ACTIVE VIBRATION CONTROL OF SMART STRUCTURES

A THESIS SUBMITTED TO
THE GRADUATE SCHOOL OF NATURAL AND APPLIED SCIENCES
OF
THE MIDDLE EAST TECHNICAL UNIVERSITY

BY

FATMA DEMET ÜLKER

IN PARTIAL FULFILLMENT OF THE REQUIREMENTS FOR THE DEGREE OF

MASTER OF SCIENCE

IN

THE DEPARTMENT OF AEROSPACE ENGINEERING

SEPTEMBER 2003

Approval of the Graduate School of Natural and Applied Sciences.

Prof. Dr. Canan Özgen
Director

I certify that this thesis satisfies all the requirements as a thesis for the degree of Master of Science.

Prof. Dr. Nafiz Alemdaroğlu
Head of Department

This is to certify that we have read this thesis and that in our opinion it is fully adequate, in scope and quality, as a thesis for the degree of Master of Science.

Dr. Volkan Nalbantoğlu
Co-Supervisor

Prof. Dr. Yavuz Yaman
Supervisor

Examining Committee Members

Prof. Dr. Mehmet A. Akgün

Prof. Dr. Yavuz Yaman

Assist. Prof. Dr. Metin Salamcı

Dr. Altan Kayran

Dr. Volkan Nalbantoğlu

ABSTRACT

ACTIVE VIBRATION CONTROL OF SMART STRUCTURES

Ülker, Fatma Demet

M.S., Department of Aerospace Engineering

Supervisor: Prof. Dr. Yavuz Yaman

Co-Supervisor: Dr. Volkan Nalbantoğlu

September 2003, 119 pages

The purpose of this thesis was to design controllers by using H_∞ and μ control strategies in order to suppress the free and forced vibrations of smart structures. The smart structures analyzed in this study were the smart beam and the smart fin. They were aluminum passive structures with surface bonded PZT (Lead-Zirconate-Titanate) patches. The structures were considered in clamped-free configuration.

The first part of this study focused on the identification of nominal system models of the smart structures from the experimental data. For the experimentally identified models the robust controllers were designed by using H_∞ and μ-synthesis strategies. In the second part, the controller implementation was carried out for the suppression of free and forced vibrations of the smart structures.

Within the framework of this study, a Smart Structures Laboratory was established in the Aerospace Engineering Department of METU. The controller implementations were carried out by considering two different experimental set-ups. In the first set-up the controller designs were

based on the strain measurements. In the second approach, the displacement measurements, which were acquired through laser displacement sensor, were considered in the controller design.

The first two flexural modes of the smart beam were successfully controlled by using H_∞ method. The vibrations of the first two flexural and first torsional modes of the smart fin were suppressed through the μ-synthesis. Satisfactory attenuation levels were achieved for both strain measurement and displacement measurement applications.

Keywords: System Identification, H_∞ and μ Synthesis Methods, Robustness Analysis, Signal Processing, Controller Implementation

ÖZ

AKILLI YAPILARIN AKTİF TİTREŞİM KONTROLÜ

Ülker, Fatma Demet

Yüksek Lisans, Havacılık ve Uzay Mühendisliği Bölümü

Tez Yöneticisi: Prof. Dr. Yavuz Yaman

Ortak Tez Yöneticisi: Dr. Volkan Nalbantoğlu

Eylül 2003, 119 sayfa

Bu çalışmada, H_∞ ve μ-sentez yöntemleri kullanılarak akıllı yapıların serbest ve zorlanmış titreşimlerini sönümlendirmek için denetçi tasarlanması amaçlanmıştır. Akıllı kiriş olarak adlandırılan bir kiriş benzeri yapı ile akıllı plak olarak adlandırılan bir plak benzeri yapı incelenmiştir. Bu yapılar, üzerlerine PZT (Lead-Zirconate-Titanate) yamaları yapıştırılmış pasif alüminyum yapılardır. Yapılar, bir kenarı tutturulmuş diğer kenarı serbest bırakılmış olarak incelenmiştir.

Çalışmanın ilk aşaması akıllı yapıların sistem modellerinin deneysel veriler kullanılarak belirlenmesi üzerine yoğunlaşmıştır. Deneysel olarak belirlenen bu modeller için H_∞ ve μ-sentez yöntemleri ile gürbüz denetçiler tasarlanmıştır. Çalışmanın ikinci kısmında, akıllı yapıların serbest ve zorlanmış titreşim denetim uygulamaları yapılmıştır.

Bu tezin kapsamında, ODTÜ Havacılık ve Uzay Mühendisliği Bölümünde bir Akıllı Yapılar Laboratuvarı kurulmuştur. Denetim uygulamalarında iki değişik yaklaşım göz önünde bulundurulmuştur. İlk yaklaşımda, denetçiler uzama ölçümlerini esas alarak tasarlanmıştır. İkinci

yaklaşımda, denetçi tasarımında yerdeğişim ölçümleri esas alınmıştır. Yerdeğişim ölçümleri laser yardımı ile yerdeğişim algılama cihazı ile yapılmıştır.

Akıllı kirişin ilk iki rezonans frekansındaki titreşimi H_∞ yöntemi kullanılarak başarılı bir şekilde denetlenmiştir. Akıllı plakın ilk iki eğilme titreşimleri ve ilk burulma titreşimi μ-sentez yöntemi ile sönümlendirilmiştir. Hem uzama ölçümleri uygulamalarında hem de yerdeğişim ölçümleri uygulamalarında yeterli titreşim sönümlenme seviyelerine ulaşılmıştır.

Anahtar Kelimeler: Sistem Belirlenmesi, H_∞ ve μ sentez methodları, Gürbüzlük Analizleri, Sinyal İşlenmesi, Denetçi Uygulanması

To my Parents

ACKNOWLEDGMENTS

I would like to thank my supervisor, Prof. Dr. Yavuz Yaman, for his guidance and support throughout my studies. I would also like to thank my co-supervisor, Dr. Volkan Nalbantoğlu, for several enlightening ideas and constructive comments which have helped to improve my views of control theory.

I am grateful to my parents for tolerating me especially for 7 years and for their love and encouragement. Also I would like to thank my sister, Buket for showing me the life at the outside of the department.

When the time comes to explain my indebtedness to Mustafa, I realize that the words are not enough. During my assistantship in the department, I benefited from his experiences related to both technical field and the real life.

I would like to thank Cağatay for his patience for my questions.

I have spent nearly everyday of my last year with Mustafa, Ömer, Gizem, yellow thing Emre, Özgür, Barbaros, Funda, Ebru, and Mehmet. I would like to thank them for opening their door whenever I was bored.

I would like to thank also Dr. Eswar Prasad, Dr. David Waechter and Bin Yan for their endless support.

This work was supported by NATO/RTO/Applied Vehicle Technology Panel through the project 'T-129, Development of Control Strategies for the Vibration Control of Smart Aeronautical Structures'. I gratefully acknowledge the support given.

TABLE OF CONTENTS

LIST OF TABLES

LIST OF FIGURES

LIST OF SYMBOLS

ROMAN SYMBOLS

ARE	Algebraic Riccati Equation
FEM	Finite Element Model
F_L	Lower Linear Fractional Transformation
F_U	Upper Linear Fractional Transformation
LFT	Linear Fractional Transformation
H	Hamiltonian Matrix
MIMO	Multi-Input Multi-Output
PZT	Lead-Zirconate-Titanate Piezoelectric Material
SISO	Single-Input Single-Output
W_{act}	Actuator Weight
W_{add}	Additive Weight
W_{dist}	Disturbance Weight
W_{noise}	Noise Weight
W_{per}	Performance Weight

GREEK SYMBOLS

δ	Real or Complex Scalar Uncertainty
Δ	Full Block Uncertainty
μ	Structured singular value
$\rho(A)$	Spectral Radius of A
$\bar{\sigma}(A)$	Largest Singular Value of A

SUPERSCRIPTS

$^{-1}$	Inverse
*	Complex Conjugate Transpose

MISCELLANEOUS SYMBOLS

$\Re$	Field of Real Numbers
$\mathcal{C}$	Field of Complex Numbers
$\in$	Belong to
$\|\|A\|\|_\infty$	Infinity norm of A
$\tilde{P}$	Perturbed Plant
sup	Supremum (the least upper bound of a set)
inf	Infimum (the greatest lower bound of a set)

CHAPTER 1

INTRODUCTION

1.1 Background to the Study

The flexible aerospace structures require the utilization of proper control strategies for the achievement of pointing and shape accuracy requirements of missions. The applications of smart structures in conjunction with the advance control techniques is proving to be an effective means for these requirements.

The purpose of this thesis is to design and implement the controllers to suppress the free and forced vibrations of some smart structures. In the controller design, H_∞ and μ-synthesis methods are used. The smart structures analyzed in this study are a beam-like structure called as smart beam and a plate-like structure called as smart fin. They are aluminum passive structures with surface bonded PZT (Lead-Zirconate-Titanate) patches. The structures are considered to be in clamped-free configuration. The surface bonded piezoelectric parches are used as actuators and strain gages and laser displacement sensor are used as sensors in this study. The first two flexural modes of the smart beam and the first flexural and the first torsional modes of the smart fin are suppressed.

Chapter 1, in addition to the thesis outline, gives a literature survey about the smart structures and some control applications used for the vibration suppression.

Chapter 2 describes H_∞ and μ-synthesis controller design methods and gives the basic

definitions of the synthesis and analysis methods. In addition, this chapter explains how these controller design methods can be employed as a tool for the vibration suppression of smart structures.

Chapter 3 presents the theoretical and the experimental studies conducted for the smart beam. The theoretical studies focus on the determination of the system models of the smart beam and the design of H_∞ controllers. The experimental studies give the implementation of the designed H_∞ controllers. The theoretical and experimental results for the smart beam are also given in this chapter.

Chapter 4 gives the theoretical and the experimental studies performed for the smart fin. The identification of the experimental system models of the smart fin and the design of controllers via μ-synthesis are presented in this chapter. The theoretical and experimental results for the smart fin are also given.

The general conclusions drawn from the study and the recommendations for the future work are given in Chapter 5.

1.2 Limitations of the Study

The system models of the smart structures of the present study are assumed to be linear time invariant and they are obtained within a limited bandwidth. The unmodelled dynamics and the parameter variations are considered as uncertainties.

Nonlinear characteristics of piezoelectric actuators and their hysteresis effects are neglected in the present study.

Only H_∞ and μ-synthesis controller design methods are considered for control applications.

The PZT locations in the smart fin are those obtained from the theoretical analysis by using Ansys v5.6. No formal optimization was conducted.

1.3 Literature Survey

1.3.1 Smart Structures

Recent progress in piezoelectric materials for distributed actuators and sensors has triggered a considerable interest in smart structures. The smart structure is a structure which can sense external disturbances and respond to those with active control in real time to maintain the mission requirements. Smart structures consist of highly distributed active devices called smart materials and controller units. The smart materials are used as sensors and/or actuators which are either embedded or attached to a passive structure [1].

The different types of smart materials may be categorized in terms of the type of energy transformation they undergo, such as:

- Thermo-Mechanical: Shape Memory alloys.
- Light-Mechanical: Fibre Optics.
- Magneto-Mechanical: Magnetostrictive materials, Magneto-Rheological Fluid.
- Electro-Mechanical: Piezoelectric materials, Electrostrictive materials, Electro-Rheological Fluid.

A detailed information on the types of the smart materials and their application areas can be found in Reference [1].

Piezoelectric effect is the two-way effect between stress/strain and electric field/voltage difference in materials having no central symmetry. The first experimental demonstration of a connection between macroscopic piezoelectric phenomena and crystallographic structure was published in 1880 by Pierre and Jacques Curie [2]. They asserted that there was an one-to-one correspondence between the electrical effects of temperature change and mechanical stress in a given crystal. They observed that any strain in the passive structure led to a voltage field to be generated through the piezoelectric material. This is known as *direct piezoelectric effect*. In two years, the Curie brothers confirmed that crystals exhibiting the direct piezoelectric effect (electricity from applied stress) would also exhibit the *converse piezoelectric effect* (stress

in response to applied electric field). In 1950's, development of the barium titanate family of piezoceramics and later the lead zirconate titanate family contributed to establishing an entirely new method of piezoelectric device development - namely, tailoring a material to a specific application. During the 1960's and 1970's, researchers discovered that various organic materials exhibit the piezo effect. Then, in 1969, a strong piezoelectric response in the polymer polyvinylidene fluoride (PVDF) was discovered, which developed far greater piezo activity than any other synthetic or natural polymer [3].

Piezoelectric materials have been used in a wide range of applications such as in ultrasonic transducers, accelerometers, gramophones, resonators, filters, ink-jet printers and as various kinds of sensors and actuators. It is quite natural to extend this list of applications to include smart structures. Comparing to piezoelectric materials, the other types mentioned previously are more difficult to integrate into existing structures and being relatively new, they lack a consistent mathematical model unlike piezoelectric materials which had been developed analytically [4].

Piezoelectric materials can have several forms such as piezoceramics (e.g. Lead Zirconate Titanate - PZT), piezopolymers (e.g. Polyvinylidene Fluoride - PVDF), piezoelectric fibers, piezoelectric fibrous/layer composites, piezoelectric films, etc. However, since PVDF actuators and sensors have very low passive stiffness values and extreme sensitivities to environmental conditions (humidity, temperature), they are not attractive for most of the engineering applications [5]. Compared to piezoelectric fibers, piezoceramics are easier and less expensive to be produced. Consequently, piezoceramics are considered to be more convenient and more available for applications of smart structures.

1.3.2 H_∞ Control Theory and μ-Synthesis

H_∞ control theory was originated by Zames [6]. He formulated the problem of sensitivity reduction by feedback as an optimization problem with an operator norm, in particular, an H_∞-norm. In the further researches, Zames and Francis [7] considered the single-variable case and extended the previous work of Zames [6] to the parametrization of unstable plants. In their

following research, the general design procedure given in [7] was improved. Sarason's theory [8] was applied to determine the optimal weighted sensitivity function and an upper bound on its norm. The problem of achieving small sensitivity over a specified frequency band and effect of non-minimum phase was studied. Also the method for handling the plant having zeros and poles on the imaginary axis, which was not covered in [7], was presented in [9]. Once the single input single output plant model have been analyzed, Francis and Helton [10] advanced their studies on the application of H_∞ control theory to a linear multi-variable systems. Starting from 1981 with Zames, the techniques for the synthesis of optimally robust stabilization controllers have been developed. These methods were first applied to the robust stabilization problem of single-input single-output systems then to the multi-variable systems by Glover [11]. In his study, Glover dealt with the stabilization of a linear system model having uncertainties in it. Reduced order controllers were also considered. Glover extended the robust stabilization problem for the multi-input multi-output systems. State space formulas were derived for all controllers solving the standard H_∞ problem by Doyle and Stein [12].

Although H_∞ control theory was shown to be very effective method to design a controller for the multi-input multi-output systems, it was found that this method was still conservative for the system having multiple sources of uncertainty. As a remedy, structured singular value, μ, was introduced allowing for the introduction of the uncertainty structure in the controller design process [13]. Currently, μ-synthesis method provides an extremely powerful technique in robust control design. For the solution of μ-synthesis problem, Young [14] introduced a *D-K* iteration method assuming that the system only has the complex uncertainty structure, which was also considered as conservative. In the following study, Young [15] developed another method, *D,G-K* iteration method, which was able to consider the real uncertainties as well as complex uncertainties. Another approach was derived by Toffner-Clausen [16], which was also straightforward extension of the *D-K* iteration method. This method was denoted as μ-*K* iteration and shown to be more easily applied to real problems than the *D,G-K* iteration method.

1.3.3 Studies on Modelling and Control of Flexible Structures

Use of piezoelectric materials offers a number of advantages over conventional actuators which are hydraulic, pneumatic and electric actuators. These advantages, low energy consumption, fast response, high efficiency and compactness, make the piezoelectric materials more preferable in the active control applications [17].

The fundamental concept in design of a controller is to have an accurate model of active structure. In the initial stages of the design Finite Element Model (FEM) is adequate. The FEM model allows one to address such issues as optimal actuator and sensor placement, size and power requirements of the actuators and open-loop and closed-loop performance comparisons. Also, the FEM determines the natural frequencies and the mode shapes of the structure. However, the FEM method can not predict the input/output transfer function parameters accurately and makes no predictions of the damping in the system [1, 18]. This problem brings to light the necessity of an experimentally identified model. Then, one can obtain the refined finite element model based on the experimentally identified model. In the controller design stage either refined finite element model or experimentally identified model can be used.

Dosch et. al. [18] investigated the model of an active flexible ribbed antenna with a two-step identification technique. Positive position feedback (PPF) and H_∞ controllers were designed based on the identified model. The closed-loop control was then implemented and resulted in the suppression of the first eight modes of the antenna.

Nalbantoglu [19, 20] studied on the derivation of multi-input multi-output system model by applying frequency domain identification techniques and the generalized orthonormal basis functions. He observed very good agrement between experiments and simulations done by parametric system identification and identification with generalized orthonormal basis functions.

In the system modelling, determination of the high frequency properties of the structure creates problem. Therefore, accurately accounting for the inevitable errors due to unmodelled dynamics is important as well as improving the mathematical model. The study performed by Balas and Young [21] contributed to the literature by presenting detailed discussion on how to model and analyze errors in natural frequency using real/complex structured singular

value algorithms. By adding the parametric uncertainty as well as the additive uncertainty on the nominal model and defining the performance criteria, set of controllers were designed with complex μ-analysis and implemented on a Mini-Mast structure. According to experimental results, it was shown that the μ-synthesis techniques could be used to account for the variations in natural frequencies and high performance controllers could be designed despite a low fidelity model [20]. Rasmussen [22] illustrated the formulation of the parametric uncertainty with clear examples.

The relation between performance specifications and error signal selection was studied by Nalbantoglu [19, 23]. He considered a four-bay experimental flexible structure as a testbed in the investigation of performance selection criterion. The closed loop tests were performed to illustrate the importance of type of desired attenuation levels and the frequency range of interest on the selection of the penalty weights, error signals and sensor locations.

Balas et al. [24] studied on the design and experimental verification of the controller for the truss structure. A number of control laws were synthesized via H_∞ and μ-synthesis techniques for different uncertainty level of descriptions. They obtained good agreement between analytically predicted attenuation and the experiment results. For the investigation of the stability robustness in the presence of numerous, closely spaced modes and the integration of system identification techniques and robust control design new trust model was designed. On this model, performance trade-offs were examined by Balas and Doyle [25]. They claimed that for the model which is not described accurately by the nominal and the uncertainty models may be unstable or exhibit poor performance when implemented on the actual system. In contrast, accurate structured uncertainty descriptions lead to controllers which achieve high performance when implemented on the experimental facility. From the results of the experiments, they obtained similar performance for a wide range of uncertain levels. As a result, it was concluded that once reasonable structured uncertainty level have been determined it may not be necessary to pin down precise levels of uncertainty.

Halim et al. [26] worked on the design and the experimental evaluation of the performance of a feedback controller to suppress the vibration of a flexible beam due to first six bending

modes. In the controller design, they focused on the minimization of spatial H_2 norm of the close-loop system. The experiments were done to show the effectiveness of the controller in reducing the structural vibrations on a piezoelectric laminate beam.

Kar et al. pointed out the spillover instability phenomenon caused by the unmodelled high-frequency modes and proposed an idea to reduce the unmodelled system uncertainties by placing actuators in the node points of the neglected mode. For the H_∞ based robust controller design, system model was expressed by augmenting the uncertainties to the nominal model. With the implementation of the controller it was confirmed that proposed feedback controller had good vibration control effect in the frequency range of interest [27]. Mei et. al. [28] also considered the spillover effects and suggested to combine the wave feedback control and quadratic optimal control. These methods were applied to beam numerically but not proven experimentally.

Yaman et al. [29] studied on an active vibration control technique applied to a smart beam. The study first investigated the effects of element selection in finite element modelling and the effects of the piezoelectric patches on the resonance frequencies. From finite element model state-space form suitable for a controller design was obtained. The design of an active vibration controller which effectively suppresses the vibrations of the smart beam due to its first two flexural modes was presented. A finite element based modelling technique was presented for a smart fin in the study of Yaman et al. [30]. An H_∞ controller was designed to suppress in-vacuo vibrations due to the first two modes of the smart fin. The effectiveness of the technique in the modelling of uncertainties was shown. It was observed that the controller guarantied the robust performance of the system in the presence of uncertainties. Yaman et al. [31] presented theoretical and experimental results of the modelling of a smart plate for active vibration control. In their study, a single-input/single-output H_∞ controller was designed to suppress the vibrations due to the first two flexural modes of the smart plate. Yaman et al. [32] applied H_∞ control to a smart-beam having PZT patches to suppress the flexural vibrations. It was shown that H_∞ active vibration controllers were very effective in suppressing the sinusoidally excited, in-vacuo forced vibrations of the smart beam.

CHAPTER 2

CONTROL THEORY

2.1 Introduction

The objective of feedback control is not only to provide the internal stability, but also to achieve certain performance specifications. However, while trying to attain these goals, two drawbacks come into picture, which are uncertainty of the system model to be controlled and the measurement errors. As a result of studies in the early 1980's, formulations of a tractable mathematical notion of uncertainty and rigorous mathematical techniques to cope with the uncertainty problems were introduced into the classical control theory [35]. First H_∞ synthesis technique was introduced to literature. Then, μ synthesis technique was derived.

The H_∞ control problem was formulated by Zames [6] and was motivated by the necessity for a control framework that could systematically incorporate errors in the plant model. The main observation in Reference [6] was that these requirements could be met by working in a Banach algebra such as H_∞ . The formulation of the H_∞ problem needed an enormous research effort into its solution. One approach for the solution of H_∞ problem is combination of function theory and state space methods, notably Riccati equations. Another approach is using the linear matrix inequality method [35].

While H_∞ theory constitutes a considerable innovation in robust control design, it still does not take into account the possible structure in the uncertainty. Thus, for multiple uncertainties

at different locations in the plant, an H_∞ design is too conservative which can lead to controllers unable to satisfy performance specifications. To cope with this problem, μ-synthesis method was derived that allows for the introduction of the uncertainty structure in the controller design process [34].

Whichever the controller synthesis method, the major objective of the feedback controller is to minimize the effects of unknown initial conditions and external influences on system behavior, subject to the constraint of not having a complete representation of the system [35].

In this thesis, H_∞ and μ-synthesis methods are applied as a tool for the vibration suppression of smart structures. This chapter describes H_∞ and μ-synthesis methods and gives the basic definitions and tools used for the formulation of the control problem and robustness analysis of the feedback system.

2.2 Basic Definitions and Tools for Control Problem Formulation

2.2.1 Linear Fractional Transformation

Linear Fractional Transformations (LFTs) are powerful and flexible approach to represent uncertainty in matrices and systems. For this reason H_∞ and μ-synthesis control problems are formulated in a linear fractional transformation framework. A LFT could be defined as follows for the matrix M.

$$\begin{bmatrix} M_{11} & M_{12} \\ M_{21} & M_{22} \end{bmatrix} \in C^{(p_1+p_2)(q_1+q_2)} \tag{2.1}$$

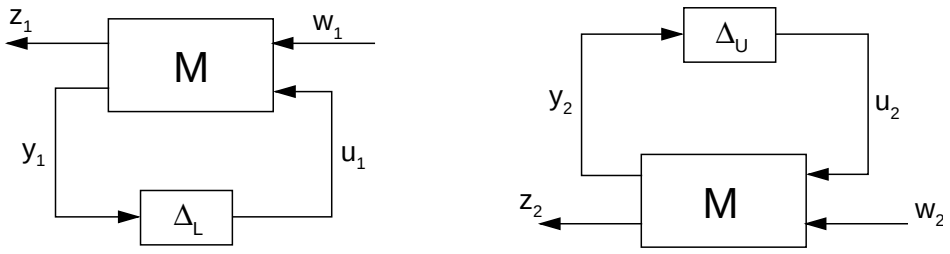

(a) Lower Fractional Transformation

(b) Upper Fractional Transformation

Figure 2.1: Linear Fractional Transformation Block Diagram

For the given matrix M, the set of equations can be written for the above diagrams as

$$\begin{bmatrix} z_1 \\ y_1 \end{bmatrix} = \begin{bmatrix} M_{11} & M_{12} \\ M_{21} & M_{22} \end{bmatrix} \begin{bmatrix} w_1 \\ u_1 \end{bmatrix} \qquad \begin{bmatrix} y_2 \\ z_2 \end{bmatrix} = \begin{bmatrix} M_{11} & M_{12} \\ M_{21} & M_{22} \end{bmatrix} \begin{bmatrix} u_2 \\ w_2 \end{bmatrix} \tag{2.2}$$

$$u_1 = \Delta_L y_1 \qquad u_2 = \Delta_U y_2$$

The meaning of an LFT in control science can be expresses if the matrix M is taken as a proper transfer function. In that case LFTs defined in Equation 2.2 give the closed loop transfer matrices from $w_1 \rightarrow z_1$ and $w_2 \rightarrow z_2$ respectively. $T_{z_1 w_1} = F_L(M, \Delta_L)$ and $T_{z_2 w_2} = F_U(M, \Delta_U)$. The derivation of $F_L(M, \Delta_L)$ is given in Equation 2.3.

$$\begin{aligned} z_1 &= M_{11} w_1 + M_{12} u_1 \\ y_1 &= M_{11} w_1 + M_{12} u_1 \\ u_1 &= \Delta_L y_1 \\ y_1 &= M_{21} w_1 + M_{22} \Delta_L y_1 \\ (I - M_{22}\Delta_L) y_1 &= M_{21} w_1 \Rightarrow y_1 = (I - M_{22}\Delta_L)^{-1} M_{21} w_1 \\ z_1 &= M_{11} w_1 + M_{12}\Delta_L (I - M_{22}\Delta_L)^{-1} M_{21} w_1 \\ z_1 &= [M_{11} + M_{12}\Delta_L (I - M_{22}\Delta_L)^{-1} M_{21}] w_1 \\ z_1 &= F_L(M(s), \Delta_L) w_1 \end{aligned} \tag{2.3}$$

From these equalities $F_L(M, \Delta_L)$ and $F_U(M, \Delta_U)$ can be expressed as

$$F_L(M(s), \Delta(s)) = M_{11} + M_{12}\Delta_L (I - M_{22}\Delta_L)^{-1} M_{21} \tag{2.4a}$$

$$F_U(M(s), \Delta(s)) = M_{22} + M_{21}\Delta_U (I - M_{11}\Delta_U)^{-1} M_{12} \tag{2.4b}$$

For the control problem formulation, the LFT form is used to pull out the unknowns Δ and controller for reducing the control problem to a general interconnection structure given in Figure 2.2.

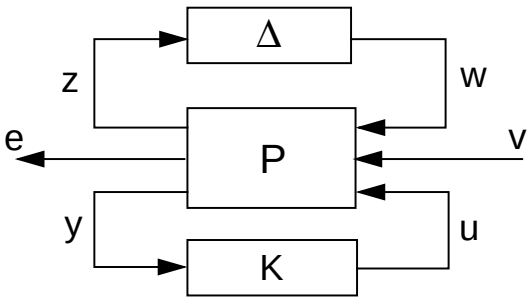

Figure 2.2: General Interconnection Structure

2.2.2 Calculation of H_∞ Norm

The infinity norm of a scalar function G is interpreted as the distance in the complex plane from origin to the farthest point on the Nyquist plot of G, and it also appears as the peak value on the Bode magnitude plot of G. Hence, the infinity norm of a transfer function can be obtained graphically. For the estimation of the infinity norm, fine grids are formed in the frequency range of interest as $\omega_1 \ldots \omega_N$ then estimate for $||G||_\infty$ is

$$||G||_\infty = \max_{1 \leq k \leq N} \bar{\sigma}(j\omega_k) \tag{2.5}$$

This value is generally read from the Bode plot.

For MIMO systems, calculation of the H_∞ norm requires checking for $j\omega$ axis eigenvalues of a Hamiltonian matrix. The Hamiltonian matrix is first formed depending on a parameter γ. Then the search over γ is performed and for each γ the eigenvalue of the Hamiltonian matrix is calculated. If non of the eigenvalues of the Hamiltonian matrix are on $j\omega$ axis, then the infinity norm of the system matrix is said to be less than γ. If the matrix $H\gamma$ does have $j\omega$ axis eigenvalues, then it is said that these occur at the frequencies where the transfer matrix has a singular value equal to γ. The detailed information can be found in Reference [13].

2.2.3 Uncertainty and Robustness

In any circumstances, the model will only be an approximate representation of the physical process. Therefore, there are unavoidable differences between the model and the reality and these are referred as model uncertainty. Since there are many assumptions made to obtain the

mathematical model, a single plant can not produce the same outputs as the true plant does. It is necessary to define a set of possible models to define the system model.

Main sources for model uncertainty can be listed as [37]

1. Incomplete knowledge on the process; this type of uncertainty may be caused if the system model has been derived from the laws of physics. On the other hand, if the model is determined experimentally, the accuracy of the model depends on whether the process has been excited by inputs, which are suited for determining a model, and to what extent the process has been influenced by disturbances during the experiment.

   In this study, the system models for the smart beam and the smart fin were obtained from experimental results and the experiments were carried out within a limited frequency range. Thus, the high frequency dynamics of the smart beam and smart fin were not considered. Also, during the experiment the system's output most probably was affected by the noise from the environment, which was again an uncertainty for the system.

2. Model simplification; In most of the processes, for the simplification of the problem, reduced order system models are used. For easiness in the controller design and controller implementation, low order system models are preferred. So the reduction in the order of the system models brings another uncertainty to a nominal system model, which must be accounted for.

3. Incomplete model structure; in general it is preferable to design controllers based on a linear model, where the nonlinearities in actuators or sensors are omitted. In the analysis, both the system dynamics of the smart beam and smart fin were considered as linear. Also, nonlinearity effects of the piezoelectric materials, such as hysteresis were omitted and the actuators were considered as linear. This negligence can be considered as an uncertainty to be added on to the nominal system model.

4. Time varying parameters also result in variation of the parameters of the model.

These uncertainties could be introduced to the system with different types of uncertainty descriptions, which are presented as follows.

2.2.3.1 Parametric Uncertainty

Parameters in a state space or transfer function representation of a system are assumed to lie in a set given as

$$\tilde{P} \in P + \omega\delta\,,\ \delta \in [\ -k \quad k\ ] \tag{2.6}$$

where $\tilde{P}$, the perturbed system model, describes the set of systems, P is defined as the nominal value of the parameter, δ is allowed to take any value between $-k$ and k, ω is the problem dependent scaling factor. This type of uncertainty is considered to be suitable in representing the uncertainty in natural frequency and the damping ratios of the flexible structures.

The formulation of the parametric uncertainty at the natural frequencies and the damping ratios was analyzed by Balas and Young [21]. In this work a method was suggested for taking into account the real parameter variations in the damping ratios and natural frequencies with complex perturbations. For a single-mode transfer function, uncertainty in the damping ratios (δ_1) and natural frequency squared terms (δ_2) is expressed as in Equation 2.7.

$$\frac{1}{s^2 + 2\zeta\omega(1+\delta_1) + \omega^2(1+\delta_2)} \tag{2.7}$$

It was shown that, the complex perturbations in the damping levels lead to variations in the structural natural frequencies as well as in the damping levels in the system model. The uncertainty of the system was formulated in state-space form by first transforming the A matrix to a bidiagonal form then perturbing only first element of each 2×2 natural frequency block. This perturbation was considered as complex uncertainty in damping levels, which results in a significant change in damping levels but small change in natural frequencies [21].

2.2.3.2 Additive and Multiplicative Uncertainties

Block diagrams of additive and multiplicative perturbations used to represent the model uncertainty are given in Figure 2.3. Here W represents the fixed stable transfer function, Δ represents a variable stable transfer function satisfying $||\Delta||_\infty < \gamma$ Also, it is assumed that none of the unstable poles of the nominal plant is cancelled in forming $\tilde{P}$.

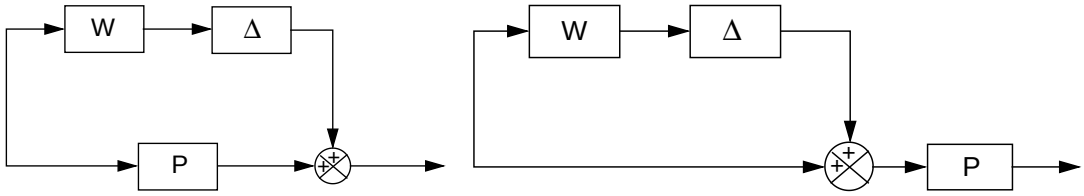

(a) Additive Uncertainty (b) Multiplicative Uncertainty

Figure 2.3: Additive and Multiplicative Uncertainty

For additive uncertainty, perturbed plant transfer function is formed as $\tilde{P} = (P + \Delta W)$. For multiplicative uncertainty, perturbed plant transfer function is formed as $\tilde{P} = (1 + \Delta W)P$.

In general, additive uncertainty is considered to account for the high frequency unmodelled dynamics and multiplicative input/output uncertainty is considered to account for actuator/sensor errors and mode shape mismatch [25].

2.2.3.3 Uncertainty Selection Criteria

In the system identification, the transfer function is obtained from input output relations and some techniques are applied to smooth the transfer function. The detailed information is given in Section 2.7. However, these techniques flatten the obtained transfer function at the natural frequency locations while smoothing it. In this thesis, the different overlap numbers were tried to estimate the transfer function by trial and error and the approximate change in the magnitude of the transfer function change was determined. The transfer function between these ranges was selected to be an estimated transfer function. Then the curve fitting method was applied to obtain the approximate representation of the system model. In the curve fitting stage, again there was error between fitted and estimated transfer function. The fitted transfer function was taken as nominal system model and additive uncertainty was added on the nominal system model to cover the uncertainties caused by fitting and the unmodelled dynamics stated in Section 2.2.3. Then the selected weights are put in Figure 2.3(a) and ± 1 was given to Δ ($||\Delta||_\infty < 1$) and the set of systems were analyzed if they were in the determined ranges. The effect of uncertainty and performance weight on the nominal model is given Figure 2.4 for the

system model used in the study. This figure illustrates the upper and the lower bounds of the set of systems under the effect of parametric uncertainty and the additive uncertainty. In Figure 2.4, Δ and δ correspond to the additive uncertainty and parametric uncertainty respectively. The system models within these bounds are shown to be perturbed system model, $\tilde{P}$ in the definitions.

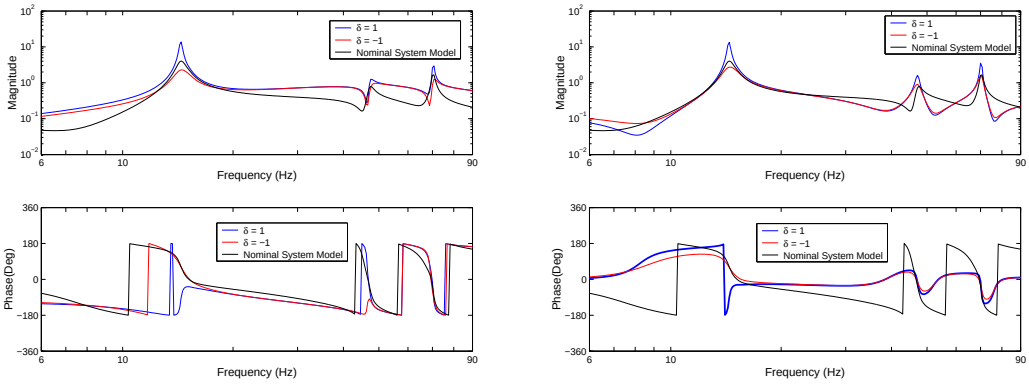

(a) $\Delta = -1$ (b) $\Delta = 1$

Figure 2.4: Uncertainty Effect on the Nominal System

2.2.4 Stability and Performance Definitions

Nominal Stability: The controller must stabilize the nominal plant (P).

Robust Stability: The controller must stabilize every plant belonging to set ($\tilde{P}$) which is defined by the proper uncertainty descriptions.

Nominal Performance: The performance specifications must be satisfied by the closed loop system for the nominal plant (P).

Robust Performance: The performance specifications must be satisfied by the closed loop system for every plant belonging to set ($\tilde{P}$) which is defined by the proper uncertainty descriptions.

Small Gain Theorem: The basis for the robust stability criteria is derived from the small gain theorem. Small gain theorem states that, if a feedback consists of stable systems and the loop gain product is less than unity then the feedback loop is internally stable. Loop gain product is defined as $||M||_\infty$ for the system given in Figure 2.5.

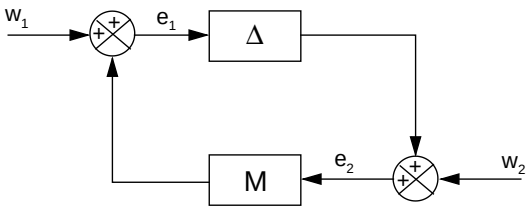

Figure 2.5: Block Diagram for Small Gain Theorem

Up to now, the definitions and the necessary tools to form the H_∞ control problem were presented. Once the appropriate uncertainty descriptions and performance characteristics are chosen, the H_∞ control problem can be formed.

2.3 H_∞ Synthesis

The general feedback diagram given in Figure 2.6 is transformed in to general interconnection structure given in Figure 2.7 by pulling out the unknown Δ uncertainty and controller block. In this block diagram v defines the vector of exogeneous inputs such as disturbances (d), noise (n) and reference input (r). e is a vector of error signals to be kept small, y is a vector of sensor measurements and u is a vector of control signals.

In Figure 2.6, SYS block represents the identified nominal system model. W_{per} is the performance weight. W_{per} is added to the feedback system to reflect the desired frequency-dependent performance objective. W_{add} is the additive weight, which defines the uncertainty of the nominal system model. Also, the uncertainty on the natural frequencies and damping ratios can be added to the nominal system. The necessity of uncertainties was discussed in Section 2.2.3. W_{act} is actuator weight, which defines the actuator limitation to prevent the actuation saturation. W_{noise} represents the signal to noise ratio. In general, the sensor dynamics are insignificant relative to the dynamics of the rest of the system. This might not be true of the sensor noise and should be added on top of the measured values. W_{noise} is added as another block diagram to state that the measured system response is affected by noise. W_{dist} is the disturbance weight. It is necessary to define level of the disturbance that affects the system. The weights could be frequency dependent or constant.

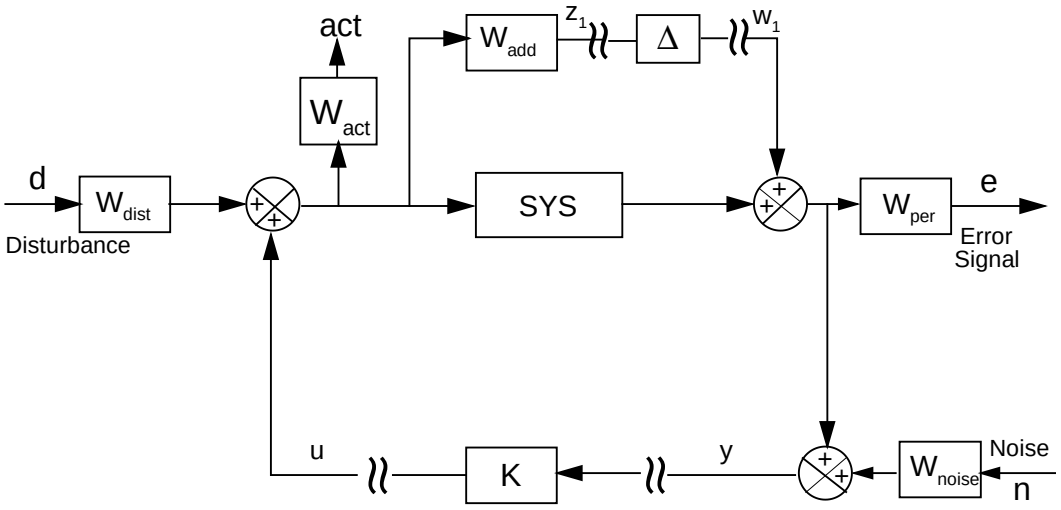

Figure 2.6: General Feedback Block Diagram

These weights are absorbed into the P matrix to form the general interconnection structure by pulling out the unknowns uncertainty Δ and controller block.

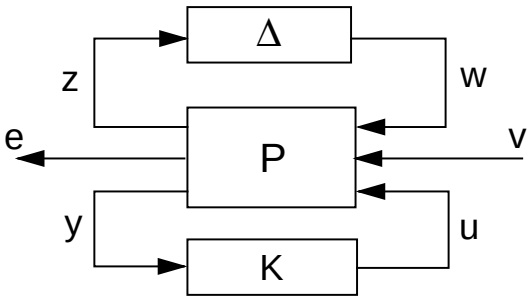

Figure 2.7: General Interconnection Structure (Figure 2.2 is repeated)

For the controller design Δ block is eliminated and input-output relation from $[\ w \quad v\ ]^T$ to $[\ z \quad e\ ]^T$ is written in LFT form as in Equation 2.8 (Equation 2.4a is repeated). The obtained structure after the elimination of Δ block is given in Figure 2.8.

$$F_L(P,K) = P_{11} + P_{12}K(I - P_{22}K)^{-1}P_{21} \tag{2.8}$$

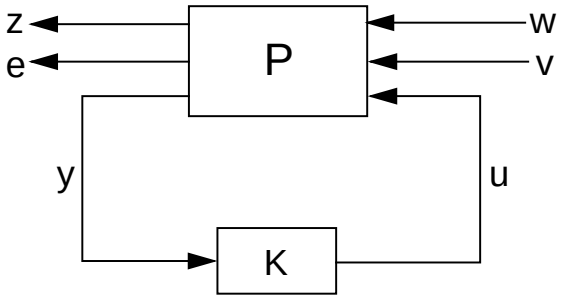

Figure 2.8: H_∞ Synthesis

The objective of the H_∞ control problem is to find a stabilizing controller K which minimizes $||F_L(P,K)||_\infty$. Once the controller is found from the minimization of $||F_L(P,K)||_\infty$, the controller is absorbed into P matrix and μ-analysis which is given in Section 2.6 is performed to check if the designed closed loop system is robust to uncertainties. The robust performance, nominal performance and robust stability tests can be done by considering the definitions given in Section 2.2.4. The robustness analysis is explained in Section 2.6.

In H_∞ controller design, the uncertainties are considered as unstructured, that is the structure of the uncertainty block Δ is not taken into account. Thus, for multiple uncertainties at different locations in the plant, an H_∞ design is too conservative which considers all the uncertainties as one full block. In order to avoid this conservatism, structured singular value concept was introduced [13].

2.4 Structured Singular Value μ

In H_∞ controller design, the structured uncertainty, which is necessary to reduce the conservatism if a system is built from components that are themselves uncertain, is not considered. The Δ block is considered as unstructured. In fact the Δ block in LFT representation has a special structure as given in Equation 2.9

$$\underline{\Delta}(s) = \{diag[\delta_1 I_{r_1}, \delta_2 I_{r_2}, ..., \delta_s I_{r_s}, \Delta_1, \Delta_2, ..., \Delta_F]\,;\, \delta_i \in \Re H_\infty, \Delta_i \in \Re H_\infty\} \qquad (2.9)$$

with $||\delta_i||_\infty < 1$ and $||\Delta_i||_\infty < 1$.

This $\underline{\Delta}(s)$ block representation involves the full blocks (Δ_i), the repeated real and complex scalars (δ_s). The repeated real scalars allow the representation of the uncertainties at the natural frequencies and damping ratios, whereas full complex blocks allow the representation of the additive or multiplicative uncertainties.

The definition of the structured singular value, μ, is given for the matrix $M \in C^{p\times q}$, and the smallest perturbation matrix $\underline{\Delta} \in C^{p\times q}$ in Equation 2.10.

$$\mu_{\underline{\Delta}} = \frac{1}{\min \bar{\sigma}(\Delta) \,:\, \Delta \in \underline{\Delta},\, det(I - M\Delta) = 0} \tag{2.10}$$

unless no $\Delta \in \underline{\Delta}$ makes $(I - M\Delta) = 0,\ \mu_{\underline{\Delta}} = 0$.

An exact solution for $\mu_{\underline{\Delta}}$ does not exist. A solution can be approximated via upper and lower bounds on $\mu_{\underline{\Delta}}$. In general, these bounds are not sufficient to estimate $\mu_{\underline{\Delta}}$. If the block does not contain any real elements the upper and lower bounds can be found by using scaling matrices U and D, which do not affect $\mu_{\underline{\Delta}}(M)$ but affect the $\bar{\sigma}$ and spectral radius ρ.

$$\bar{U} = \{U \in \underline{\Delta} \,:\, U^*U = I_n\} \tag{2.11}$$

$$\bar{D} = \{Diag[D_1, ..., D_s, d_1 I_{m_1}, ..., d_F I_{m_F}]\ , D_i \in C^{r_i \times r_i},\ D_i = D_i^* > 0,\ d_j \in \Re, d_j > 0\}$$

For any $\Delta \in \underline{\Delta}$, $U \in \bar{U}$ and $D \in \bar{D}$

$U^* \in \bar{U}$, $U\Delta \in \underline{\Delta}$, $\Delta U \in \underline{\Delta}$, $\bar{\sigma}(U\Delta) = \bar{\sigma}(\Delta U)$ and $D\Delta = \Delta D$. Therefore the bounds can be tightened to

$$\max_{U\in\bar{U}} \rho(UM) \le \mu_{\Delta}(M) \le \inf_{D\in\bar{D}} \bar{\sigma}(DMD^{-1}) \tag{2.12}$$

These upper and lower bounds have shown to be useful predictions of $\mu_{\underline{\Delta}}$. The case when $\underline{\Delta}$ contains real elements is more complicated. A detailed explanation is given in Reference [13]. The structured singular value is used for the robustness analysis given in Section 2.6 of a linear system having structured uncertainty.

2.5 μ-Synthesis

In the controller design it is aimed to find a controller K which satisfies the property given in Equation 2.13.

$$\min_{K} ||F_L(P,K)||_\alpha \; for \; \alpha = \infty \; or \; \mu \tag{2.13}$$

$\alpha = \infty$ case was given in Section 2.3 resulting a design of H_∞ controller.

$\alpha = \mu$ case brings the μ-synthesis method. For the solution of it, D-K iteration technique is used. The detailed information can be found in Reference [13]. For this technique, stable and minimum phase scaling matrix $D(s)$ is chosen such that $D(s)\Delta(s) = \Delta(s)D(s)$. Once fixed scaling matrix D, search for $\min_K ||DF_L(P,K)D^{-1}||_\infty$ turns out to classical optimization problem. Also for a given stabilizing K,

$\inf_{D,D^{-1}\in H_\infty} ||DF_L(P,K)D^{-1}||_\infty$ can be solved by searching in the frequency domain as in Equation 2.14.

$$\sup_{\omega} \inf_{D_\omega \in \bar{D}} \bar{\sigma}[D(\omega)F_L(P,K)(j\omega)D^{-1}(\omega)] \tag{2.14}$$

The μ-synthesis via scaling is given in Figure 2.9. D-K iterations proceed by performing two parameter minimization in sequential order, first minimizing over K by keeping $D(\omega)$ fixed, then minimizing over $D(\omega)$ keeping K fixed. The steps for the D-K iteration can be summarized as follows [42]:

1. The first step in the D-K iteration is to design a controller K_o for the unscaled matrix P. This controller can be H_∞ controller and for this case the first step block diagram representation comes out to be same as the block diagram for H_∞ synthesis problem (Figure 2.8).

2. The second step involves the computation of the closed loop system for the designed controller and μ-analysis for the closed loop system.

3. In the third step the iteration is initialized by estimating the scaling matrix $D(\omega) \in D$ for each point across a frequency according to μ-analysis result. The scalar transfer matrices $d_i(s), d_i^{-1}(s) \; for \; i = 1, 2, \ldots, (F-1)$ (F is the number of full blocks) are obtained by fitting a transfer function. Once the $D(s) = diag(d_1(s)I, d_2(s), \ldots, d_{F-1}(s)I, I)$ are obtained

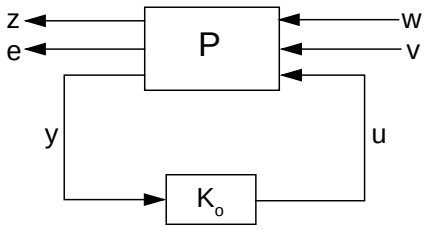

(a) First Step

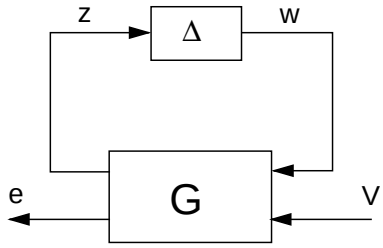

(b) Second Step

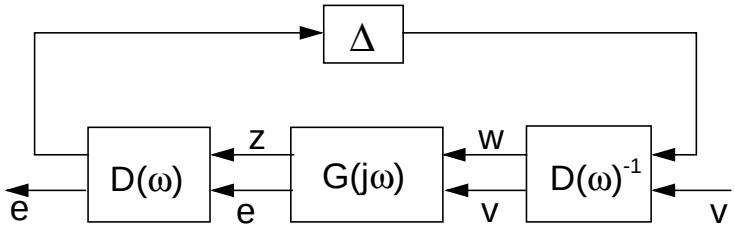

(c) Third Step

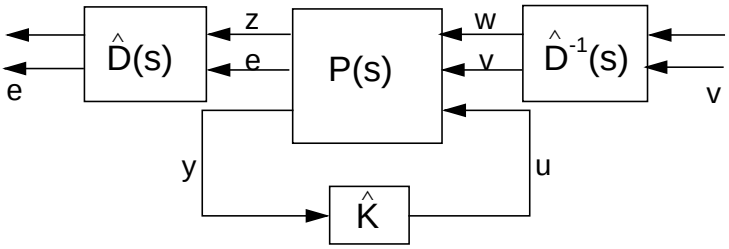

(d) Fourth Step

Figure 2.9: *D-K* Iteration Steps

new state space model are constructed by scaling the G matrix.

$$\hat{P}(s) = \begin{bmatrix} D(s) & \\ & I \end{bmatrix} P(s) \begin{bmatrix} D^{-1}(s) & \\ & I \end{bmatrix} \tag{2.15}$$

4. In this step, a minimization of $||F_L(\hat{P}, K)||$ over all stabilizing controllers K is done. It becomes a H_∞ controller problem but for this time since the minimization problem uses the scaled matrix $\hat{P}$, the resulting controller is represented as $\hat{K}$.

5. By using the controller $\hat{K}$, found in the last step and unscaled P, $\bar{\sigma}(D(\omega)F_L(P, \hat{K})D^{-1}(\omega))$ is minimized over $D(\omega)$. This procedure produces another scaling matrix call $\hat{D}(\omega)$.

6. As a last step these two scaling matrices are compared and if these are found as close to each other the iteration step stops otherwise after replacing $D(\omega)$ with $\hat{D}(\omega)$ iteration continues up to desired closeness is obtained.

Although, there are some global convergence problems in *D-K* iteration process, it was shown that the controllers designed by using this approach work well. However, since this method is less conservative, the definition of system uncertainty should be carefully selected.

The preceding sections give brief information about both H_∞ and μ-syntheses. The controller can be designed with any of these methods but one should check the robustness properties of the designed controller.

2.6 Robustness Analysis

Structured Robust Stability: This analysis provides a test for the robust stability of the system given in Figure 2.10. The structured singular value, $\mu_{\underline{\Delta}}$, can be used to evaluate the robustness margins for a system having structured uncertainty. And it is shown that robust stability is satisfied for all perturbations if and only if the condition given in Equation 2.16 is satisfied.

$$sup_w \mu_{\underline{\Delta}}(G_{11}(j\omega)) \leq 1,\ 0 \leq \omega \leq \infty \tag{2.16}$$

In this equation, G_{11} corresponds to the interconnection with uncertainty channel, Δ. The value in Equation 2.16 can be found graphically from the definition of $\mu_{\underline{\Delta}}$ and by searching over a fine grid formed in the frequency range of interest, and the peak value of the plot $\mu_{\underline{\Delta}}(G_{11}(j\omega))$ determines the size of the perturbations that makes the loop unstable.

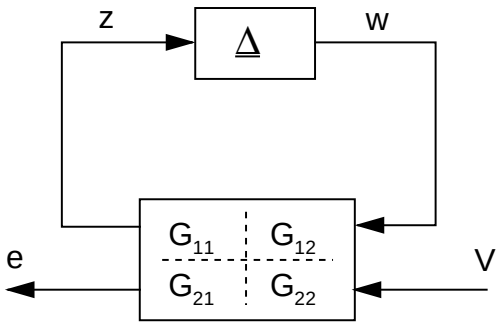

Figure 2.10: Robust Stability Analysis Block Diagram

This theorem provides a test for the stability of the system shown in Figure 2.10 for all allowable perturbations. However, usually stability is not the only condition that must be satisfied for a feedback system. Since in most of the cases, before the onset of instability, the closed-loop performance degrades significantly when the nominal plant is perturbed. A robust performance test is necessary to indicate the worst case level of performance associated with a given level of perturbations.

Robust Performance: The robust performance problem can be formulated as a robust stability problem by defining a fictitious full block of uncertainty Δ_{per} with the performance inputs and outputs. The only difference between the robust performance and the robust stability lies on the definition of the Δ structure, which is defined as in Equation 2.17 and block diagram representation is given in Figure 2.11.

$$\underline{\Delta}_P = \{ \begin{bmatrix} \Delta & 0 \\ 0 & \Delta_{per} \end{bmatrix} : \Delta \in \underline{\Delta},\ \Delta_{per} \in \mathcal{C}^{q_2 \times p_2} \} \tag{2.17}$$

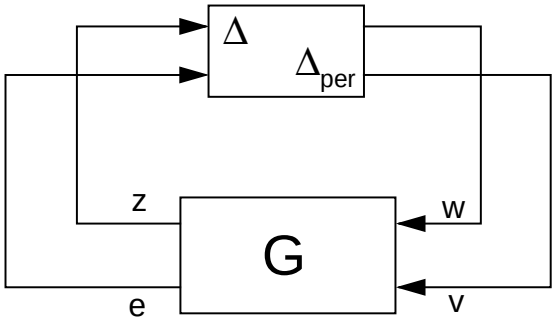

Figure 2.11: Robust Performance Analysis Block Diagram

Theorem for the robust performance states that $F_U(G, \Delta)$ is stable and $||F_U(G, \Delta)||_\infty < 1$

$$sup_w \mu_{\underline{\Delta}_P}(G(j\omega)) \leq 1,\ 0 \leq \omega \leq \infty \tag{2.18}$$

This value can be found graphically from the definition of $\mu_{\underline{\Delta}}$ and by searching over all frequencies in a frequency range of interest.

2.7 System Identification

Mathematical modelling is a procedure by which a mathematical description of the system behavior is extracted either from the physical laws known as white-box modelling or from experimental data, which is called as black-box modelling. Also, the mathematical model can be obtained by using both experimental data and physical laws. This is known as grey-box modelling.

Experimental results show that the modelling of flexible structures via finite element method may not be accurate enough for high performance active control design purposes. For this reason determination of a system model from the experimental data is the preferable method that can be applied to derive the model of the system. The construction of a model from data involves three basic entities: the experimental data, a set of candidate models and a rule by which candidate models can be evaluated using the data.

The experiments should be performed in a way that sufficient information about the system is obtained. A model set is constructed to fit to the data by using the model parameters. It should be noted that this model set does not necessarily reflect the physical consideration in the system. Particular solution is obtained by considering the listed entities, then the constructed model is validated. The loop for the system identification is given in Figure 2.12 [38].

System identification techniques can be studied in two main titles as parametric and non-parametric identification. In parametric identification process the set of models is expressed with the parameter vector, which must be estimated. It is required to adjust the coefficients of the matrices of a state-space model so as to achieve the best possible match between the frequency responses generated by this model and those coming from the experiment. For non-parametric identification system model is obtained without selecting a confined set of possible models in other words this method does not employ a finite-dimensional parameter vector in the search for a best description of the system model.

Nonparametric system identification involves the analysis of impulse response, step response and sine-wave testing. Since giving impulse type of input could make the system exhibit non-linear effects resulting in the disturbance of linearized behavior of system model and giving a

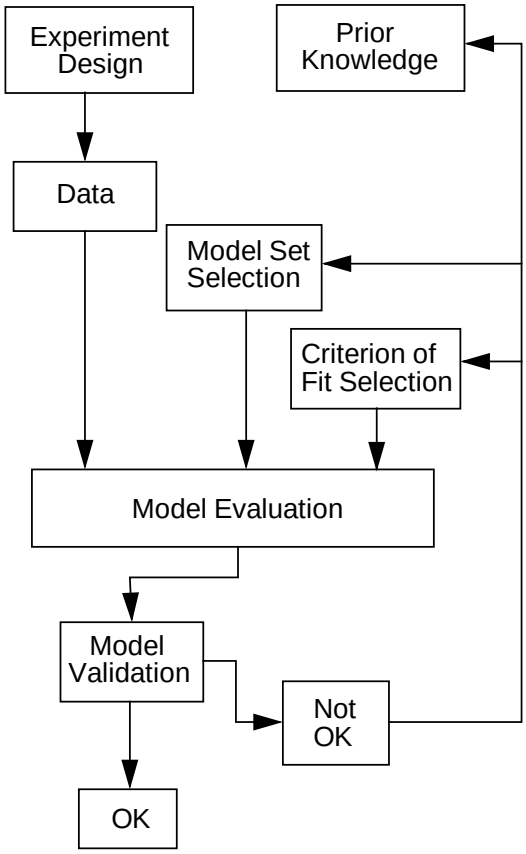

Figure 2.12: The System Identification Loop

step type input causes large error on system modelling, it is advised to construct the system model from sine-wave testing. This is known as a frequency analysis and is a simple method for obtaining detailed information about a linear system in the frequency range of interest [38].

In the sine-wave testing, the system to be identified is excited with an input signal of sine-wave $x(t)$ in the frequency range of interest and the output signal $y(t)$ is measured. The input-output relation of a linear time invariant system can be used to estimate the transfer function of the system. The detailed information can be found in Reference [38].

The outcome of unsmoothed transfer function computed from the input output relation may give a spiky appearance, which causes the interpretation of the estimated transfer function difficult. For this reason, a smoothing method is necessary to be applied. In this thesis the Welch method and windowing is used for smoothing the estimated transfer function [39].

Finally, the parametric identification is applied to determine the system model by fitting

a curve to the transfer function, which had been already obtained from nonparametric system identification. The transfer function is expressed as

$$g(z) = \frac{\sum_{j=1}^{p} n_j z^j}{z^p + \sum_{j=1}^{p-1} d_j z^j} \tag{2.19}$$

Here p is the order of the system and n and d are the coefficients of the numerator and denominator of the transfer function respectively. The equation can be rearranged by multiplying both sides by denominator

$$\sum_{j=1}^{p-1} d_j z^j g(z) - \sum_{j=1}^{p} n_j z^j = -g(z) z^p \tag{2.20}$$

$z_{i=1}^{M}$ represents the points on the unit circle obtained by mapping the discrete frequency points, w_i, of the experimental transfer function. These frequency values had been determined as a result of nonparametric identification. $z_i = e^{j\frac{w_i}{T}}$, T is the sampling frequency.

The problem was arranged to form the standard least square problem as given in

$$Z_o = \begin{bmatrix} 1 & z_1 & z_1^2 & \dots & z_1^{p-1} \\ 1 & z_2 & z_2^2 & \dots & z_2^{p-1} \\ . & . & . & \dots & \\ 1 & z_m & z_m^2 & \dots & z_m^{p-1} \end{bmatrix} \qquad Z = \begin{bmatrix} 1 & z_1 & z_1^2 & \dots & z_1^{p} \\ 1 & z_2 & z_2^2 & \dots & z_2^{p} \\ . & . & . & \dots & \dots \\ 1 & z_m & z_m^2 & \dots & z_m^{p} \end{bmatrix}$$

$$\begin{aligned} D &= [g(z_1), g(z_2), \dots, g(z_M)] \\ \hat{n} &= [n_0, n_1, \dots, n_p] \\ \hat{d} &= [d_0, d_1, \dots, d_{p-1}] \\ y &= [g(z_1)z_1^p, g(z_2)z_2^p, \dots, g(z_M)z_M^p] \end{aligned} \tag{2.21}$$

The matrix representation of the Equation 2.20 is given in Equation 2.22

$$\begin{bmatrix} DZ_o & -Z \end{bmatrix} \begin{pmatrix} \hat{d} \\ \\ \hat{n} \end{pmatrix} = -y \tag{2.22}$$

The problem now turns out to be standard least square problem. For the solution of the problem, direct method explained in Reference [40] is used. An iterative solution approach is added to remove the high frequency emphasis by means of weighting coefficients. The obtained transfer function from the solution of least square problem was transferred to a continuous system.

CHAPTER 3

THEORETICAL AND EXPERIMENTAL STUDIES OF THE SMART BEAM

3.1 Introduction

This chapter presents the theoretical and the experimental studies conducted on the smart beam. The studies were done by considering two different approaches. In the first approach, the system model of the smart beam was derived by considering the piezoelectric actuator voltage as an input and strain gage result as an output of the system. For this application, the H_∞ control was performed by using a four-channel programmable controller *SensorTech SS10* which was specifically designed for smart structure applications. In the second application, the system model of the smart beam was obtained by considering the piezoelectric actuator voltage as an input and the beam tip flexural displacement as an output. The H_∞ controller of this approach was implemented by using a *LabVIEW v5.0* based program. In the following sections, the derivation of the system models, H_∞ controller design and implementations are given for both applications.

3.1.1 Description of the Smart Beam

The smart beam was modelled by symmetrically attaching eight PZT (Lead-Zirconate-Titanate) actuators (25 $mm \times 20\ mm \times 0.5\ mm$, *Sensortech BM500* type) and two strain gages

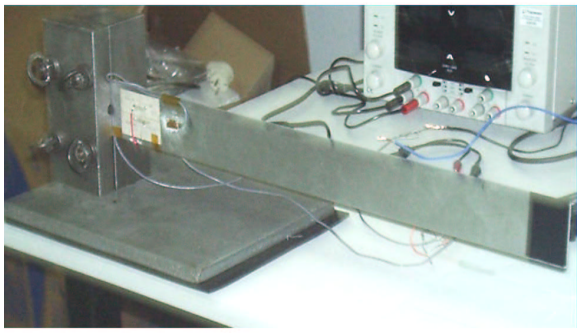

Figure 3.1: The Smart Beam Used in the Study

(*OMEGA-SG-7/350-LY13*) as sensors on a passive aluminum beam having the dimensions of 507 $mm \times 51\ mm \times 2\ mm$. In the analysis the smart beam was considered in clamped-free configuration. The structural modelling of the smart beam was performed and the theoretical characteristics were found by Çalışkan [1] using *ANSYS v5.6* package program. The structural model of the smart beam is given in Figure A.1 in Appendix A. The actuators and sensors were placed on a section with highest possible strain. Figure 3.1 gives the smart beam used in the study.

Open loop experiments were also performed on the smart beam for the determination of the structural characteristics and for the verification of the theoretical results. Table 3.1, gives the theoretically determined resonance frequencies together with the experimentally obtained resonance frequencies and the damping coefficients [1].

Table 3.1: Theoretically and Experimentally Obtained Resonance Frequencies and the Experimentally Found Damping Coefficients of the Smart Beam

FEM	Experimental	
$f_n(Hz)$	$f_n(Hz)$	Damping(ζ)
7.30	7.29	$7.71 \cdot 10^{-2}$
44.11	40.07	$1.78 \cdot 10^{-2}$
117.28	110.62	$7.06 \cdot 10^{-3}$

3.2 System Identification of the Smart Beam

The system model of a structure can be obtained either theoretically or experimentally. Various studies usually point out the effectiveness of the experimentally identified models in the controller design. In this study, the experimentally identified models were determined and

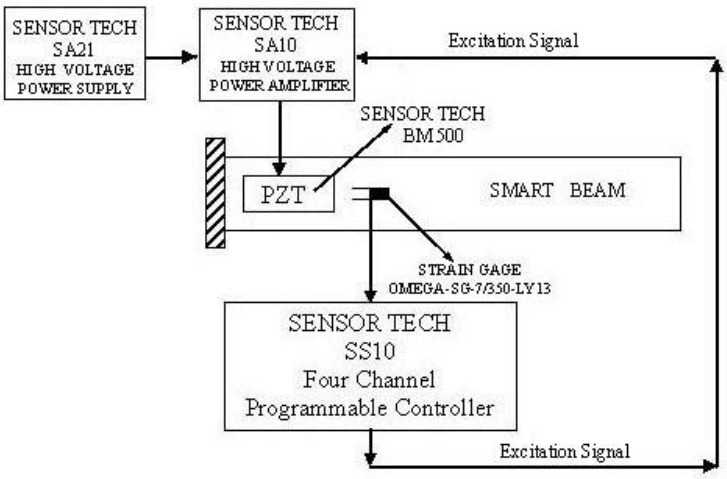

Figure 3.2: Experimental Setup for the System Identification of the Smart Beam for Strain Measurement

used in the controller design. The system model of the smart beam was obtained by applying both nonparametric and parametric system identification techniques. Nonparametric system identification involves the analysis of impulse response, step response and sine-wave testing. Due to the disadvantages of first two analysis type, mentioned previously in Chapter 2, it was thought to construct the system model from sine-wave testing. This is known as a frequency analysis and is a simple method for obtaining the detailed information about a linear system in the frequency of interest. As a result of the nonparametric system identification, transfer function of the system was obtained first, then the least square curve fitting method was applied to find the approximate representation of the model. As discussed in Chapter 2, the least square curve fitting method is a parametric identification in which the coefficients of the numerator and denominator of the transfer function, with a desired order, are estimated.

3.2.1 System Identification of the Smart Beam Based on Strain Measurements

The smart beam was excited with sinusoidal chirp signal ($x(t)$) in the frequency range of interest, which covers the first two flexural modes (0.1 Hz to 60 Hz) and the response of the smart beam ($y(t)$) was acquired via the strain gages defined before acting as sensor. The sinusoidal chirp signal of amplitude 10 V peak-to-peak was generated by four channel dedicated controller

unit (*SensorTech SS10*) and amplified 30 times before applied on the piezoelectric materials. For the amplification of the excitation signal, high voltage power amplifier *SensorTech SA10* and high voltage power supply *SensorTech SA21*, which supplies the necessary DC voltage to the *SensorTech SA10* were used. These are dedicated instruments specifically developed for piezoelectric applications. *SensorTech SS10* has its own internal strain gage preamplifier and the strain values were amplified before stored in a computer. The program written in *C* language was used for data acquisition. The experimental setup for the system identification process is given in Figure 3.2.

The excitation signal in time domain is given in Figure 3.3(a). The strain values were measured by the controller unit and these values were converted to some numbers which were meaningful for the controller unit. Figure 3.3(b) shows the measured strain values according to these numbers for a duration of 60 *secs*.

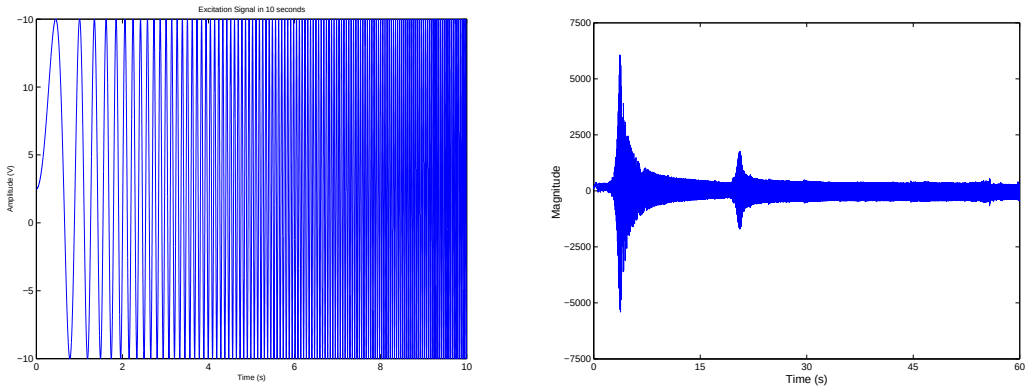

(a) Excitation Signal

(b) Time Response of the Smart Beam

Figure 3.3: Excitation Signal and Time Response of the Smart Beam for Strain Measurement

One of the main problems in measuring the strain values is the electrical noise. To generate the necessary bending moment on the smart beam, piezoelectric materials must be driven by high voltage value ($150-300\ V$). On the other hand, the strain signal induced is generally within a range of $10^{-3}\ V$. The usage of high voltage and low voltage simultaneously increases the noise effect on the strain values. For the reduction of the noise effect, half bridge configuration was used in strain gage circuit, which doubled the strain value and provided temperature compensation. Also, strain values were amplified before stored in a computer. Although the

noise effect had been reduced in some extent, the measured strain values had also sensor noise and noise from environment on top of the actual strain values. The correlation technique was applied to reduce the effect of these on the resulting transfer function. Then the least-square curve fitting method was applied to obtain the approximate representation of the estimated transfer function. The frequency responses of the smart beam in terms of the estimated and fitted transfer functions with different orders, and the error between them are given in Figure 3.4.

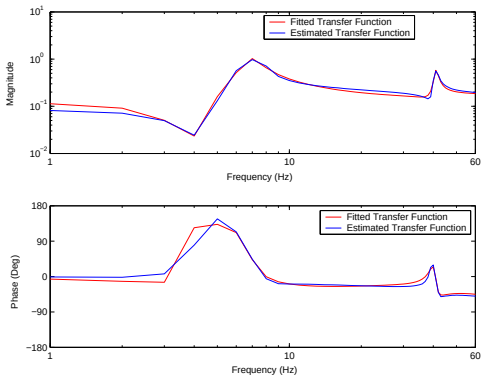

(a) 8^{th} Order Transfer Function

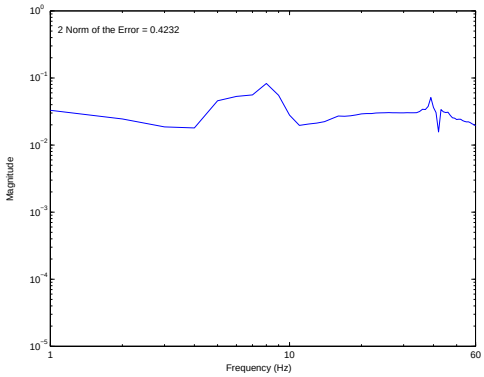

(b) Error for 8^{th} Order Transfer Function

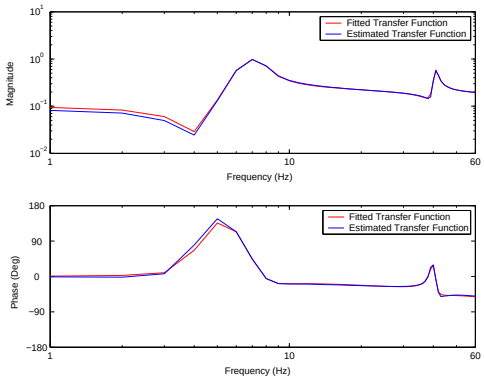

(c) 10^{th} Order Transfer Function

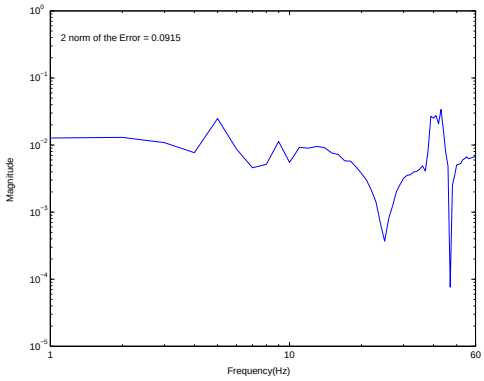

(d) Error for 10^{th} Order Transfer Function

Figure 3.4: Estimated and Fitted Transfer Functions and Error for the Smart Beam for Strain Measurement

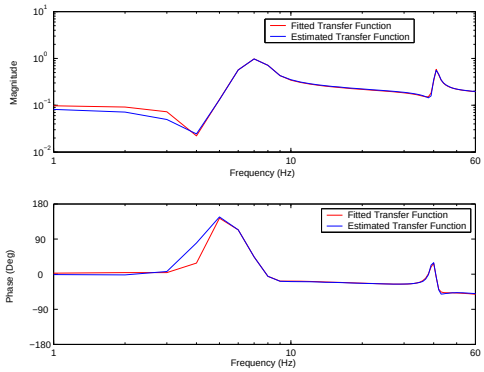

(e) 12^{th} Order Transfer Function

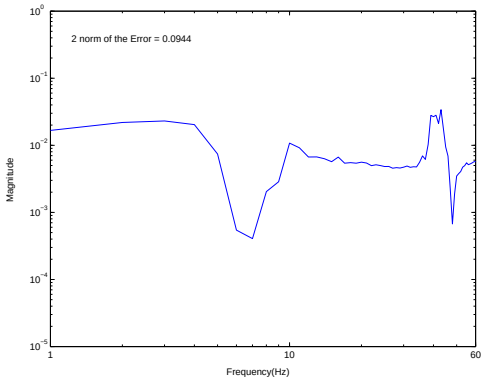

(f) Error for 12^{th} Order Transfer Function

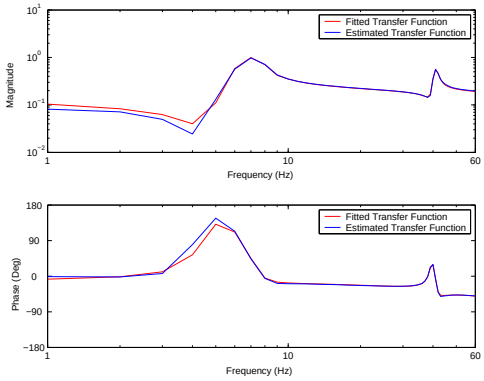

(g) 20^{th} Order Transfer Function

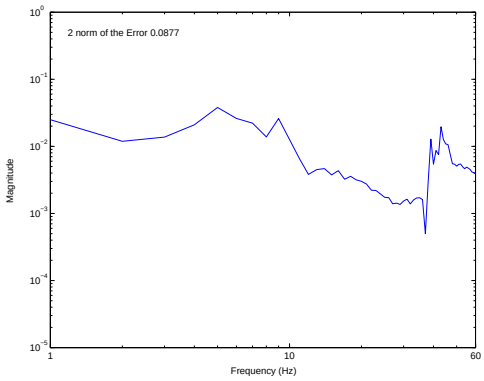

(h) Error for 20^{th} Order Transfer Function

Figure 3.4: Estimated and Fitted Transfer Functions and Error for the Smart Beam for Strain Measurement (Continued)

The 2-norm of the error between the estimated and fitted transfer functions was calculated for several transfer function orders. The order of the transfer function for the controller design of the smart beam was selected by considering the error at the natural frequencies and the 2-norm of the error between estimated and fitted transfer function. Although, the system model of order 20 has less error compared to lower order system models have, it was better to choose the low order system model in the controller design. Since the 10^{th} order system model had less error compared to 8^{th} order system model, the controller was designed is of 10^{th} order. In Equation 3.1, the 10^{th} order system model is given.

$$G(s) = \frac{-0.129s^{10} + 119.7s^9 + 1219s^8 + 7.06 \cdot 10^7 s^7 + 3.761 \cdot 10^{10} s^6 + 5.618 \cdot 10^{12} s^5}{s^{10} + 1462s^9 + 9.092 \cdot 10^5 s^8 + 8.336 \cdot 10^8 s^7 + 2.192 \cdot 10^{11} s^6 + 5.491 \cdot 10^{13} s^5} \quad (3.1)$$
$$\frac{+2.317 \cdot 10^{15} s^4 + 6.037 \cdot 10^{16} s^3 + 6.308 \cdot 10^{18} s^2 + 4.998 \cdot 10^{19} s + 2.988 \cdot 10^{21}}{+1.099 \cdot 10^{16} s^4 + 3.514 \cdot 10^{17} s^3 + 3.828 \cdot 10^{19} s^2 + 4.641 \cdot 10^{20} s + 3.234 \cdot 10^{22}}$$

3.2.2 System Identification of the Smart Beam Based on Displacement Measurements

The general procedure used in the previous section was repeated, this time by considering the beam tip flexural displacement measurements instead of strain gage measurements. For the measurement of the tip displacement, a *Laser Displacement Sensor* (*LB 1201(W)LB 300*) was used. The smart beam was excited with a sinusoidal chirp signal, ($x(t)$) of frequency 0.1 *Hz* to 120 *Hz*, which covers the first three flexural modes. The chirp signal was generated by using *HP33120A* signal generator. The flexural displacement of the beam tip, ($y(t)$) was stored in a computer by using the program written in *Labview v5.0*. The experimental setup for the system identification of the smart beam based on the displacement measurement is given in Figure 3.5. The *Labview* program written for data acquisition is shown in Figure A.4 in Appendix A.

In Section 3.2.1, the system model of the smart beam was obtained by considering the piezoelectric actuator voltage as an input and strain gage result as an output of the system. In that application, the sinusoidal chirp signal was generated by *SensorTech SS10* for a frequency range of 0.1 *Hz* to 60 *Hz*. *SensorTech SS10* has an internal output filter, whose cutoff frequency is set to 100 *Hz* [43]. Hence, it is not possible to generate excitation for frequencies higher than 100 *Hz* and consequently the third flexural mode was not included in the system identification. However, in this section the third flexural mode was also included since this time the sinusoidal chirp signal was generated by signal generator *HP33120A* rather than *SensorTech SS10*.

Each loop in the program given in Figure A.4 in Appendix A corresponds to a single simultaneous input sampling period. The chirp signal of 10 *V* amplitude was amplified to 300 *V* before applied on the piezoelectric materials. For the amplification of the excitation signal, high voltage power amplifier *Sensortech SA10* and high voltage power supply *Sensortech SA21*

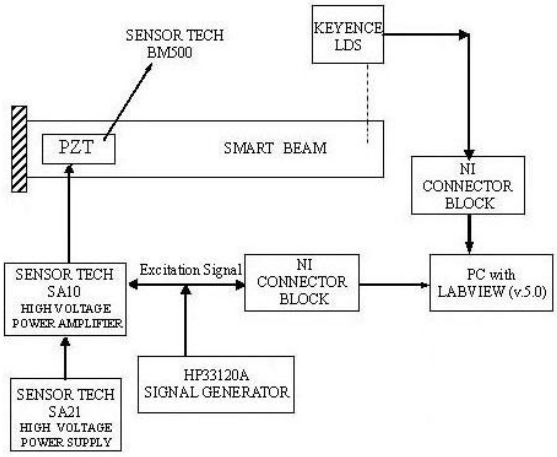

Figure 3.5: Experimental Setup for the System Identification of the Smart Beam for Displacement Measurement

were again used. The displacement of the smart beam at the tip was measured with the head of *laser displacement sensor LB 300* and it was converted to a voltage value by *1201(W)* unit. The displacement values and the applied voltage on the piezoelectric patches were transmitted to the analog-to-digital card via connector block then stored in a computer by using the program given in Figure A.4 in Appendix A. The displacement values were measured by the laser displacement sensor head and these values were converted to the meaningful numbers for the laser displacement sensor unit. The resulting time response of the smart beam is given in Figure 3.6 according to these converted numbers.

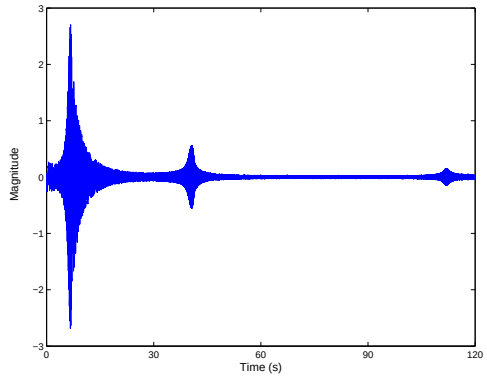

Figure 3.6: Time Response of the Smart Beam for Displacement Measurement

The required transfer function was estimated from the relevant input output relations.Then the least-square curve fitting method was applied to obtain the approximate representation of the estimated transfer function. The frequency responses of the smart beam in terms of the

estimated and fitted transfer functions with different orders, and the error between them are given in Figure 3.7.

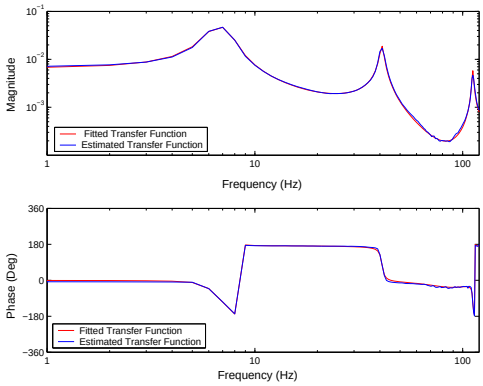

(a) 8^{th} Order Transfer Function

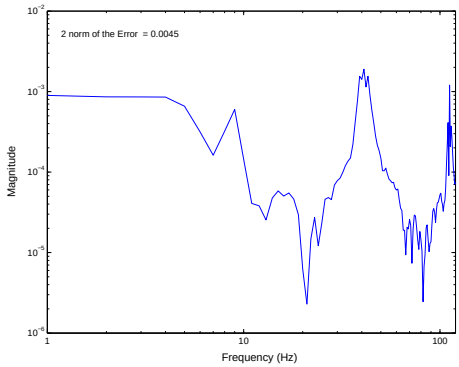

(b) Error for 8^{th} Order Transfer Function

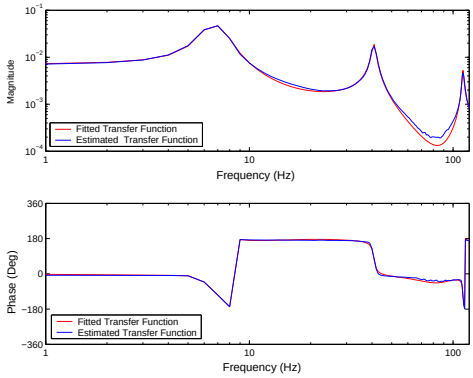

(c) 10^{th} Order Transfer Function

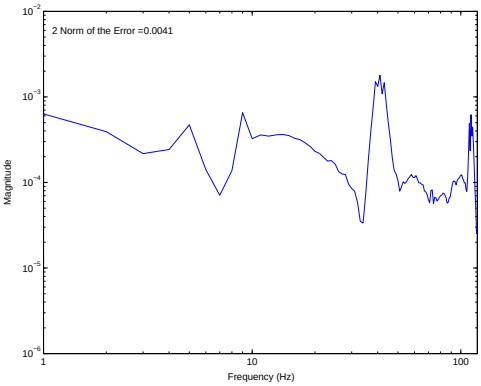

(d) Error for 10^{th} Order Transfer Function

Figure 3.7: Estimated and Fitted Transfer Functions and Error for the Smart Beam for Displacement Measurement

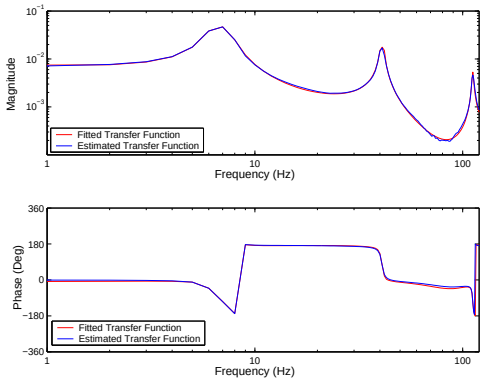

(e) 12^{th} Order Transfer Function

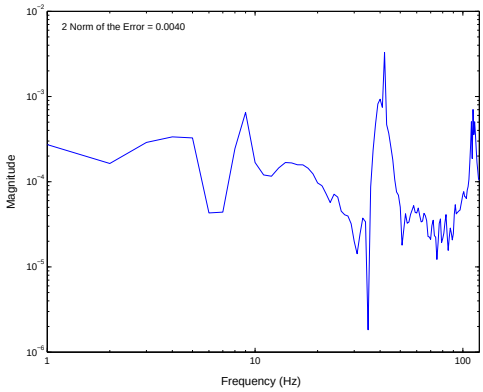

(f) Error for 12^{th} Order Transfer Function

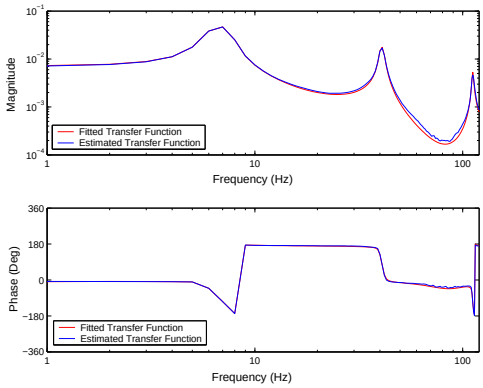

(g) 20^{th} Order Transfer Function

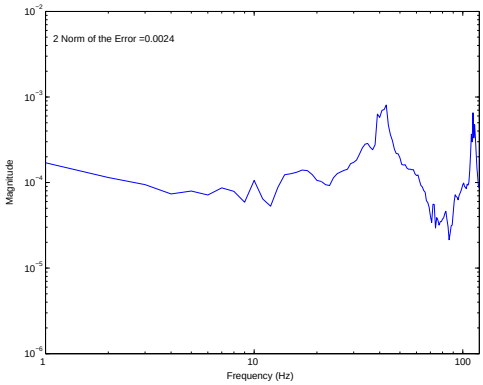

(h) Error for 20^{th} Order Transfer Function

Figure 3.7: Estimated and Fitted Transfer Functions and Error for the Smart Beam for Displacement Measurement (Continued)

Being a smaller order and having an acceptable error, 8^{th} order system model was used in the controller design process. Equation 3.2 gives the transfer function of the 8^{th} order system model.

$$G(s) = \frac{-0.00024s^8 - 0.01185s^7 - 128.9s^6 + 3552s^5 - 2.294 \cdot 10^7 s^4 - 9.158 \cdot 10^8 s^3}{s^8 + 41.43s^7 + 5.648 \cdot 10^5 s^6 + 1.637 \cdot 10^7 s^5 + 3.492 \cdot 10^{10} s^4 + 6.383 \cdot 10^{11} s^3}$$
$$\frac{+3.117 \cdot 10^{11} s^2 + 6.433 \cdot 10^{12} s + 7.224 \cdot 10^{14}}{+1.262 \cdot 10^{14} s^2 + 1.134 \cdot 10^{15} s + 1.1 \cdot 10^{17}} \quad (3.2)$$

3.3 H_∞ Controller Design

Once the system descriptions of the smart beam were obtained, the H_∞ controller problem was formulated by specifying the performance criteria and uncertainty characteristics of the

identified models. Then the controllers were designed, μ analyses were performed and open loop and closed loop frequency responses of the smart beam were analyzed. In the frequency response analysis it was assumed that the smart beam was disturbed from its equilibrium position by the disturbance given from PZT's. The block diagram formulation of the H_∞ controller is highlighted in Figure 3.8.

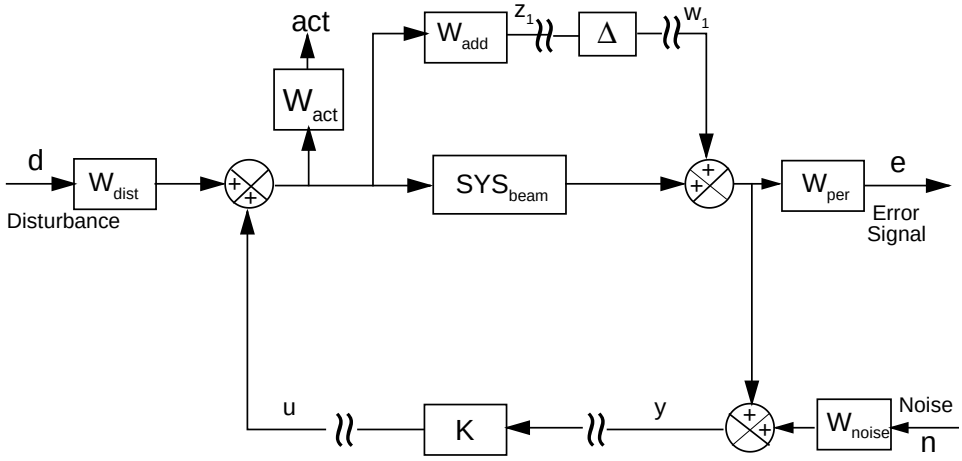

Figure 3.8: Block Diagram Representation of the Controller Design for the Smart Beam

In this Figure SYS_{beam} block represents the identified nominal system model. W_{per} is the performance weight, W_{add} is the additive weight to define the additive uncertainty of the structure. W_{act} is necessary to define the actuator limitation, W_{noise} represents the signal to noise ratio and W_{dist} is the disturbance weight. The terms were defined in Section 2.3. By inserting the values of selected weights in the general block diagram, a new controller can be obtained. For each application different controllers were designed for the smart beam.

3.3.1 H_∞ Controller Design Based on Strain Measurements

In this part of the study, an H_∞ controller was designed on the system model obtained from the strain gage readings. According to the controller objectives, the performance weight was selected such that the suppression of the vibration of the smart beam at its first two natural frequencies had to be achieved. Thus, it was desired from controller to have high performance in

the frequency range covering the first two modes and not to affect the system at high frequencies. Additive weight represents the uncertainty of the system. The influencing factors for the system uncertainty were mentioned in detail in Section 2.2.3. Additive weight was selected to cover the unmodelled dynamics and high sensor noise at high frequencies. In general, at high frequency, the amplitude of the strain value is low compared to that at low frequency region and, the effect of noise is more prominent. In addition to the noise effect, since the system model was obtained for the frequency range of $0.1\ Hz - 60\ Hz$, the modes outside the desired control bandwidth may cause instability in the closed loop system, if they were unaccounted in the design model.

According to this objectives, the selected performance weight and the additive weight are shown in Figure 3.9.

Disturbance weight was selected as unity, which means that the disturbance coming from outside was directly sensed by the system. Signal to noise ratio was chosen as 100 equivalence of this; W_{noise} was equal to 0.01. Actuator weight was selected as 0.1, which is equal to non-dimensional maximum voltage applied on the piezoelectric materials.

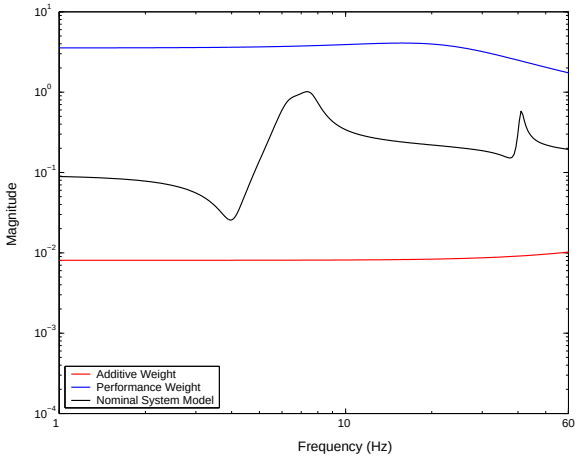

Figure 3.9: Performance and Additive Weights for the Smart Beam for Strain Measurement

H_∞ controller was designed for the smart beam according to defined performance and uncertainty specifications and μ-analysis was done for the closed loop system. The calculated structured singular values for robust performance, robust stability and nominal performance are given in Figure 3.10

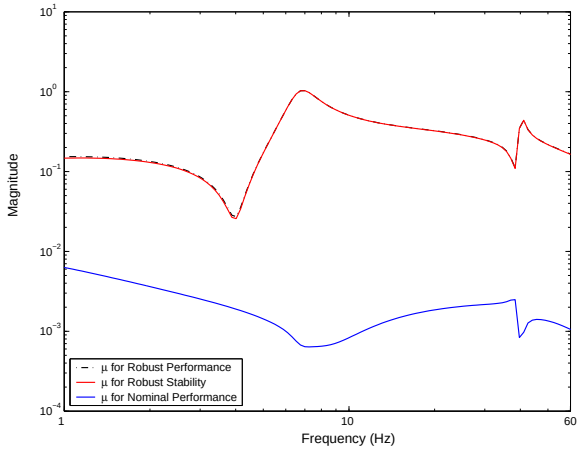

Figure 3.10: μ-Analysis Results for the Smart Beam for Strain Measurement

According to μ analysis, structured singular values must be less than unity, where the underlying theory was given in Chapter 2. As a result of the μ-analysis, it can be concluded that the designed controller is admissible. In addition to that the attenuation levels at the frequency response peaks must also be satisfactory. This was tested by performing the open-loop and closed-loop frequency response simulations in MATLAB v6.5. In Figure 3.11, the simulation results of the open-loop frequency response of the smart beam where the controller is off and the closed-loop frequency response where the controller is on are given. As it can be seen from the figure, the controller was able to suppress the vibration at the first two modes of the smart beam.

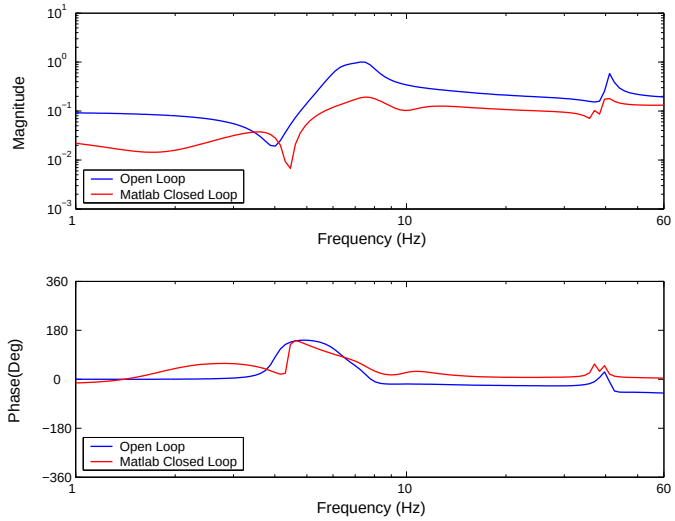

Figure 3.11: Open-Loop and Closed-Loop Frequency Responses of the Smart Beam for Strain Measurement

3.3.2 H_∞ Controller Design Based on Displacement Measurements

In Section 3.3.1, the strain gage measurements were considered as the controller input. In this section, the beam tip flexural displacement measurements were considered as controller input. The H_∞ controller block diagram previously given in Figure 3.8 was again used. However, now different weights were chosen for the system model obtained in Section 3.2.1.

By considering the objective of the controller the performance weight was selected to suppress the vibration of the smart beam at its first two natural frequencies. For the uncertainty description of the system, in addition to additive uncertainty which corresponds to the unmodelled high frequency dynamics, parametric uncertainty was added to the damping ratios and the natural frequencies in the frequency range of interest. It should be noted that the parametric uncertainty was not included in the H_∞ control synthesis of the smart beam based on the strain measurement given in Section 3.3.1 since a successful controller could be designed without need of parametric uncertainty. In Figure 3.12 the selected weights are presented.

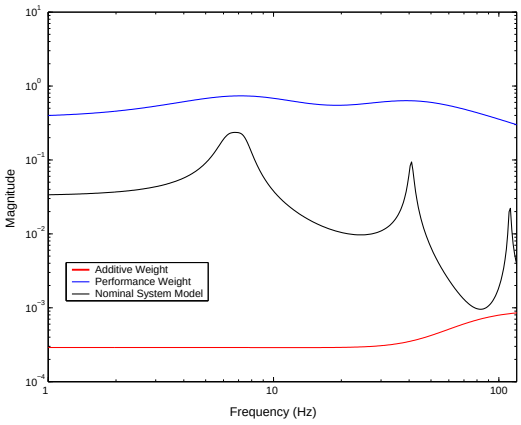

Figure 3.12: Performance and Additive Weights for the Smart Beam for Displacement Measurement

The disturbance weight was selected as unity, the noise weight was selected as 0.01, the actuator weight was selected as 0.2.

H_∞ controller was designed for the smart beam according to defined performance and uncertainty specifications and μ-analysis was done for the closed loop system. The calculated structured singular values for robust performance, robust stability and nominal performance are given in Figure 3.13

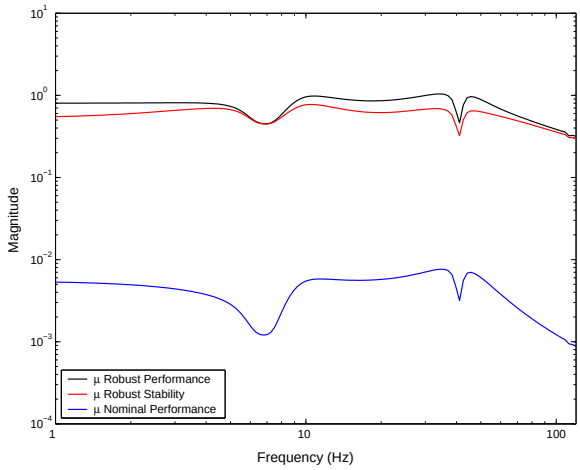

Figure 3.13: μ-Analysis Results for the Smart Beam for Displacement Measurement

The obtained structured singular values are less than unity, so it can be concluded that the designed controller is admissible according to μ analysis. In addition to that the attenuation levels at the frequency response peaks must also be satisfactory. This was checked by the open-loop and closed-loop frequency response simulations in MATLAB v6.5. In Figure 3.14 the simulation result of the closed-loop and open-loop frequency responses of the smart beam are given. The figure yields that the controller is able to suppress the vibration at the first two modes of the smart beam.

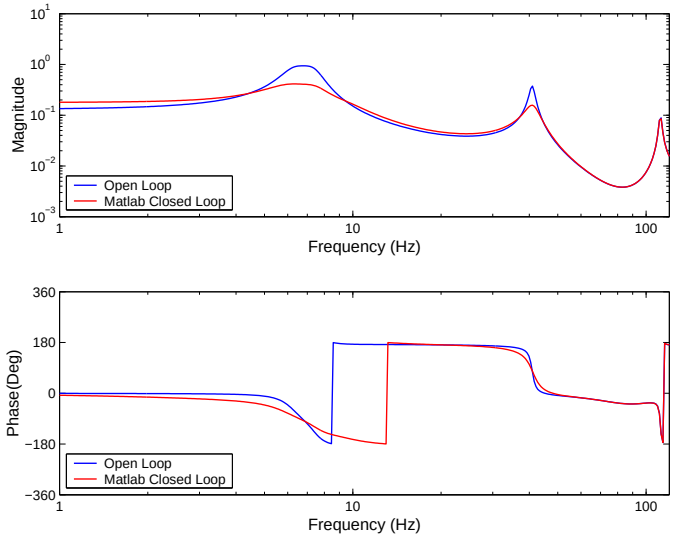

Figure 3.14: Open-Loop and Closed-Loop Frequency Responses of the Smart Beam for Displacement Measurement

For both strain and the displacement applications, the attenuation levels of the frequency response peaks at the first two natural frequencies are given in Table 3.2. Attenuation level is defined as the ratio of open loop frequency response magnitude to closed loop frequency response magnitude at the defined mode.

Table 3.2: Comparison of the Simulated Attenuation Levels of the Smart Beam for Strain and Displacement Measurements

Modes	First	Second	Third
For Strain Measurement	5.19	3.23	NA
For Displacement Measurement	2.28	2.33	1.03

Table 3.2 shows that the higher attenuation can be achieved for the strain gage application. Two possible effects may contribute to this to happen. First, during the controller design for the displacement measurements, the parametric uncertainty was also added to the nominal system model in addition to the additive uncertainty. This may increase the uncertainty on the nominal model preventing it from producing higher performance. Second reason may stem from the fact that higher actuator limitation was present in the displacement application when the signals were normalized.

3.4 H_∞ Controller Implementation

In Section 3.3, it was shown that the designed controllers achieved satisfactory performance during MATLAB v6.5 frequency domain simulations. This section gives the experimental studies conducted for the implementation and the verification of the designed controllers. Both open-loop and closed-loop experiments were performed.

The following sections present the computer programs, controller algorithms, the experimental setups and the results for open-loop and closed-loop experiments.

3.4.1 Applications Based on Strain Measurements

In this application a four-channel programmable controller unit is used. The unit, *SensorTech SS10*, is a computer based real-time tool specially developed for piezoelectric applications. It provides inputs up to eight strain gages and four variable low-voltage outputs that can

be programmed to respond the input signals. The system comprises a single-board computer powered by an Intel CPU with up to 64 *MB* RAM, high speed analog to digital and digital to analog converters and eight channel strain gage preamplifier board. The system is integrated into a sturdy steel case that also houses the necessary power supplies.

The connections to the strain gage amplifiers are made through eight five-pin self-locking connectors on the front panel for the transmission of the strain signals and outputs are available through four *BNC* connectors mounted on the front panel. Input channels are appropriate for both half bridge and full bridge configuration and for the strain gage circuit, default strain gage resistance is taken as 350 Ω. The gain of the strain gage amplifier can be adjusted 1000$\times$ to 2000$\times$ from specified potentiometer locations for each input channel. The four output channels are capable of providing 10 V peak-to-peak. These outputs also incorporate a low pass filter set to 100 Hz.

The main function of the *SensorTech SS10* system focuses on the heavy computing application of real-time signal processing and control. Powerful Intel CPU, large volume RAM, high speed analog to digital, digital to analog conversion and high efficient *C* or *C++* code make it easy to develop, these characteristics make *SensorTech SS10* different from simple PC. *SensorTech SS10* is controlled by a host computer, which operates under *RedHat6.2 Linux*. Once the control algorithm is coded and compiled, the executable file is embedded in to *SensorTech SS10* via network file system then it is downloaded to the single board computer flash disk [43].

The algorithm written in *C* programming language consists of main program and functions for the analog to digital conversion, digital to analog conversion and the controller algorithm. The input channel and output channel numbers are input to the program at the beginning of the experiment, where each channel number represents the corresponding ADC-Port or DAC-Port. Once the port numbers are defined, the program starts to convert the analog signal to digits to make the amplified strain values ready for the controller algorithm. It should be noted that, before the main controller calculation loop, bias on each of the strain gage is calculated and subtracted from the strain gage readings. Controller algorithm solves the basic state space

problem given in Equation 3.3 with zero initial condition.

$$\begin{bmatrix} \dot{x} \\ y \end{bmatrix} = \begin{bmatrix} A & B \\ C & D \end{bmatrix} \cdot \begin{bmatrix} x \\ u \end{bmatrix} \tag{3.3}$$

In Equation 3.3, the A, B, C and D matrices represents the state space realization of the designed controller. In the solution of this problem *Runge-Kutta* 4 integration method was used because of the unstability in the solution of Euler integration. However, it was observed that, when the controller was order of less than or equal to four, Euler solution converged also. The reason is that, for higher order controllers the computation time between two data acquisition cycles increases resulting a large time step. For large step sizes, Euler solution becomes unstable.

Once the necessary output for the vibration suppression is calculated, the program converts digits to analog signal. The control signal is then amplified by *SensorTech SA10* before sent to the piezoelectric patches. The C algorithm of *SensorTech SS10* is given in Figure 3.15.

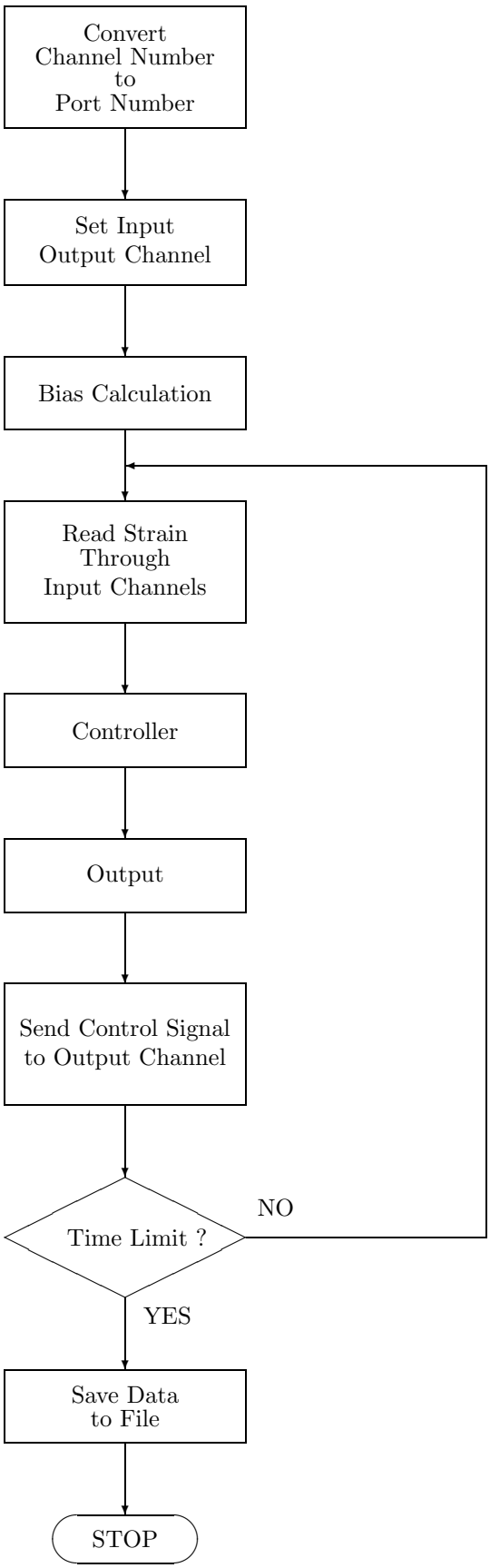

Figure 3.15: C Algorithm for the Controller Implementation for Strain Measurement

3.4.1.1 Experimental Results for Free and Forced Vibrations of the Smart Beam for Strain Measurements

The free vibration and forced vibration analyses were performed for the smart beam. For the free vibration analysis, 5 cm initial tip displacement and zero initial tip velocity were applied to the smart beam and the open-loop and closed-loop time responses were analyzed. For the forced vibration analysis, a sinusoidal chirp signal ($10\,V$ peak-to-peak amplitude and 0.1 $Hz - 60$ Hz frequency range) was applied through a Ling Dynamic Systems *LDS V106* shaker located near the root, next to the piezoelectric materials. The open-loop and closed-loop frequency responses of the smart beam were again analyzed. Figure 3.16 gives the layout of the experimental set-up.

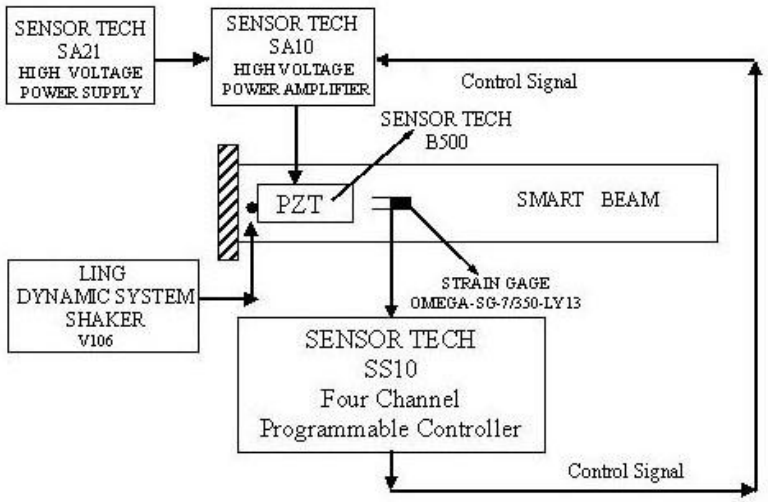

Figure 3.16: Experimental Setup for Controller Implementation of the Smart Beam for Strain Measurement

Experimental Results of the Free Vibration Analysis of the Smart Beam

The open loop and closed loop time responses of the smart beam for free vibration analyses are given in Figure 3.17.

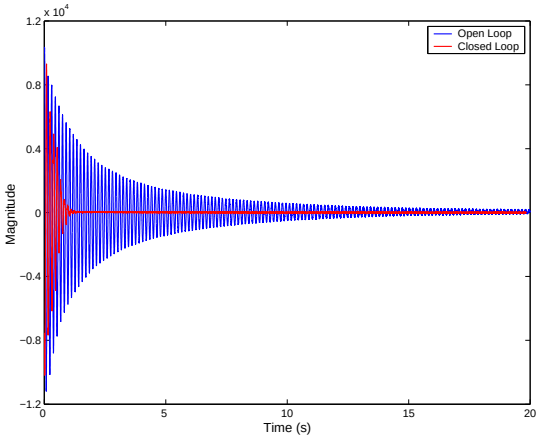

Figure 3.17: Open Loop and Closed Loop Time Responses of the Smart Beam for Strain Measurement

Figure 3.17 shows that while the smart beam continues to vibrate even at 20 *sec* in the open loop case, a significant vibration suppression is achieved in less than 1.3 *sec* for the closed loop case.

Experimental Results of the Forced Vibration Analysis of the Smart Beam

Figure 3.18 gives the comparison of the experimental open loop frequency response together with the closed loop frequency responses obtained from both experiments and Matlab simulation for the forced vibration analyses of the smart beam. The block diagram for the simulations is given in Figure A.3 in Appendix A.

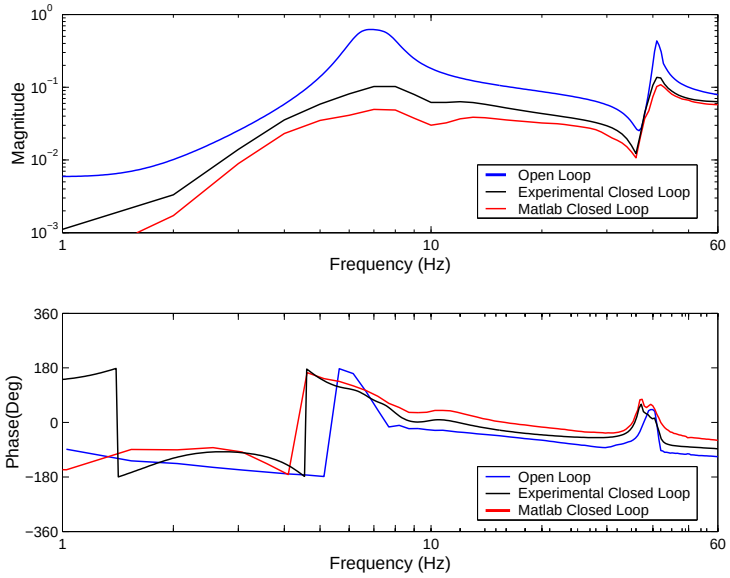

Figure 3.18: Open Loop and Closed Loop Forced Vibration Frequency Responses of the Smart Beam for Strain Measurement

It can be seen from Figure 3.18 that the required vibration suppression at first two natural frequencies is achieved. It was determined that the experimental result produced better vibration suppression than the simulation result. This can be explained by the error in the uncertainty definition, that is the system model showed less error than expected. Table 3.3 gives the achieved attenuation levels for experiment and the simulation.

Table 3.3: Comparison of the Experimentally Obtained and Simulated Attenuation Levels of the Smart Beam Undergoing an Excitation given by Shaker for Strain Measurement

Modes	First	Second
Simulated Attenuation Levels	6.03	3.16
Experimentally Obtained Attenuation Levels	12.02	3.98

3.4.2 Applications Based on Displacement Measurements

In this implementation, Labview v5.0 program was used for the data acquisition, loop generation and control algorithm purposes [44]. For the active vibration control the required controller algorithm was generated by using built-in functions of *Labview v.5.0* as well as the external codes. In the previous section, the algorithm of the C program for the solution of the state space problem was explained. The same C code was modified to be understood by *Labview* and compiled as a dynamic link library that could be linked to *Labview*. The program written in *Labview v.5.0* format is given in Appendix A.

This program consists of three sequence structures, which allows the execution of each layer sequentially. In the first layer (Figure A.5 in Appendix A), the input, output numbers and controller matrices are read from the file and these values are transmitted to the outward of the loop. Second layer allows the measurement of displacement values and conversion of them to digits via analog-to-digital card National Instrument *PCI-MIO-16XE-50*. From displacement measurements, the bias value of the laser displacement sensor is calculated. In the last layer which is the actual control algorithm, the displacement measurement is performed and the control signal is calculated one at a time. The calculated control signal is converted to analog signal by using digital-to-analog card National Instrument *PCI-6713* and sent to high voltage power amplifier via the terminal block. The calculation of the control signal from measured displacement values repeats itself up to time limit of the experiment is reached. The measured

displacement values and applied force are written in a file at the end of the control loop.

The stated multifunction input-output card used for analog-to-digital conversion is *PCI-MIO-16XE-50*. Analog input channel capacity of this card is 16 for single-ended or is 8 for differential connections. The maximum sampling rate is guaranteed to 20 $kSample/s$. Input signal ranges are software selectable and maximum input voltage is defined as 10 V. It allows only two analog output channels with a maximum update rate of 20 $kSample/s$. Also maximum allowable output voltage level is set to 10 V. For digital-to-analog conversion National Instruments *PCI-6713* card is used. The maximum output voltage of this card is set to 10 V. It has a capacity of 1 $MSample/s$ per channel on eight analog outputs. However, this rate depends on the number of channels used.

When this algorithm was tested, it was observed that even the *PCI-MIO-16XE-50* and *PCI-6713* cards have a capacity of 20 $kSample/s$ and 1 $MSample/s$ respectively, in the real time application these values could not be achieved. Higher sampling rates can be achieved by collecting and sending the data with the usage of memory buffer property of the *Labview*. But in the active vibration control, the collected data must be used for the output calculations and result must be converted to the analog form sequentially, in which memory buffer property must be waived. In the case of waiving the memory buffering, sampling rate decreases to approximately 100 $Sample/s$. To increase the sampling rate to higher values, two methods were considered. In the first one, the time spent when calling the built-in functions of *Labview* and the external codes (dynamic link libraries) was decreased by loading them to the memory of the operating system. This type of function calling is called as function calling by reference. This is analogous to passing data by reference (address of the data in memory) in programming languages. The second method is also based on this idea, in which all the variables used in *Labview* program are passed to the dynamic link libraries as reference. With these two approaches, sampling rate increases at most 2048 $Sample/s$.

In the experiments where the layout is given in Figure 3.19, beam flexural tip displacement of the smart beam was measured by a *Laser Displacement Sensor* (*LB 1201(W)LB 300*) measured displacement values were then transferred to a computer via terminal (connector) block of type

SCB86, which was connected to a computer by *SH-6868-EP* type shielded cable. The system response was acquired by the *Labview* program then digitized by the analog to digital card *PCI-MIO-16XE-50*. Once the displacement data became ready for the controller algorithm, the *Labview* program calculated the necessary output for the vibration suppression. The output signal converted to analog signal by *PCI-6713* card and sent to *Sensortech SA10*. The high voltage power amplifier increased the gain of the control signal 30 times then sent to piezoelectric patches.

3.4.2.1 Experimental Results for Free and Forced Vibrations of the Smart Beam for Displacement Measurement

The free vibration and forced vibration analyses were performed for the smart beam. For free vibration analysis, 5 *cm* initial tip displacement and zero initial tip velocity were applied to the smart beam and the open-loop and closed-loop time responses were analyzed. For the forced vibration analysis, a sinusoidal chirp signal (0.1 $Hz - 120$ Hz frequency range) was applied through a *Ling Dynamic Systems LDS V106* shaker located near the root, next to the piezoelectric patches. The chirp signal was generated by signal generator *HP33120A*. Again the open-loop and . Figure 3.19 gives the layo

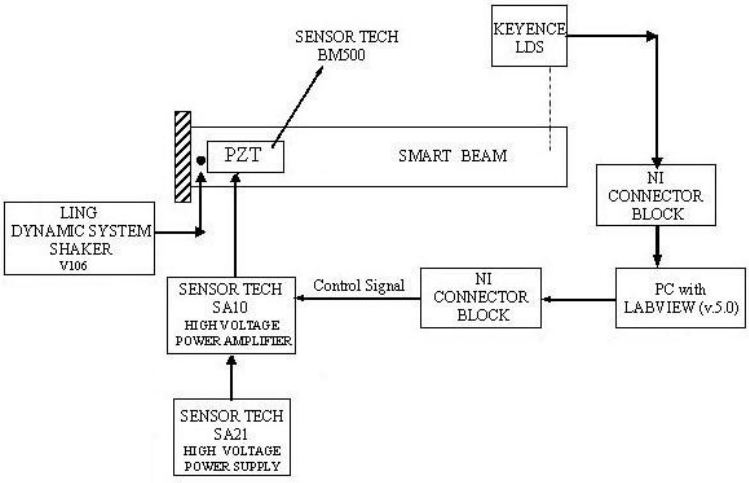

Figure 3.19: Experimental Setup for Controller Implementation of the Smart Beam for Displacement Measurement

Experimental Results of the Free Vibration Analysis of the Smart Beam

The open loop and closed loop time responses of the smart beam for free vibration analyses are given in Figure 3.20.

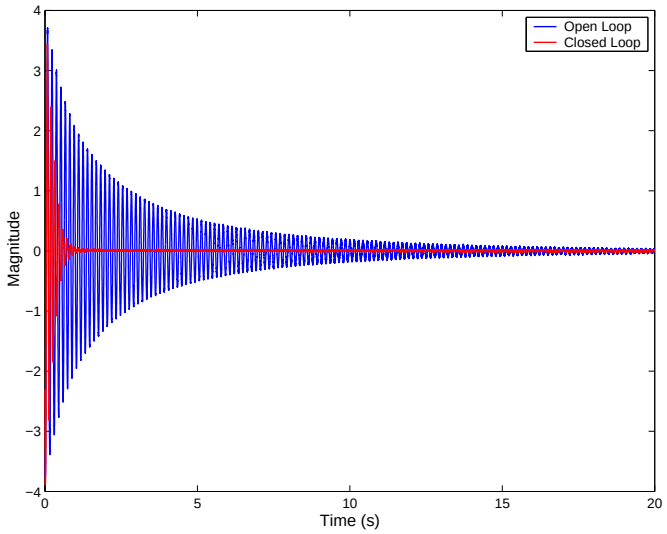

Figure 3.20: Open Loop and Closed Loop Time Responses of the Smart Beam for Displacement Measurement

Figure 3.20 reveals that again a significant vibration suppression is achieved in less than 1.3 seconds.

Experimental Results of the Forced Vibration Analysis of the Smart Beam

Figure 3.21 gives the comparison of the experimental open loop frequency response together with the closed loop frequency responses obtained from both experiments and simulation for the forced vibration analyses of the smart beam. The block diagram for the simulations is given in Figure A.3 in Appendix A.

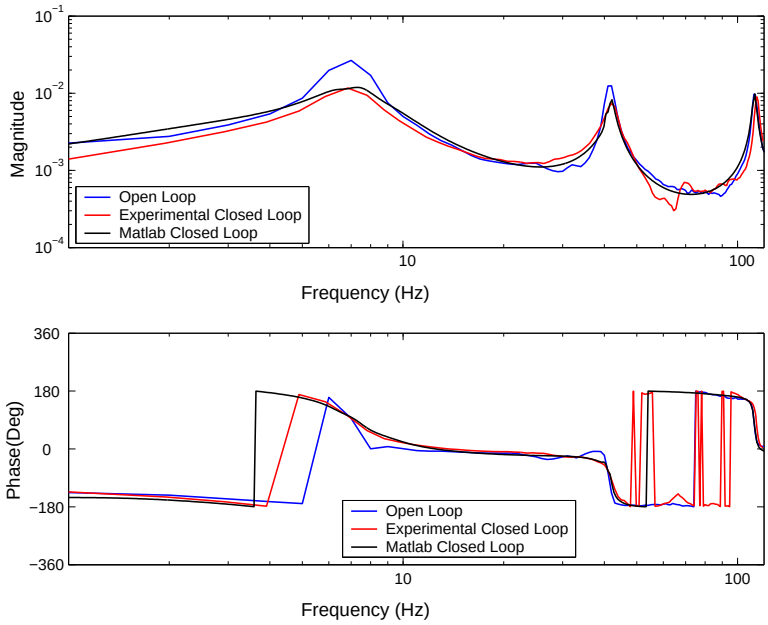

Figure 3.21: Open Loop and Closed Loop Forced Vibration Frequency Responses of the Smart Beam for Displacement Measurement

As it can be seen from Figure 3.21 the required vibration attenuation is satisfactorily obtained at the first two flexural resonances.

Table 3.4 gives the achieved attenuation levels for this application.

Table 3.4: Comparison of the Experimental and Simulated Attenuation Levels of the Smart Beam Undergoing an Excitation given by Shaker for Displacement Measurement

Modes	First	Second	Third
Simulated Attenuation Levels	2.35	2.18	0.99
Experimentally Obtained Attenuation Levels	2.29	1.95	1.08

3.5 Conclusions

This chapter focused on the design and implementation of the H_∞ controllers for vibration suppression of the smart beam based on either strain or displacement measurements.

The suppression of the free and forced vibrations of the smart beam was successfully achieved by the designed H_∞ controllers. The attenuation levels at first two flexural resonances were satisfactory in both applications based on the strain and displacement measurements.

In the implementation of the designed H_∞ controller based on the strain measurement, the attenuation level at first mode was higher than the simulation results. This could be explained

by the lower uncertainty of the actual model then the chosen uncertainty during the controller design. However, it should be noted that although the high uncertainty decreases performance of the controller, it safeguards against the instability of the controller.

CHAPTER 4

THEORETICAL AND EXPERIMENTAL STUDIES OF THE SMART FIN

4.1 Introduction

This chapter deals with the theoretical and the experimental studies conducted on the smart fin. The theoretical studies focused on the determination of the single input single output system models for the smart fin and the design of controllers via μ-synthesis to suppress the vibrations of the smart fin due to its first flexural and first torsional modes. The studies were carried out by considering two different approaches. In the first approach, the system model of the smart fin was derived by considering the piezoelectric actuator voltage as an input and three strain gage measurements as the outputs of the system. For this application, the active vibration control was performed by using a four-channel programmable controller. In the second application, the system model of the smart fin was obtained by considering the piezoelectric actuator voltage as an input and the fin tip flexural displacement as an output. The designed controller of this approach was implemented by using a *LabVIEW v5.0* based program. In the following sections, the derivation of the system models, controller design by synthesis, and implementations are given for both applications.

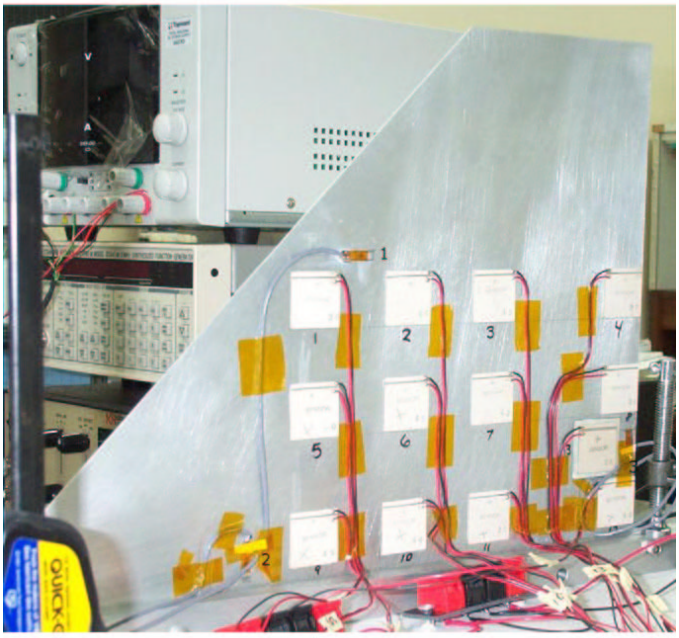

Figure 4.1: Smart Fin Used in the Study

4.1.1 Description of the Smart Fin Model

The smart fin was constructed by symmetrically attaching twenty-four PZT (Lead-Zirconate-Titanate, 25 $mm \times 25\ mm \times 0.5\ mm$, *SensorTech BM500* type) as actuators and six strain gages (*OMEGA-SG-7/350-LY13*) as sensors on a passive aluminum plate-like structure called the fin. In the analysis, the smart fin was considered as being in clamped-free configuration.

The actuators and sensors were placed on determined locations having high strain as a result of the finite element analysis [1]. The structural model of the smart fin is given in Figure A.2 in Appendix A. Although in the structural modelling, PZT's on both side of the smart fin were aimed to be used; during the real time implementations, the piezoelectric actuators of only one side were utilized. This inevitably halved the desired actuation authority.

Figure 4.1 gives the smart fin model used in the study together with the coordinate axes and the sensor locations. The open loop experiments were performed for the determination of the structural characteristics of the smart fin. In Table 4.1, the theoretically determined resonance frequencies together with the experimentally obtained resonance frequencies and the damping coefficients of the smart fin are presented [1].

Table 4.1: Theoretically and Experimentally Obtained Resonance Frequencies and the Experimentally Found Damping Coefficients of the Smart Fin

FEM	Experimental	
$f_n(Hz)$	$f_n(Hz)$	Damping(ζ)
14.96	14.51	$4.8 \cdot 10^{-2}$
45.74	48.94	$2.02 \cdot 10^{-2}$
68.25	69.43	$1.79 \cdot 10^{-3}$

4.2 System Identification of the Smart Fin

The single-input single-output system models of the smart fin were obtained by applying both nonparametric and parametric system identification techniques, which were explained in Chapter 2. The single input single output (*SISO*) models based on each strain and/or displacement measurement were obtained for an excitation given by all the piezoelectric actuators on one side of the smart fin.

4.2.1 System Identification of the Smart Fin Based on Strain Measurements

The general procedure followed for the system identification of the smart beam was repeated for the smart fin. The smart fin was excited by a sinusoidal chirp signal with a frequency range of 0.1 *Hz* to 90 *Hz*, which covers the first three modes of the smart fin. 10 *V* peak-to-peak amplitude chirp signal was generated by the four-channel programmable controller unit, *SensorTech SS10*. First, the amplitude of the chirp signal was amplified 30 times by high voltage power amplifier *SensorTech SA10*, then sent to all the piezoelectric actuators on one side of the smart fin. The response of the smart fin was acquired by using the program written in C via strain gages located at three different locations on the smart fin. One of the strain gages was designated to measure the strain in x-direction, the others were located to measure the strain in y-direction The experimental setup for the system identification process is given in Figure 4.2.

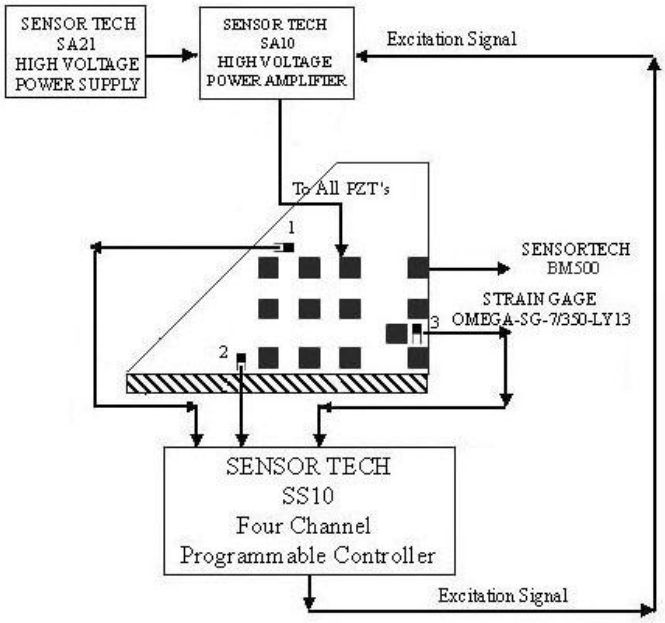

Figure 4.2: Experimental Setup for the System Identification of the Smart Fin for Strain Measurement

In the experiments, the strain gages were connected in half bridge configuration and strain values were amplified before stored in a computer by the internal strain gage preamplifiers of the controller unit, *SensorTech SS10*. The time response of the smart fin measured by strain gages undergoing the sinusoidal chirp signal excitation are given in Figure 4.3 for a duration of 90 seconds.

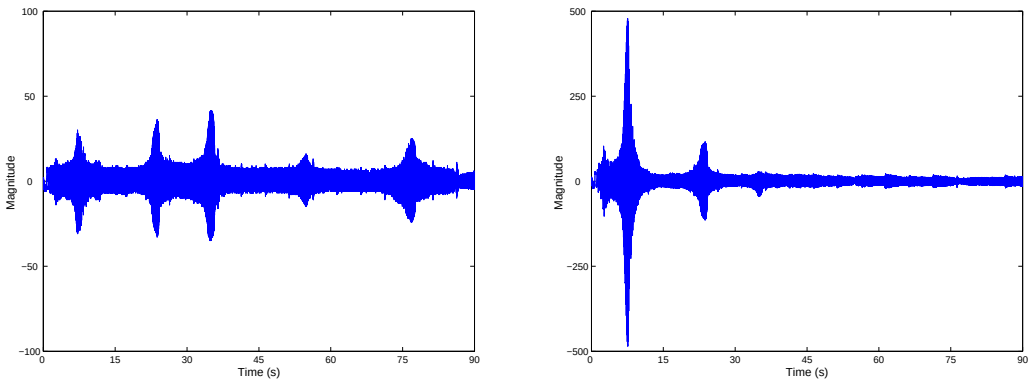

(a) Strain Gage 1

(b) Strain Gage 2

Figure 4.3: Time Response of the Smart Fin for Strain Measurement

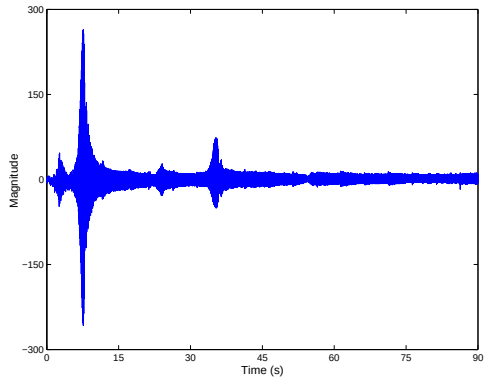

(c) Strain Gage 3

Figure 4.3: Time Response of the Smart Fin for Strain Measurement (Continued)

The spectrum analysis was done to estimate the frequency response of the smart fin from the input output relations. Then the least-square curve fitting method was applied to obtain the approximate representation of the estimated transfer function. The approach was repeated for each strain data to get the single-input single-output transfer functions. The estimated and fitted transfer functions and the error between the estimated and fitted transfer functions for each strain gage measurement were obtained. As a result of these analysis order of the system models was determined.

The system models of order 6, 8, 10, 12 and 20 and the errors between the estimated and fitted transfer functions were obtained for strain gage 1. The 2-norm of the error for the system model of order 6 was 0.0112 and for the system model of order 8 the error was 0.0044. The error level did not change for the higher order system models. For this reason, the 8^{th} order system model for strain gage 1 was chosen to be used in the controller design. Equation 4.1 gives the 8^{th} order system model of the smart fin corresponding to strain gage 1 response.

$$G(s) = \frac{0.0008379s^8 - 1.223s^7 - 909.5s^6 - 3.506 \cdot 10^5 s^5 - 3.276 \cdot 10^8 s^4}{s^8 + 1058s^7 + 6.79 \cdot 10^5 s^6 + 3.146 \cdot 10^8 s^5 + 1.268 \cdot 10^{11} s^4} \\ \frac{-2.962 \cdot 10^{10} s^3 - 2.186 \cdot 10^{13} s^2 - 2.524 \cdot 10^{14} s - 1.842 \cdot 10^{17}}{+2.223 \cdot 10^{13} s^3 + 6.921 \cdot 10^{15} s^2 + 2.168 \cdot 10^{17} s + 4.547 \cdot 10^{19}} \tag{4.1}$$

In the determination of the system model for strain gage 2, again the 2-norm of the error between the estimated and fitted transfer functions and the error graphs were obtained for different order system models. Since, the 2-norm of the error for the 6^{th} order transfer function was 0.025 whereas for the 8^th order transfer function was 0.018, for the strain gage 2 the system model of order 8 was found to be appropriate for the controller design. Moreover, 6^{th} order transfer function had some difficulties at the natural frequencies. In Equation 4.2, the 8^{th} order system model, corresponding to strain gage 2 response, is given.

$$\begin{aligned} G(s) &= \frac{-0.0013s^8 - 1.486s^7 - 932.3s^6 - 2.9 \cdot 10^5 s^5 - 9.715 \cdot 10^7 s^4}{s^8 + 245.7s^7 + 3.089 \cdot 10^5 s^6 + 4.401 \cdot 10^7 s^5 + 2.359 \cdot 10^{10} s^4} \\ & \\ & \frac{-9.957 \cdot 10^9 s^3 - 1.994 \cdot 10^{12} s^2 - 9.388 \cdot 10^{13} s - 2.308 \cdot 10^{16}}{+2 \cdot 10^{12} s^3 + 3.954 \cdot 10^{14} s^2 + 1.412 \cdot 10^{16} s + 1.68 \cdot 10^{18}} \end{aligned} \tag{4.2}$$

The procedure was repeated to determine the order of the system model. The 2-norm of the errors were obtained as 0.045 and 0.032 for the system models of order 8 and 10 respectively. Since the 10^{th} order system model was better in fitting to the estimated transfer function for strain gage 3, 10^{th} order system model was used in the controller design. However, this system model at low frequency region (6 *Hz* to 11 *Hz*) was not quite accurate. This mismatch was accounted as an uncertainty in the controller design. The Equation 4.3 gives the 10^{th} order system model used in the controller design for the response from strain gage 3 only.

$$\begin{aligned} G(s) &= \frac{0.0003386s^{10} - 1.74s^9 + 667.3s^8 - 5.024 \cdot 10^5 s^7 + 1.463 \cdot 10^8 s^6 - 3.503 \cdot 10^{10} s^5}{s^{10} + 417.7s^9 + 3.491 \cdot 10^5 s^8 + 1.238 \cdot 10^8 s^7 + 3.564 \cdot 10^{10} s^6 + 9.066 \cdot 10^{12} s^5} \\ & \\ & \frac{+8.485 \cdot 10^{12} s^4 - 4.544 \cdot 10^{14} s^3 + 8.027 \cdot 10^{16} s^2 - 1.909 \cdot 10^{18} s + 1.317 \cdot 10^{20}}{+1.229 \cdot 10^{15} s^4 + 1.352 \cdot 10^{17} s^3 + 1.353 \cdot 10^{19} s^2 + 5.655 \cdot 10^{20} s + 4.606 \cdot 10^{22}} \end{aligned} \tag{4.3}$$

4.2.2 System Identification of the Smart Fin Based on Displacement Measurements

The smart fin was excited with sinusoidal chirp signal, $(x(t))$, of frequency 0.1 *Hz* to 90 *Hz* which covers the first three modes of the smart fin. The chirp signal of 10 *V* peak-to-peak amplitude was generated by *HP33120A* signal generator and sent to *SensorTech SA10*. The

excitation signal was amplified 30 times by high voltage power amplifier *SensorTech SA10* and then sent to all piezoelectric actuators located on one side of the smart fin. The response of the smart fin was measured by a *Laser Displacement Sensor* (*LB 1201(W)LB 300*) from the tip of the smart fin. The displacement of the fin tip, $(y(t))$ was stored in a computer by using the program written in *Labview v5.0*. The experimental setup for the system identification of the smart fin based on the displacement measurement is given in Figure 4.4. The Labview program written for data acquisition is shown in Appendix A.

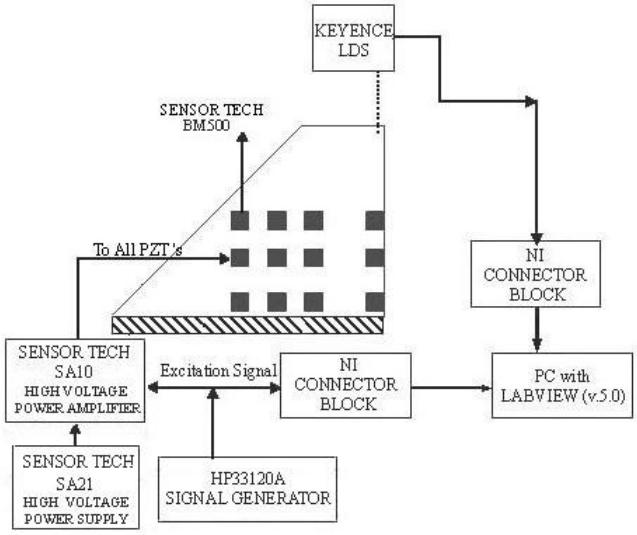

Figure 4.4: Experimental Setup for the System Identification of the Smart Fin for Displacement Measurement

The time response of the smart fin measured by a laser displacement sensor unit undergoing the sinusoidal chirp signal excitation are given in Figure 4.5 for a duration of 90 seconds.

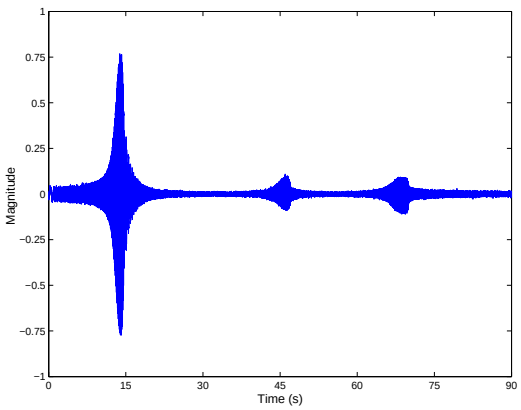

Figure 4.5: Time Response of the Smart Fin for Displacement Measurement

The spectrum analysis was done and the transfer function was estimated from input output relations. Then least square curve fitting method was applied to obtain the approximate representation of the estimated transfer function. The error between the estimated and fitted transfer functions was analyzed for different orders and being a smaller order and having an acceptable error, 6^{th} order system model was chosen to be used in the controller design. Equation 4.4 gives the transfer function of 6^{th} order system model.

$$\begin{aligned} G(s) &= \frac{0.0001179s^6 - 0.02197s^5 + 162.4s^4 - 1302s^3}{s^6 + 46.71s^5 + 2.758 \cdot 10^5 s^4 + 7.644 \cdot 10^6 s^3} \\ &\quad \frac{+2.339 \cdot 10^7 s^2 + 6.697 \cdot 10^7 s + 5.913 \cdot 10^{11}}{+1.748 \cdot 10^{10} s^2 + 1.623 \cdot 10^{11} s + 1.179 \cdot 10^{14}} \end{aligned} \tag{4.4}$$

4.3 Controller Design via μ-Synthesis

This section deals with the design of the controllers via μ-synthesis based on the models obtained in Section 4.2, to suppress the vibration of the smart fin at its first flexural and first torsional modes without exciting the higher order modes.

Unlike the controller design of the smart beam for which H_∞ controllers were designed, μ-synthesis technique given in Section 2.5 was used for the controller design of the smart fin. μ-synthesis method is known to be less conservative than the H_∞ controller design method [36]. And since the smart fin has difficulties in vibration suppression due to actuation limitation, it was desired to use less conservative method to increase performance of the controller.

The block diagram given in Figure 4.6 was used in the controller design of the smart fin. In the controller design of the smart fin, both single-input single-output (*SISO*) and single-input multi-output (*SIMO*) system models were considered and controllers were designed based on these models.

In Figure 4.6, SYS_{fin} block represents the block represents the *SISO* or *SIMO* identified nominal system model. W_{per} is the performance weight formed by augmenting the performance characteristics of each sensor, W_{add} represents the additive uncertainty of each identified model. W_{act} is necessary to define the actuator limitation. W_{noise} represents the signal to noise ratio

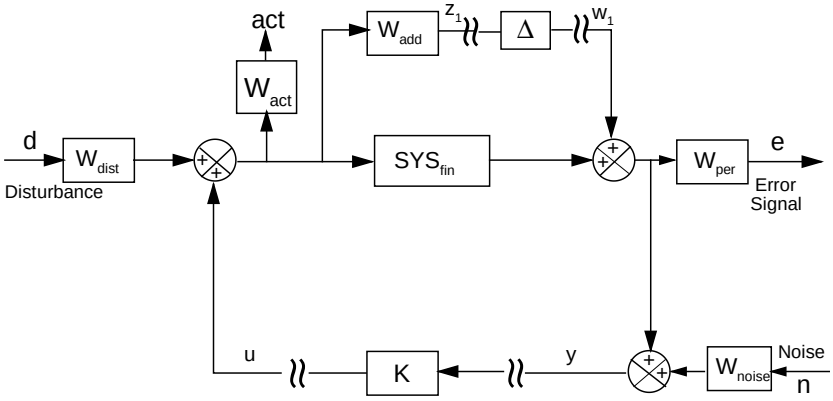

Figure 4.6: Block Diagram Representation of the Controller Design for the Smart Fin

at each sensor measurement, W_{dist} is the disturbance weight.

For the controller design, performance criteria and uncertainty characteristics of the identified models and the actuator limitations were determined. Inserting the values of different weights in the general block diagram, robust controllers were designed. Then μ analyses were performed and open loop and closed loop frequency responses of the smart fin were analyzed. In the frequency response analysis, it was assumed that the smart fin was disturbed from its equilibrium position by the disturbance given from PZT's.

4.3.1 Controller Design Based on Strain Measurements

In this part of the study the design of the controllers, conducted via μ-synthesis for the system models obtained from the strain gage readings is presented. In the controller design, both single-input single-output and single-input multi-output system models were considered.

4.3.1.1 Controller Design for Single-Input Single-Output System Models

In this analysis, the system models obtained from strain gage 2 and strain gage 3 were considered separately for the controller design. The controller design steps were followed starting from the selection of the performance characteristics, uncertainty descriptions of nominal model and actuator limitations. μ-synthesis problem was formulated and solved by *D-K* iteration technique, which was explained in Section 2.5.

Both strain gage 2 and strain gage 3 can primarily sense the flexural vibrations and the controllers based on them perform according to the strain signals sensed by the strain gages. Since both can sense the flexural vibrations, it is expected that both can perform satisfactorily for the first mode. But because of the mode shapes of the smart fin, the strain gage 2 can also sense the vibrations of the second mode whereas the strain gage 3 can not. For this reason, it was thought that the strain gage 2 may be effective in vibration suppression at the second mode when used as the controller input.

Performance and uncertainty weights were selected considering the design goals and the modelling errors of the nominal system model. Figure 4.7 gives the sample selected weights for the controller design where the strain gage 2 was used as controller input. The additive weight was selected to cover the modelling error at the low frequency region and unmodelled dynamics at the high frequency region. In addition to an additive uncertainty, parametric uncertainty was added on top of the nominal system model. Performance weight selection was done to suppress the vibration of the smart fin at its first flexural and first torsional modes.

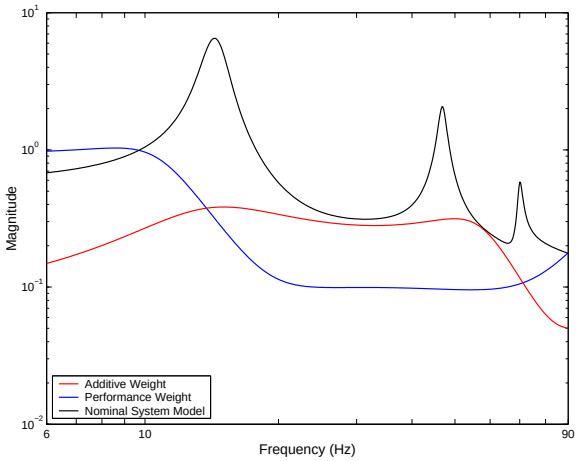

Figure 4.7: Performance and Additive Weights for Smart Fin for Strain Measurement (Controller Input is from Strain Gage 2)

Disturbance weight was selected as unity, W_{noise} was selected as 0.01. Actuator weight was taken as 0.1, which is equal to non-dimensional maximum voltage applied on the piezoelectric actuators.

The controller problem was formed for the smart fin by inserting the defined performance and uncertainty specifications into the corresponding blocks given in Figure 4.6 and following

the controller design steps given in Section 2.5. The controller was designed by using μ-synthesis method and analysis was performed for the closed loop system.

Figure 4.8 gives the calculated structured singular value plots for robust performance, robust stability and nominal performance.

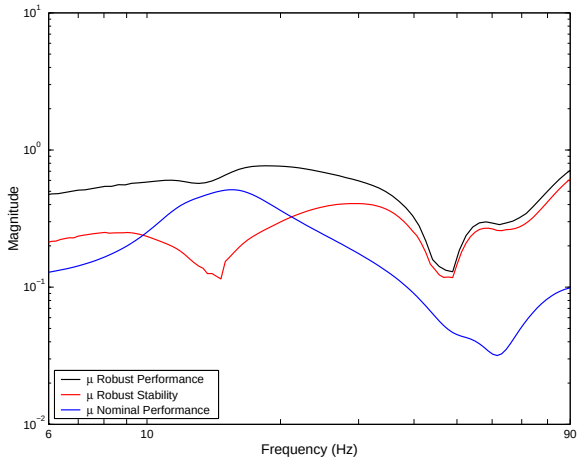

Figure 4.8: μ-Analysis Results for the Smart Fin for Strain Measurement (Controller Input is from Strain Gage 2)

μ-analysis results gave the structured singular values less than unity, thereby indicating that the designed controller was admissible according to μ-analysis. Although the robustness analysis results were satisfactory, the open-loop and closed-loop frequency responses of the smart fin should be checked. The comparison of open loop and closed loop frequency responses was performed for both strain gage 2 and strain gage 3. The closed loop frequency response of the smart fin obtained from strain gage 2 was analyzed to determine the effectiveness of the controller whose input is strain gage 2. However, the response of the system should be also checked at different location other than the controller input sensor location to determine how the response of the whole structure is affected when the controller is integrated to the system. For this reason, the closed loop response analysis was performed for strain gage 3 also. Figure 4.9 gives the comparison of open loop and closed loop responses of the smart fin obtained from both strain gage 2 and strain gage 3. As seen from the figure, the vibration levels at the first two resonance frequencies were attenuated.

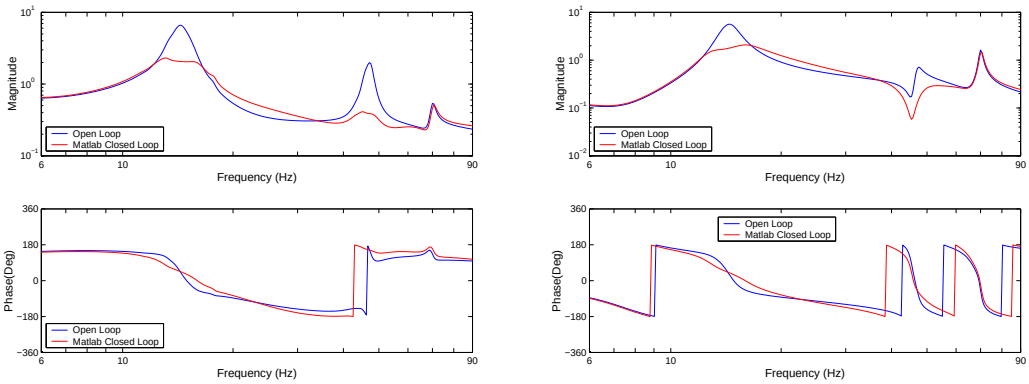

(a) Strain Gage 2

(b) Strain Gage 3

Figure 4.9: Open-Loop and Closed-Loop Frequency Responses of the Smart Fin for Strain Measurement (Controller Input is from Strain Gage 2)

As stated before, the controller was also designed based on the system model obtained from strain gage 3 measurements. From the frequency response plot of the system model, it was observed that the strain gage 3 could sense the vibration at the third natural frequency of the smart fin effectively. Therefore, it was concluded that by using the strain gage 3 measurements, the vibration at the second flexural mode may also be suppressed.

The controller design procedure was also followed for strain gage 3 measurements by referring to the general block diagram given in Figure 4.6. The selected weights were embedded in this block diagram representation, the μ-synthesis problem was formulated and solved by D-K iteration method. Figure 4.10 gives the selected performance and uncertainty descriptions of the system model. In the controller design, in addition to the additive uncertainty at the low and high frequency region, the parametric uncertainties at the natural frequencies and damping ratios were also considered. Disturbance weight was selected as unity, W_{noise} was selected as 0.01. Actuator weight was taken as 0.1.

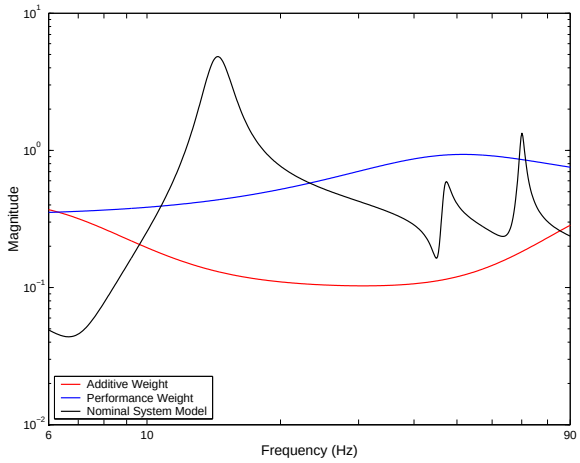

Figure 4.10: Performance and Additive Weights for the Smart Fin for Strain Measurement (Controller Input is from Strain Gage 3)

Figure 4.11 gives the μ bounds for robust performance, robust stability and nominal stability of the designed controller for strain gage 3 measurements.

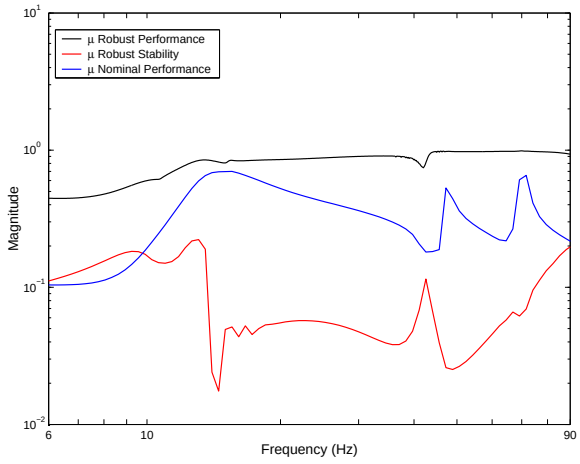

Figure 4.11: μ-Analysis Results for the Smart Fin for Strain Measurement (Controller Input is from Strain Gage 3)

The peak value of μ bound for the robust performance was obtained as less than unity. Moreover, comparison of open loop and closed loop frequency responses was analyzed. Figure 4.12 gives the open loop and closed loop frequency responses of the smart fin.

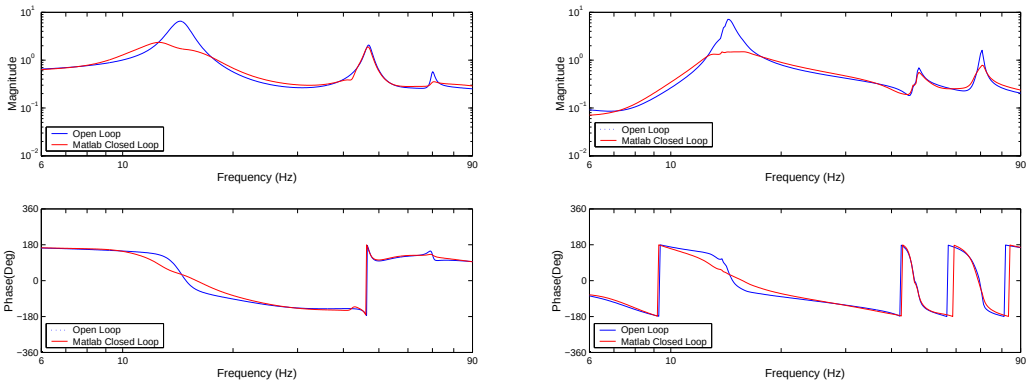

(a) Strain Gage 2

(b) Strain Gage 3

Figure 4.12: Open-Loop and Closed-Loop Frequency Responses of the Smart Fin for Strain Measurement (Controller Input is from Strain Gage 3)

As it can be seen from the open loop and closed loop frequency responses of Figure 4.12, although the controller achieved vibration attenuation at the first two flexural modes (actually first and third modes of the fin), it could not suppress the vibration of the smart fin at the first torsional mode. The reason is that, strain gage 3 could not sense the vibration of the smart fin at the first torsional mode.

Table 4.2 gives the comparisons of the achieved vibration attenuation levels for the two controllers designed for the single-input single-output system models. In the first one, the controller was designed for the system model based on the strain gage 2 measurements (i.e. controller input is the strain read from strain gage 2) and for the second one the controller was designed for the system model based on the strain gage 3 measurements (i.e. controller input is the strain read from strain gage 3).

Table 4.2: Comparison of the Simulated Attenuation Levels of the Smart Fin for Strain Measurement

Modes		First	Second	Third
Controller input is from Strain Gage 2	*Attenuation at SG* 2	3.16	5.22	1.15
	Attenuation at SG 3	3.16	4.60	1.15
Controller input is from Strain Gage 3	*Attenuation at SG* 2	3.73	1.12	1.65
	Attenuation at SG 3	3.76	1.15	1.65

As it can be seen from Table 4.2 that for the first mode, which is predominantly flexural, both controllers performed satisfactorily. Whereas for the second mode which is predominantly

torsional, the controller designed by considering the strain gage 2 as an input had achieved better vibration suppression. These results can be explained on the grounds of the smart fin mode shapes.

In the following section these two system models were combined to form a single-input multi-output system model. The aim in doing that was to achieve possible vibration suppression at all modes within the frequency range of interest for the whole structure.

4.3.1.2 Controller Design for Single-Input Multi-Output System Model (Controller Inputs are Strain Gages 2 and 3)

For the single-input multi-output system model, system identification procedure was repeated for the data obtained from both strain gages 2 and 3. The vibration suppression levels for the *SISO* models at the first three modes were given in Table 4.2. As seen from Table 4.2, the strain gage 2 could effectively suppress the vibration at the first two modes (first flexural and first torsional in order) and strain gage 3 was effective at the first and third modes (first flexural and second flexural in order). Taking this into consideration, it was aimed to use both of them to suppress or at least not to excite the vibration at the third mode. The controller design based on the single-input multi-output system model was designed by applying *D-K* iteration method.

The selected additive and performance weights are given in Figure 4.13.

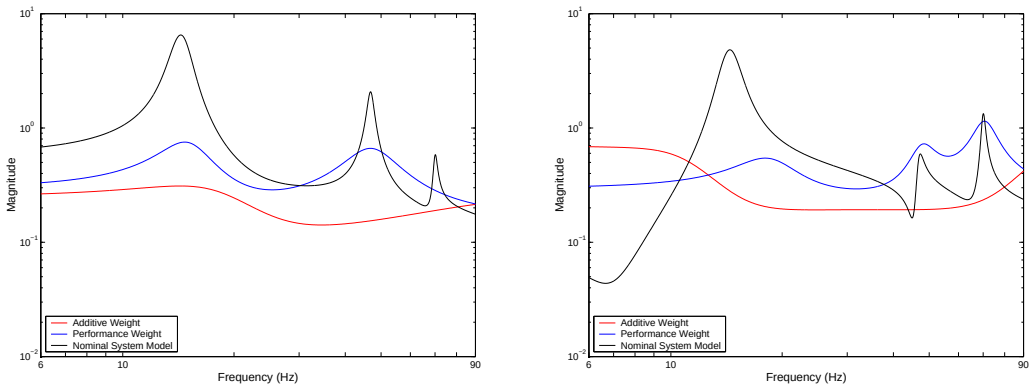

(a) Strain Gage 2

(b) Strain Gage 3

Figure 4.13: Performance and Additive Weights for Smart Fin for Strain Measurement (Controller Inputs are from both Strain Gages 2 and 3)

μ-analysis results are given in Figure 4.14 and comparison of the open loop and closed loop frequency responses are given in Figure 4.15.

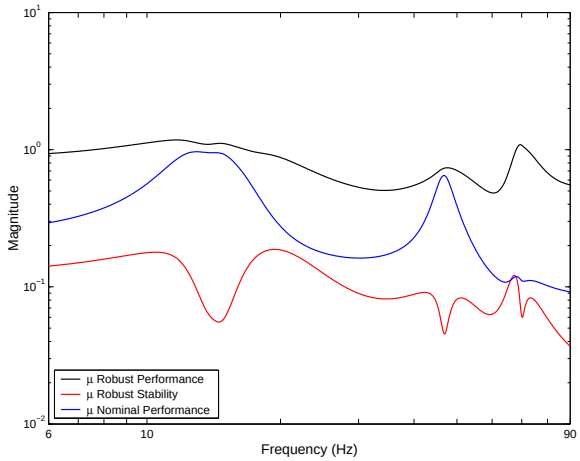

Figure 4.14: μ Analysis Results for the Smart Fin for Strain Measurement (Controller Inputs are from both Strain Gages 2 and 3)

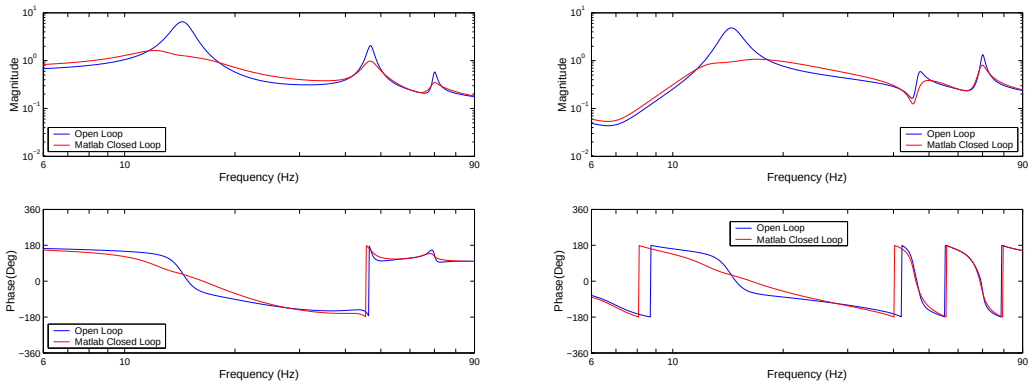

(a) Strain Gage 2

(b) Strain Gage 3

Figure 4.15: Open-Loop and Closed-Loop Frequency Responses of the Smart Fin for Strain Measurement (Controller Inputs are from both Strain Gages 2 and 3)

Table 4.3 gives the simulated attenuation levels of the closed loop system obtained from Matlab v6.5.

Table 4.3: Comparison of the Simulated Attenuation Levels of the Smart Fin for Strain Measurements (Controller Inputs are from both Strain Gages 2 and 3)

Modes	First	Second	Third
Attenuation at SG 2	5.11	2.13	1.66
Attenuation at SG 3	5.11	1.95	1.66

The attenuation level at the first mode was improved for each strain gage when both strain gages were used as controller inputs. Also, vibration attenuation at the third mode is achieved whereas the attenuation level at the second mode diminished approximately 60% compared to the attenuation level obtained when the strain gage 2 was used alone as a controller input.

4.3.2 Controller Design Based on Displacement Measurements

The general feedback controller block diagram given in Figure 4.6 was taken as a reference point to start a controller design for the smart fin using displacement measurement results. In this block diagram, the system model obtained from fin flexural tip displacement measurements as a result of piezoelectric actuation was taken as nominal model. The uncertainty and the performance weights were selected according to the modelling errors in the system identification process and controller objectives respectively.

During least square curve fitting process, 6^{th} order system model had difficulties to model the system at very low frequency region. Thus, it came out that the estimated transfer function had larger amplitude frequency response at very low frequency range than the original transfer function had. This difference introduced to the nominal system an uncertainty as well as the unmodelled high frequency system dynamics. In addition to additive uncertainty, parametric uncertainty was also added to the damping ratios and the natural frequencies in the frequency range of interest. Performance weight was selected such that the controller could suppress the vibration of the smart fin at its first two modes. Disturbance weight was selected as unity and W_{noise} was selected as 0.01 as in the previous cases. Due to the limitation in the actuation voltage, actuator weight was selected as 0.1. In Figure 4.16 the selected weights are presented.

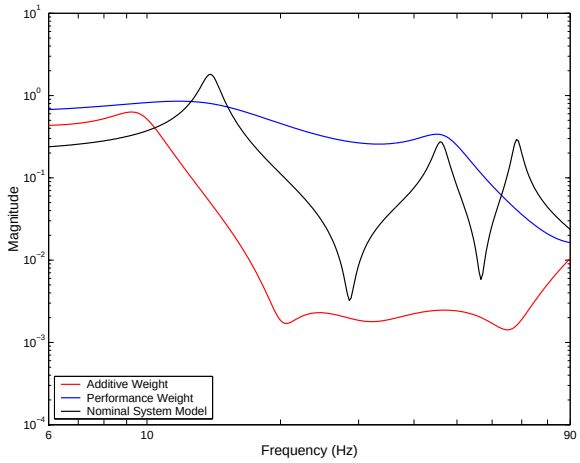

Figure 4.16: Performance and Additive Weights for the Smart Fin for Displacement Measurement (Controller Input is Fin Flexural Tip Displacement)

The controller was designed via μ-synthesis for the smart fin according to defined performance and uncertainty specifications and μ-analysis was done for the closed loop system. Figure 4.17 gives the resulting μ-analysis plots for the closed loop system.

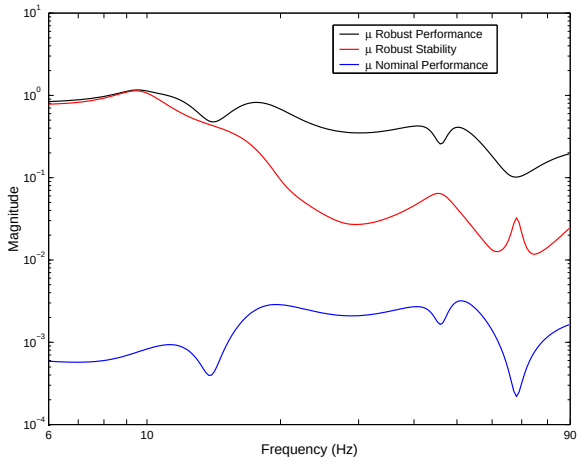

Figure 4.17: μ-Analysis Results for the Smart Fin for Displacement Measurement (Controller Input is Fin Flexural Tip Displacement)

The structured singular values were obtained as being less than unity in the frequency range of interest. Thus μ-analysis assured that the controller can be used in the vibration suppression of the smart fin. Open loop and closed loop frequency responses of the smart fin were also analyzed and the results are presented in Figure 4.18.

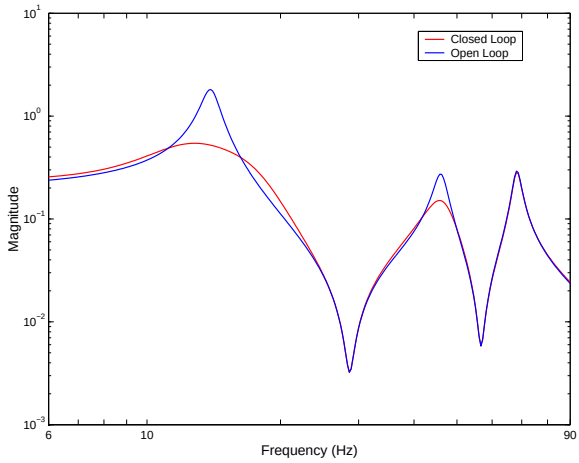

Figure 4.18: Comparison of Open-Loop and Closed-Loop Frequency Responses of the Smart Fin for Displacement Measurement (Controller Input is Tip Displacement)

As seen from the frequency response analysis graph, the vibrations of the smart fin at its first two modes were suppressed. Table 4.4 gives the attenuation levels for the closed loop system.

Table 4.4: Comparison of the Simulated Attenuation Levels of the Smart Fin for Displacement Measurement (Controller Input is Fin Flexural Tip Displacement)

Modes	First	Second	Third
Attenuation Level	3.48	1.81	1.03

4.4 Controller Implementation

The preceding sections dealt with the controller design via μ-synthesis to suppress the vibration of the smart fin. The computer based simulations were performed by using Matlab v.6.5 and it was observed that the controllers could achieve satisfactory performances. However, the real-time implementations should also be performed for all of the designed controllers.

For the controller implementation, two different experimental setups were used. They are given in Figure 4.19 and Figure 4.29. Both open-loop and closed loop experiments were performed for the smart fin.

4.4.1 Applications Based on Strain Measurements

In the real time implementation of the controllers, which were designed based on strain measurements, *SensorTech SS10* four-channel programmable controller unit was used. The same C algorithm given in Figure 3.15 was also utilized. The program first acquired the response of the smart fin via the strain gage(s) and then calculated the necessary output for the vibration suppression. The calculated control signal is then sent to *SensorTech SA10* to be amplified by 30 times before being sent to the piezoelectric patches.

4.4.1.1 Experimental Results for Free and Forced Vibrations of the Smart Fin for Strain Measurements

The free vibration and forced vibration analyses were performed for the smart fin. For the free vibration analysis, an initial tip displacement of approximately 3 cm and zero tip velocity was applied to the smart fin. The open loop and closed loop characteristics of the system were recorded. For the forced vibration analysis, the smart fin was excited by Ling Dynamic System shakers placed near its clamped edge. The sinusoidal chirp signal of frequency $0.1\ Hz - 90\ Hz$ was generated by *SensorTech SS10* and sent to one of the shakers. The block diagram of the simulated closed loop for the smart fin is given in Figure A.3 in Appendix A. It should be noted that both shakers can excite the flexural vibration of the smart fin. However, since the location of the shaker denoted as SL1 was approximately on the nodal line of the second mode, the second mode could not be excited as much as the first mode. The open-loop and closed-loop frequency responses of the smart fin were analyzed. Figure 4.19 gives the layout of the experimental set-up.

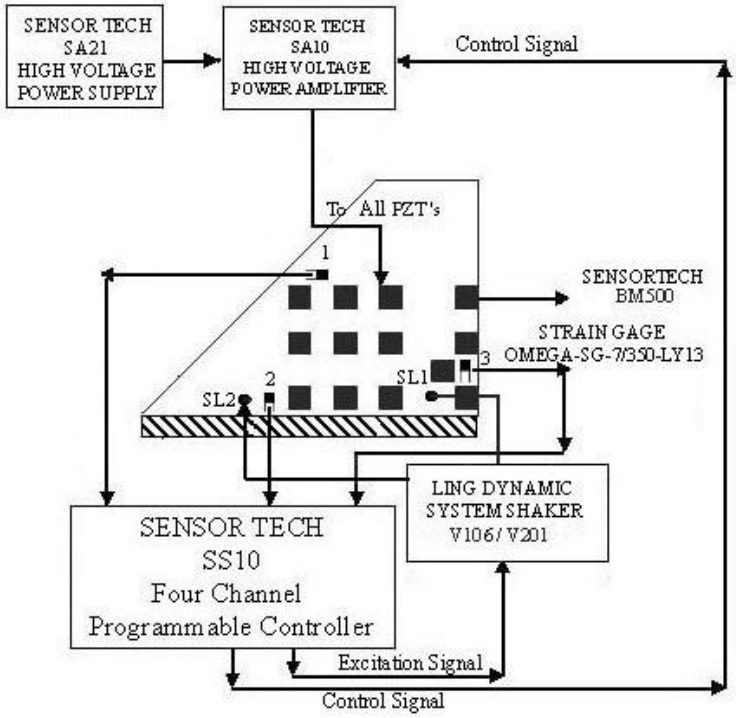

Figure 4.19: Experimental Setup for Controller Implementation of the Smart Fin for Strain Measurement

Free Vibration Experiments of the Smart Fin (Controller Input is from Strain Gage 2)

The open loop and closed loop time responses of the smart fin measured by strain gage 2 and 3 are given in Figure 4.20.

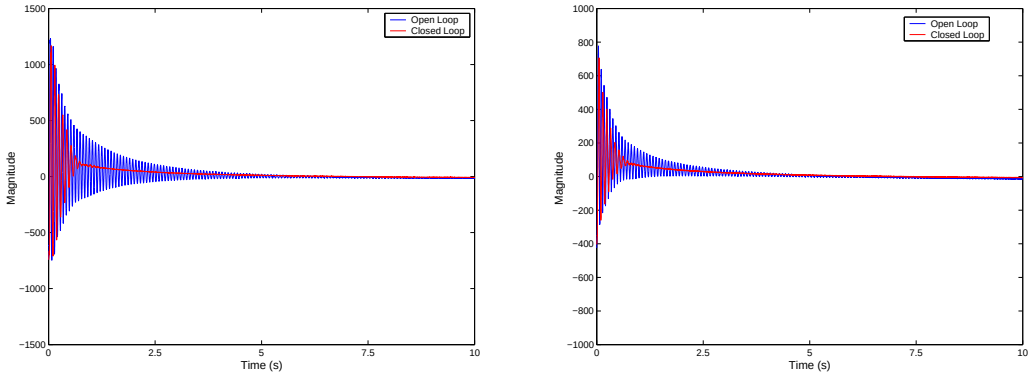

(a) Strain Gage 2

(b) Strain Gage 3

Figure 4.20: Open Loop and Closed Loop Time Responses of the Smart Fin for Strain Measurement (Controller Input is from Strain Gage 2)

As seen from the figure, the vibration suppression was achieved for the smart fin within a second in closed loop case.

Forced Vibration Experiments of the Smart Fin (Controller Input is from Strain Gage 2)

In Figure 4.21 and Figure 4.22 the comparison of the experimental open loop frequency response, closed loop frequency responses obtained from both experiments and simulation results are given. In the first analysis, the smart fin was excited by the shaker which is denoted as SL1 in Figure 4.19. In the second analysis, the smart fin was excited by the shaker which is denoted as SL2. Although, the strain gage 2 was used as the controller input, strain gage 3 measurements were also considered to observe the effectiveness of the controller throughout the structure.

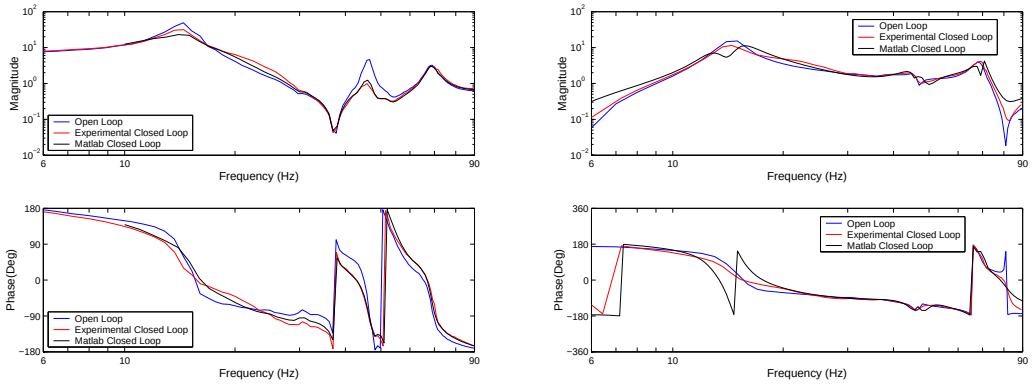

(a) Strain Gage 2

(b) Strain Gage 3

Figure 4.21: Open Loop and Closed Loop Forced Vibration Frequency Responses of the Smart Fin for Strain Measurement (Controller Input is from Strain Gage 2, Excited by Shaker SL1)

The open loop and closed loop frequency responses of the smart fin obtained from strain gage 2 measurements shows that the vibration was suppressed at first two resonance frequencies. However, the measurements obtained from strain gage number 3 indicate that the vibration attenuation could not be achieved successfully at the second mode. This means that the vibration could not be suppressed through the whole structure. In Table 4.5 the obtained attenuation levels at the defined modes are presented.

Table 4.5: Comparison of the Simulated and Experimental Attenuation Levels of the Smart Fin an Excitation given by Shaker (SL1) for Strain Measurement (Controller Input is from Strain Gage 2)

Modes		First	Second	Third
Simulated Attenuation Levels	*Attenuation at SG* 2	2.43	3.52	1.29
	Attenuation at SG 3	2.17	0.76	1.10
Experimentally Obtained Attenuation Levels	*Attenuation at SG* 2	1.55	5.76	1.05
	Attenuation at SG 3	1.55	1.00	0.98

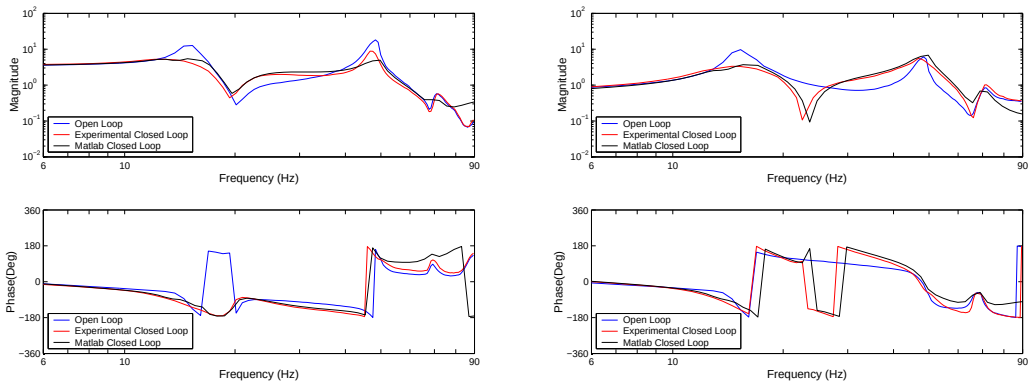

(a) Strain Gage 2

(b) Strain Gage 3

Figure 4.22: Open Loop and Closed Loop Forced Vibration Frequency Responses of the Smart Fin for Strain Measurement (Controller Input is from Strain Gage 2, Excited by Shaker SL2)

As stated before the excitation at the torsional mode of the smart fin given by the shaker, which was located at SL2, was comparable with excitation at the first flexural mode of the smart fin. However, since the excitation capacity of this shaker (*LDS V106*) was less than that of the shaker (*LDS V201*) located at SL1, it could not excite the first mode of the smart fin as much as the shaker located at SL1. Therefore the available PZT actuation authority was apparently sufficient to suppress the vibration at the first mode at this level of excitation.

When the open loop and closed loop frequency responses were compared for the strain gage 3 measurements (Figure 4.22(b)), it was observed that the closed loop frequency response was quite discrepant than that of open loop. It seems that while trying to suppress the torsional vibration, the controller altered the system characteristics. This can be considered as another disadvantage of using a single sensor as a controller input.

Table 4.6 gives the simulated and experimentally obtained attenuation levels of the smart fin.

Table 4.6: Comparison of the Simulated and Experimental Attenuation Levels of the Smart Fin Undergoing an Excitation given by Shaker (SL2) for Strain Measurement (Controller Input is from Strain Gage 2)

Modes		First	Second	Third
Simulated Attenuation Levels	*Attenuation at SG* 2	2.33	3.67	1.51
	Attenuation at SG 3	2.77	0.93	1.28
Experimentally Obtained Attenuation Levels	*Attenuation at SG* 2	3.18	2.44	1.03
	Attenuation at SG 3	2.95	1.23	0.83

Free Vibration Experiments of the Smart Fin (Controller Input is from Strain Gage 3)

The open loop and closed loop time responses of the smart fin measured by strain gage 2 and 3 are given in Figure 4.23.

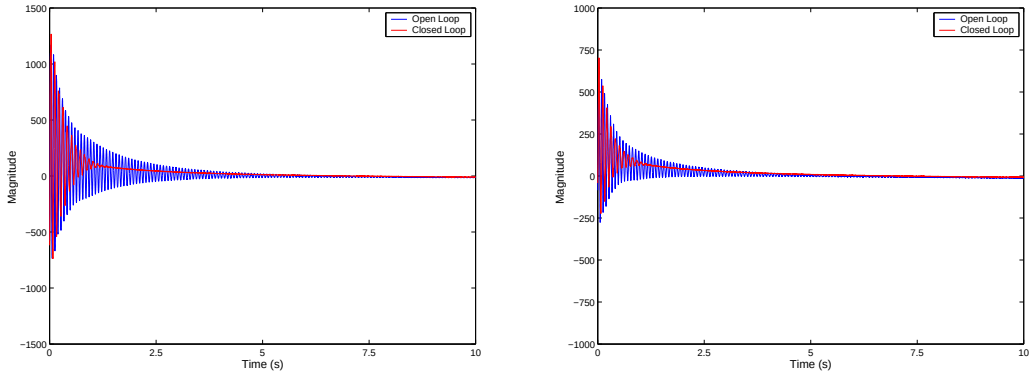

(a) Strain Gage 2

(b) Strain Gage 3

Figure 4.23: Open Loop and Closed Loop Time Responses of the Smart Fin for Strain Measurement (Controller Input is from Strain Gage 3)

As seen from the figure, the vibration suppression was achieved for the smart fin within a second in closed loop case.

Forced Vibration Experiments of the Smart Fin (Controller Input is from Strain Gage 3)

Figure 4.24 and Figure 4.25 give the comparison of the experimental open loop frequency response, closed loop frequency responses obtained from both experiments and simulation results.

The first figure corresponds to the response of the smart fin undergoing a shaker excitation. The shaker used in the experiments is denoted as SL1 in Figure 4.19. The second figure gives the response of the smart fin excited by the shaker which is denoted as SL2. In this analysis, controller input was the measurements from strain gage 3. In addition to strain gage 3, strain gage 2 measurements were also analyzed to observe the effect of the controller actuation to the whole structure.

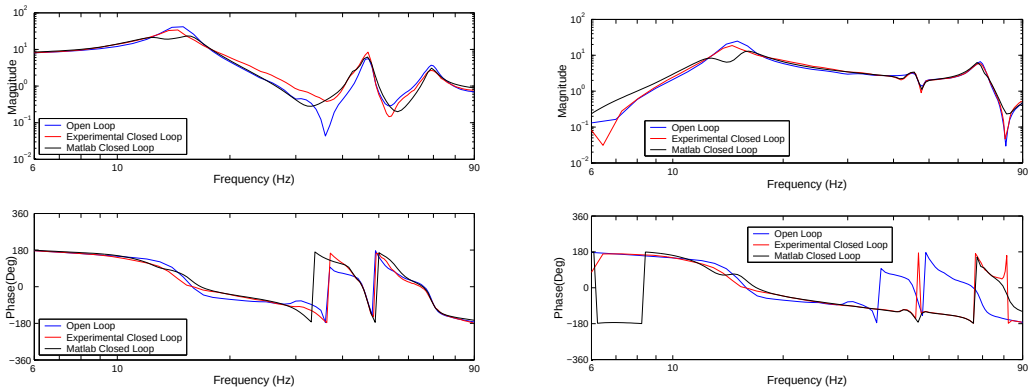

(a) Strain Gage 2

(b) Strain Gage 3

Figure 4.24: Open Loop and Closed Loop Forced Vibration Frequency Responses of the Smart Fin for Strain Measurement (Controller Input is from Strain Gage 3, Excited by Shaker SL1)

Although the aim was to suppress the vibration at the first flexural and first torsional modes (first two modes), the vibration attenuation was achieved only at first two flexural modes (first and third modes). The result was expected since strain gage 3 could not sense the vibration of the smart fin at the second mode.

The comparison of the experimentally obtained and simulated attenuation levels of the smart fin is presented in Table 4.7.

Table 4.7: Comparison of the Simulated and Experimentally Attenuation Levels of the Smart Fin an Excitation given by Shaker (SL1) for Strain Measurement (Controller Input is from Strain Gage 3)

Modes		First	Second	Third
Simulated Attenuation Levels	*Attenuation at SG 2*	1.98	0.90	1.20
	Attenuation at SG 2	2.76	0.92	1.06
Experimentally Obtained Attenuation Levels	*Attenuation at SG 2*	1.40	0.66	1.40
	Attenuation at SG 2	1.33	0.96	1.13

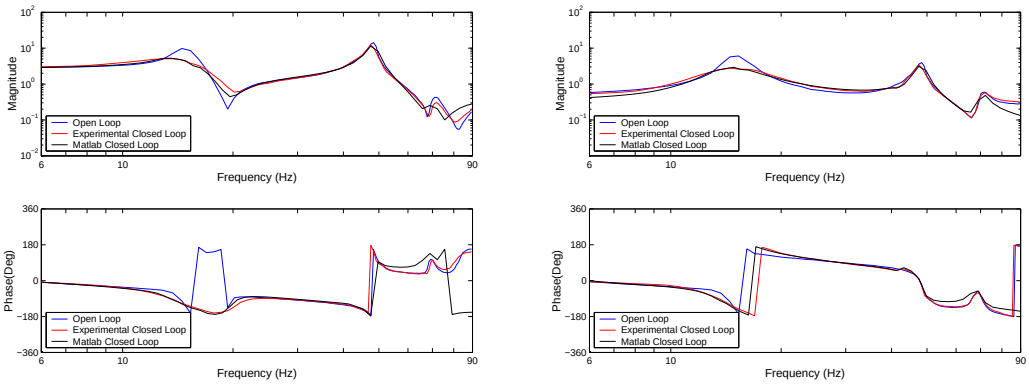

(a) Strain Gage 2

(b) Strain Gage 3

Figure 4.25: Open Loop and Closed Loop Forced Vibration Frequency Responses of the Smart Fin for Strain Measurement (Controller Input is from Strain Gage 3, Excited by Shaker SL2)

When the experimentally obtained attenuation levels for the controller whose input was strain gage 2 measurements were compared to those of the controller whose input was strain gage 3, it was observed that the latter controller achieved lower attenuation levels. However, it did not change the system characteristics unlike the other controller.

The comparison of the experimentally obtained and simulated attenuation levels of the smart fin is presented in Table 4.8.

Table 4.8: Comparison of the Simulated and Experimental Obtained Attenuation Levels of the Smart Fin an Excitation given by Shaker (SL2) for Strain Measurement (Controller Input is from Strain Gage 3)

Modes		First	Second	Third
Simulated Attenuation Levels	*Attenuation at SG* 2	2.09	1.46	1.85
	Attenuation at SG 2	2.05	1.28	1.23
Experimentally Obtained Attenuation Levels	*Attenuation at SG* 2	2.08	1.40	1.40
	Attenuation at SG 2	2.06	1.40	1.05

Free Vibration Experiments of the Smart Fin (Controller Inputs are from both Strain Gages 2 and 3)

In the preceding sections, the controllers were designed based on the *SISO* model. It was concluded that a single controller input was not enough to estimate the vibration of the overall structure. Thus the controller could not provide the necessary control signal for the vibration suppression. For this reason, *SIMO* model was thought to be more convenient and was used to

design the controller presented in this section. The open loop and closed loop time responses of the smart fin measured by strain gages 2 and 3 are given in Figure 4.26.

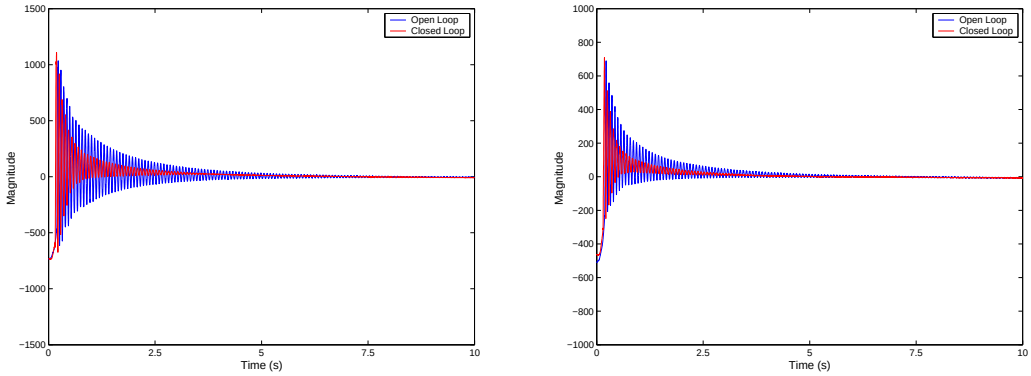

(a) Strain Gage 2

(b) Strain Gage 3

Figure 4.26: Open Loop and Closed Loop Time Responses of the Smart Fin for Strain Measurement (Controller Inputs are from both Strain Gages 2 and 3)

It was obvious from the comparison of open loop and closed loop time responses plot that the free vibration of the smart fin was suppressed less than a second when the control signal was applied on the system.

Forced Vibration Experiments of the Smart Fin (Controller Inputs are from both Strain Gages 2 and 3)

The disadvantages of the controller based on the *SISO* model were mentioned previously. The implementation of a controller based on the *SIMO* model to suppress the free vibration did not give enough information about its effectiveness. Therefore forced vibration suppression analysis was also performed. Figures 4.27 and 4.28 give the comparison of the experimental open loop frequency response and the closed loop frequency responses obtained from both experiments and simulation results. In the first analysis, the smart fin was excited only by the shaker shown as SL1 in Figure 4.19, and in the second analysis, the smart fin was excited by the shaker shown as SL2 in the same figure.

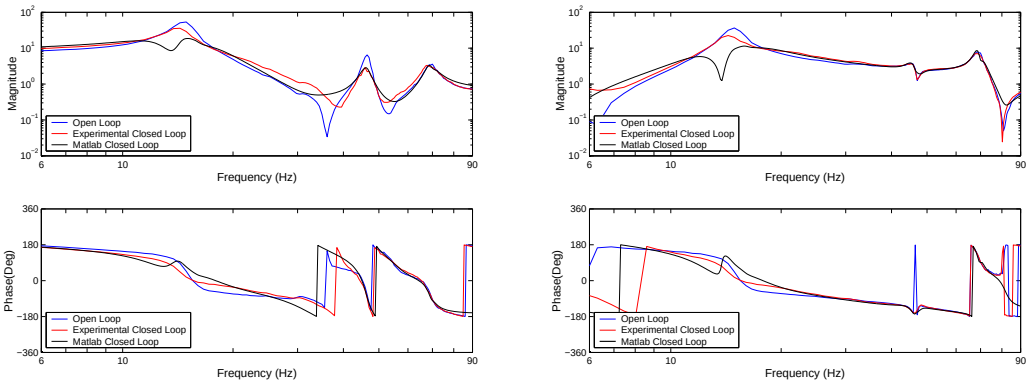

(a) Strain Gage 2

(b) Strain Gage 3

Figure 4.27: Open Loop and Closed Loop Forced Vibration Frequency Responses of the Smart Fin for Strain Measurement (Controller Inputs are from both Strain Gages 2 and 3, Excited by Shaker SL1)

Table 4.9 shows the simulated and experimentally obtained attenuation levels at three modes of the smart fin which was continuously excited by a single shaker.

Table 4.9: Comparison of the Simulated and Experimental Attenuation Levels of the Smart Fin an Excitation given by Shaker (SL1) for Strain Measurement (Controller Inputs are from both Strain Gages 2 and 3)

Modes		First	Second	Third
Simulated Attenuation Levels	*Attenuation at SG* 2	2.04	1.42	1.13
	Attenuation at SG 2	2.66	0.89	0.70
Experimentally Obtained Attenuation Levels	*Attenuation at SG* 2	2.76	1.99	1.39
	Attenuation at SG 2	2.72	1.02	1.26

When the ratio of the peak value of open loop frequency response to that of closed loop frequency response was compared for each strain gage with the *SISO* cases explained previously (Table 4.5 and Table 4.7), the vibration attenuation at the first mode was improved. However, at the second mode, the attenuation level degraded approximately 65% at the strain gage 2 location when compared with the result of the controller whose controller input was the strain gage 2.

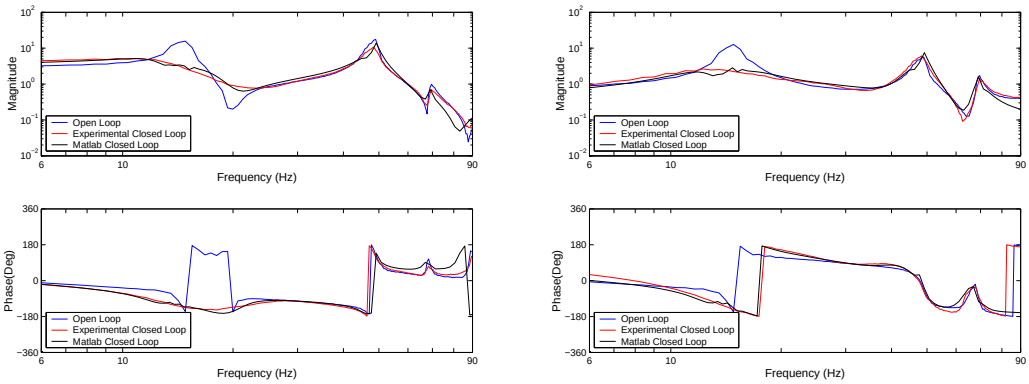

(a) Strain Gage 2

(b) Strain Gage 3

Figure 4.28: Open Loop and Closed Loop Forced Vibration Frequency Responses of the Smart Fin for Strain Measurement (Controller Inputs are from both Strain Gages 2 and 3, Excited by Shaker SL2)

Table 4.10 gives the simulated and experimentally obtained attenuation levels of the smart fin.

Table 4.10: Comparison of the Simulated and Experimental Attenuation Levels of the Smart Fin an Excitation given by Shaker (SL2) for Strain Measurement (Controller Inputs are from both Strain Gages 2 and 3)

Modes		First	Second	Third
Simulated Attenuation Levels	*Attenuation at SG* 2	4.90	1.27	1.42
	Attenuation at SG 2	4.47	0.80	1.02
Experimentally Obtained Attenuation Levels	*Attenuation at SG* 2	5.86	1.97	1.41
	Attenuation at SG 2	5.66	1.13	1.19

The experimental results in Table 4.10 clearly indicate the enhancement of the vibration attenuation at the first mode. However, a high attenuation level at the second mode could not be achieved.

The aim of using two strain gages as controller inputs was to improve the vibration suppression within a frequency range of interest. However, with the available structural configuration the torsional vibration could not be suppressed. Structural modelling is left to be improved in the future works.

4.4.2 Applications Based on Displacement Measurements

In the implementation of the designed controller, *Labview v5.0* program was used for the data acquisition, loop generation and control algorithm purposes. The schematic representation of the program is given in Figure A.5 of Appendix A. The effectiveness of controller was analyzed for both free vibration and forced vibration of the smart fin.

In the experiments, the disturbance was given to the smart fin as being either initial tip displacement or continuous shaker excitation. The response of the smart fin was sensed by laser displacement sensor head *LB300* and converted to a voltage value by *LB 1201(W)* unit. Passing through connector block (*SCB68*), the output voltage values were acquired by analog-to-digital card of *PCI-MIO-16XE-50*. The digitized response of the smart fin was used in the controller algorithm to calculate the control signal for the attenuation of the vibration. The resulting control signal converted to analog signal by *PCI-6713* digital-to-analog card and sent to high voltage power amplifier (*SensorTech SA10*) to be amplified. Then the amplified signal given to piezoelectric actuators. In the forced vibration experiments, disturbance signal was generated by signal generator *HP33120A*, and sent to amplifier *PA25E*. The amplified voltage was given to Ling Dynamic System *LDS V106* and *V201* shakers. For this application, in addition to the response of the smart fin, the excitation signal was also stored in a computer by using analog-to-digital card of *PCI-MIO-16XE-50* and the connector block (*SCB68*).

4.4.2.1 Experimental Results for Free and Forced Vibrations of the Smart Fin for Displacement Application

The free vibration and forced vibration analyses were performed for the smart fin. For free vibration analysis, approximately $3cm$ tip displacement was given to smart fin. The open-loop and closed-loop time responses of the smart fin were analyzed. For the forced vibration analysis, a sinusoidal chirp signal ($0.1\ Hz - 90\ Hz$ frequency range) was applied through a Ling Dynamic Systems *LDS V106* and *V201* shakers located next to clamped edge. The chirp signal was generated by signal generator *HP33120A*. Again the open-loop and closed-loop frequency responses of the smart fin were analyzed.

Figure 4.29 gives the layout of the experimental set-up.

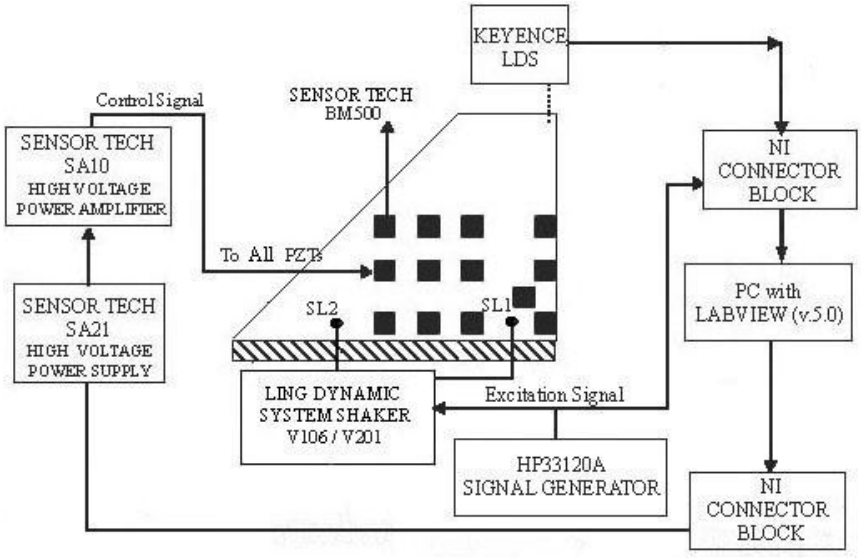

Figure 4.29: Experimental Setup for Controller Implementation of the Smart Fin for Displacement Measurement

Free Vibration Experiments of the Smart Fin (Controller Input is from Fin Flexural Tip Displacement)

The resulting open loop and closed loop time responses of the smart fin for a period of 10 *sec.* are given in Figure 4.30.

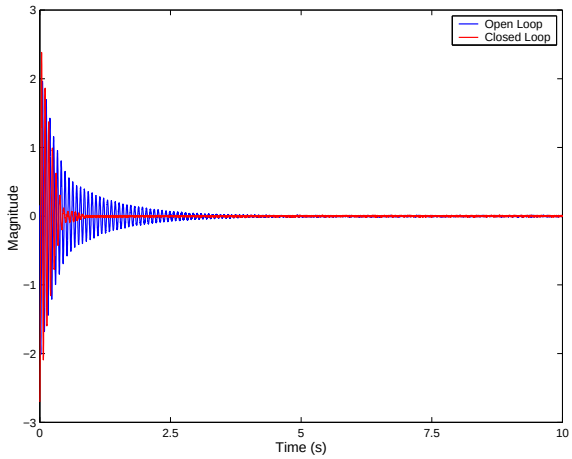

Figure 4.30: Open Loop and Closed Loop Time Responses of the Smart Fin for Displacement Measurement (Controller Input is Fin Flexural Tip Displacement)

As seen from Figure 4.30, the vibration attenuation due to tip displacement was achieved in less than 1 *second*.

Forced Vibration Experiments of the Smart Fin (Controller Input is from Fin Flexural Tip Displacement)

The resulting experimental and simulated closed loop and experimental open loop frequency responses of the smart fin are presented in Figure 4.31.

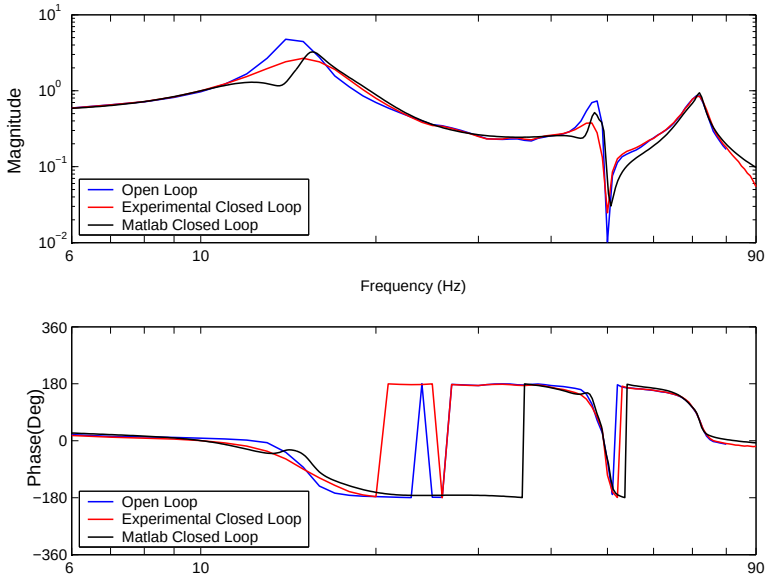

Figure 4.31: Open Loop and Closed Loop Forced Vibration Frequency Responses of the Smart Fin for Displacement Measurement (Controller Input is Fin Flexural Tip Displacement, Excited by Shaker SL1)

As seen from the Figure 4.31, expected attenuation levels at the first two resonance frequencies were achieved. Table 4.11 gives the comparison of the experimental attenuation levels and simulated attenuation levels.

Table 4.11: Comparison of the Simulated and Experimental Attenuation Levels of the Smart Fin an Excitation given by Shaker (SL1) for Displacement Measurement (Controller Input is from Fin Flexural Tip Displacement)

Modes	First	Second	Third
Simulated Attenuation Levels	2.75	1.42	0.91
Experimentally Obtained Attenuation Levels	1.78	1.95	1.00

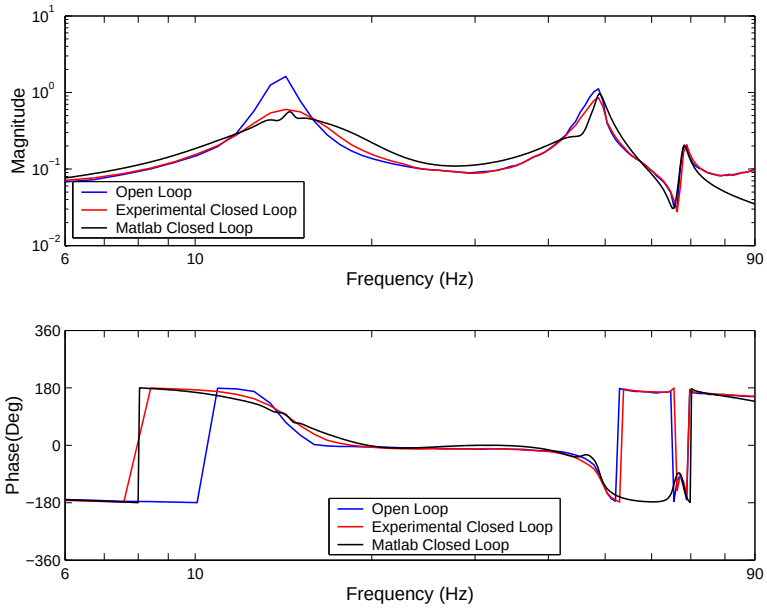

Figure 4.32: Open Loop and Closed Loop Forced Vibration Frequency Responses of the Smart Fin for Displacement Measurement (Controller Input is from Fin Flexural Tip Displacement, Excited by Shaker SL2)

As seen from the Figure 4.32, the vibration of the smart fin at the first mode was suppressed. However, as in the previously designed controllers the attenuation levels at the second resonance frequency was not satisfactory. Table 4.12 gives the comparison of the experimentally obtained attenuation levels and simulated attenuation levels.

Table 4.12: Comparison of the Simulated and Experimental Attenuation Levels of the Smart Fin an Excitation given by Shaker (SL2) for Displacement Measurement (Controller Input is Fin Flexural Tip Displacement)

Modes	First	Second	Third
Simulated Attenuation Levels	2.90	1.16	0.96
Experimentally Obtained Attenuation Levels	2.69	1.31	0.95

4.5 Conclusions

In this chapter, the controllers were designed to suppress both free and sinusoidally forced vibrations of a smart fin via μ-synthesis method and the designed controllers were implemented. Two different experiments were conducted where the first one used strain gages as sensor and the second one utilized a laser displacement sensor. For both applications, the PZTs were used as actuators to suppress the vibration levels.

The controller implementations showed that the piezoelectric actuator authority was not enough to suppress the vibrations of the smart fin. That was due to the fact that, the PZTs of only one face were effectively utilized because of experimental limitations. So half of the actuator authority was not enough to obtain a high level of attenuation if a high level of shaker excitation is given to the smart fin (Table 4.5, 4.7, 4.9, 4.11). However, if the smart fin was given a low level of shaker excitation, the obtained attenuation levels became more satisfactory (Table 4.6, 4.8, 4.10, 4.12).

In the analysis, controllers were designed based on *SISO* and *SIMO* models. But, for both cases, only one control signal was given to all the PZT's on one side of the smart fin. This was advantageous for the vibration suppression of the smart fin at its first mode since all of the PZT's were excited with the same control signal. However, for the vibration suppression of the torsional mode, giving the same control signal to all of the PZT's was not very effective. Therefore, it was thought that the PZT's can be separated in to two groups and one of them may be used for the flexural vibration suppression the other may be used for the torsional vibration suppression. However, since the actuation authority was not enough this case was left to be analyzed as a future work.

It was shown that the usage of one sensor as a controller input was not appropriate for the two dimensional structures. Although, the designed controller could suppress the vibration at the controller input sensor location, since because not having enough information for the whole structure, the controller may cause an excitation at the other parts of the structure. It is believed that a multi-input multi-output system model, which could be used by setting one of the controller output for the flexural vibration suppression and the other one for the torsional vibration suppression, may yield more satisfactory results.

Another conclusion drawn from the controller implementations is that, the real time implementations may not always be possible due to the hardware limitations, such as sampling rate limitations during the signal processing.

CHAPTER 5

CONCLUSIONS

5.1 General Conclusions

This study aimed to illustrate the effectiveness of H_∞ and μ synthesis methods in the free and in-vacuo forced vibration suppression of smart structures. The structures analyzed in this thesis were the smart beam and the smart fin, which were both aluminum passive structures with surface bonded PZT (Lead-Zirconate-Titanate) patches. The structures were considered in clamped-free configuration. The surface bonded PZT patches were used as actuators whereas the strain gages and the laser displacement sensor were used as sensors.

The first part of the study was dedicated to the smart beam. The experiments were performed to obtain the single-input single-output system models from either strain or displacement measurements. H_∞ controllers were designed based on these models for the vibration suppression of the smart beam due to its first two flexural modes. For the validation of the designed controllers, experiments were performed for both free vibration and forced vibration analyses. The excitation for the forced vibration was given by a shaker. As a result of the experiments, it was observed that the designed H_∞ controllers could effectively suppress the free and in-vacuo forced vibrations of the smart beam at its first two modes.

The second part of the study focussed on the experimental and theoretical works conducted for the smart fin. The first experiments were carried out to determine the single-input single-

output system models of the smart fin from either strain or displacement measurements. The controllers were designed via μ synthesis method. In the controller design, both *SISO* and *SIMO* models were used to suppress the free and in-vacuo forced vibrations of the smart fin due to its first flexural and first torsional modes. As in the case of the smart beam, the excitation for the forced vibration was again given by a shaker. The second part of the experiments were performed for the validation of the designed controllers.

The controller implementations showed that the piezoelectric actuation authority was not enough to suppress the vibration of the smart fin due to its first two modes. In the structural design performed using Ansys v5.6 [1], the piezoelectric actuators were placed on both side of the smart fin and it was aimed to use all of the piezoelectric actuators for the vibration suppression purposes. However, PZT actuators being only on one side of the smart fin could be used in the experiments. Thus, half of the actuator authority could be utilized, which was not enough to obtain high level of attenuation. Although the actuation authority was not enough to suppress the vibrations due to high level of shaker excitations, the designed controllers were still effective to suppress the in-vacuo forced vibrations of the smart fin.

It can be concluded that both H_∞ and μ synthesis methods are appropriate for the vibration suppression of the smart structures. It should be noted that both methods are able to include the uncertainty characteristics of the nominal system in the controller design. However, these controller synthesis methods are inevitably based on the frequency response of the system and hence finding the transfer function of the system requires longer times.

In this study, the experiments were carried out by using two different experimental set-up. The first one was based on the strain gage measurements and a dedicated four-channel programmable controller was used in the control applications. In these applications C code was used for data acquisition and control purposes. The high sampling rate (at least 2048 $Sample/s$) could be considered as an advantage of this system. High sampling rate allows the implementation of the higher order controllers. However, this system can only utilize the strain measurements and, though strain gages are not expensive instruments, the system is not very advantageous in terms of the accuracy. The reason stems from the fact that the strain gages

are very sensitive to electrical noise and noise from environment. For the smart structure applications high voltage is required and the amplifiers and DC supplies used in these applications create electrical noise. Also, the strain gages are located on the specific location of the structure and it brings cabling and gluing problems. Furthermore they can only be used once. Another disadvantage was the output filter of the controller unit. The filter has cutoff frequency of 100 Hz and this limits the frequency range of the experiments.

The second set-up was based on displacement measurements and laser displacement sensor, data acquisition cards and *Labview v 5.0* were used for the data acquisition and control purposes. The main disadvantage of this system was low sampling rate (at most 2048 $Sample/s$). Since sampling rate was low, all of the designed controllers could not be implemented. The reason may be due to cards used or due to the program used. Since *Labview* program is high level language it takes time to convert the code to machine code. Another disadvantage of this system is the price of the laser displacement sensor unit. However, a system utilizing data acquisition cards and *Labview* can use any measurements as controller input such as displacement measurements, strain gage measurements or accelerometer measurements. In this study, the displacement measurements were performed by using laser displacement sensor and it had cleaner signal when compared with the strain gage measurements. This is advantageous for controller implementations. Also, the laser displacement sensor can be directed to different locations to measure the displacement of the structure and since it is a way of non-contacting measurement, that does not bring extra mass loading to the structure.

5.2 Future Work

As a result of controller implementations, it was observed that the piezoelectric actuator authority was not enough to suppress the vibration of the smart fin. In the structural modelling, the PZT locations for the smart fin was determined by conducting a parametric study rather than an optimization process. In the future studies, the PZT locations and sizes may be optimized to maximize the attenuation levels at the desired structural modes.

Further improvement is necessary for the experimental hardware. The first improvement

is needed to increase the data acquisition rate. In the controller implementation, low data acquisition rate caused problems in the displacement measurements applications. The second improvement is about the use of PZT's as sensor, for which a more expensive hardware, charge amplifier will be required.

As mentioned in Section 1.2, the hysteresis effects of the piezoelectric actuators were neglected in the present study. Further research is in progress to consider nonlinear properties of the piezoelectric actuators for actuator modelling under the hysteresis effect.

Another future work is to design the controllers using different controller design methods. This thesis work dealt with only the active vibration control. If the necessary hardware is provided, the adaptive control approach, which requires fast data acquisition rate and fast computer processing, may also be implemented in the future.

Aeroelastic effects may also be taken into consideration in the future work. The present study covers the active control of in-vacuo free and forced vibrations of the smart structures. Including the aeroelastic effects will enable to perform the controller experiments in a wind tunnel.

REFERENCES

[1] Çalışkan T., *Smart Materials and Their Applications in Aerospace Structures*, PhD Thesis, Middle East Technical University, September 2002

[2] http:\\www.piezo.com\history.html

[3] Bar-Cohen Y., Xue T. and Lih S., *Polymer Piezoelectric Transducers for Ultrasonic NDE*, NDTnet, Vol.1 No.09, September 1996

[4] Chee C. Y. K., *Static Shape Control of Composite Laminated Plate Smart Structures Using Piezoelectric Actuators*, PhD Thesis, University of Sydney, September 2000

[5] Ikeda T., *Fundamentals of Piezoelectricity*, Oxford University Press, 1996

[6] Zames G., *Feedback and Optimal Sensitivity: Model Reference Transformations, Multiplicative Seminorms, and Approximate Inverses*, IEEE Transactions on Automatic Control, Vol., AC-26, No.2, April 1981

[7] Zames G., Francis B. A., *Feedback, Minimax Sensitivity and Optimal Robustness*, IEEE Transactions on Automatic Control, Vol., AC-28, No.5, May 1983

[8] Sarason D., *Generalized Interpolation in* H_∞ , Trans. AMS, vol. 127, pp.179-203, 1967

[9] Francis B. A., Zames G., *On* H_∞ *Optimal Sensitivity Theory for SISO Feedback Systems*, IEEE Transactions on Automatic Control, Vol., AC-29, No.1, January 1984

[10] Francis B. A., Helton W. J., Zames G., H_∞ *Optimal Feedback Controllers for Linear Multivariable Systems*, IEEE Transactions on Automatic Control, Vol., AC-29, No.10, October 1984

[11] Glover K., *Robust Stabilization of Linear Multivariable Systems: Relations to Approximation*, International Journal of Control, Vol. 43, No.3, pp.41-66, 1986

[12] Doyle J. C., Stein G., *Multi-variable Feedback Design: Concepts for classical/modern Synthesis*, I.E.E.E. Transaction on automatic Control,Vol., AC-26, pp.4-16, February, 1981

[13] Balas G. J., Doyle J. C., Glover K., Packard A., Smith R., μ*-Analysis and Synthesis Toolbox* Musyn Inc. and MathWorks Inc., Minneapolis, MN, 1993

[14] Young P.M., *Robustness with Parametric and Dynamic Uncertainty*, PhD Dissertation, California Inst. of Technology, Pasadena, CA, May 1993

[15] Young P.M., *Controller Design with Mixed Uncertainties*, In Proceedings of American Control Conference, pp. 23332337, Baltimore, Maryland, 1994

[16] Tffner-Clausen S., Andersen P., Stoustrup J., and Niemann H. H., *A new approach to* μ*-synthesis for mixed perturbation sets*, In Proceedings of the 3^{rd} European Control Conference, pp. 147152, Rome, Italy, September 1995.

[17] Mavroidis C., Pfeiffer C. and Mosley M., *Conventional Actuators, Shape Memory Alloy, And Electrorheological Fluids*, Invited Chapter in Automation, Miniature Robotics and Sensors for Non-Destructive Testing and Evaluation, Y. Bar-Cohen Editor, April 1999

[18] Dosch J.,Leo D. and Inmann J.,*Modeling and Control for Vibration Suppression of a Flexible Active Structure*, Journal of Guidance, Control and Dynamics, Vol. 18, pp. 340-346, Apr. 1995

[19] Nalbantoglu V., *Robust Control and System Identification for Flexible Structures*, PhD Thesis,University of Minnesota, July 1998

[20] Nalbantoglu V., Bokor J., Balas G., Gaspar P., *System Identification with Generalized Orthonormal Basis Functions: an Application to Flexible Structures*, Control Engineering Practice , Vol. 11, pp.245-259, 2003

[21] Balas G., Young P. M., *Control Design For Variations in Structural Natural Frequencies*,Journal of Guidance, Control and Dynamics, Vol. 18, No. 2, March-April 1995

[22] Rasmussen K. H., Jørgensen, *Parametric Uncertainty Modelling for Robust Control: a Link to Identification*, Computers and Chemical Engineering 23, pp.987-1003, 1999

[23] Nalbantoglu V., Balas G., Thomson P.,*The Role of Performance Criteria Selection in the Control of Flexible Structures*, AIAA Guidance Navigation and Control Conference San Diego, CA, pp. 1-9, 1996

[24] Balas G., Lukich M., Dailey L. R., Doyle, J. C., *Robust Control of Truss Experiment*, Proceedings of the American Control Conference, Atlanta, GA, pp. 245-252, June 1988.

[25] Balas G., Doyle J. C., *Robustness and Performance Trade-Offs in Control Design for Flexible Structures*, IEEE Transactions on Control systems Technology, Vol. 2, No.4, December 1994

[26] Halim D., Moheimani S. O., *Spatial H_2 Control of a Piezoelectric Laminate Beam: Experimental Implementation* , IEEE Transactions on Control systems Technology, Vol. 10, No.4, July 2002

[27] Kar I. N., Miyakura T., Seto K., *Bending and Torsional Vibration Control of a Flexible Plate Structure Using H_∞ -Based Robust Control Law*, IEEE Transactions on Control systems Technology, Vol. 8, No.3, May 2000

[28] Mei C., Mace B. R., *Reduction of Control Spillover in Active Vibration Control of Distibuted Structures Using Multioptimal Schemes*, Journal of Sound and Vibration, 251(1), 184-192, 2002

[29] Yaman Y., Çalışkan T., Nalbantoğlu V., Prasad E., Waechter D., Yan B., *Active Vibration Control of a Smart Beam*, Canada-US Cansmart Workshop on Smart Materials and Structures, 2001 Montreal, Canada Proceedings pp:137-147

[30] Yaman Y., Çalışkan T., Nalbantoğlu V., Ülker F. D., Prasad E., Waechter D., Yan B., *Active Vibration Control of Smart Plates by Using Piezoelectric Actuators*, ESDA2002, 6th Biennial Conference on Engineering Systems Design and Analysis, Paper APM-018, Istanbul, Turkey, July 8-11, 2002

[31] Yaman Y., Çalışkan T., Nalbantoğlu V., Prasad E., Waechter D., *Active Vibration Control of a Smart Plate*, ICAS2002, International Council of the Aeronautical Sciences, Paper 424, Toronto, Canada, September 8-13, 2002

[32] Yaman Y., Ülker F. D., Nalbantoğlu V., Çalışkan T., Prasad E., Waechter D., Yan B., *Application of H_∞ Active Vibration Control Strategy in Smart Structures*, AED2003, 3rd International Conference on Advanced Engineering Design, Paper A5.3, Prague, Czech Republic, 01-04 June, 2003

[33] Doyle J., Francis B., Tannenbaum A., *Feedback Control Theory*, Macmillan Publishing, 1990

[34] Buschek H., *Synthesis of Fixed Order Controllers with Robustness to Mixed Real/Complex Uncertainties*, PhD Thesis, Georgia Institute of Technology, February 1995

[35] Dullerud G. D., Paganini F., *A course in Robust Control Theory*, Springer, 1999

[36] Zhou K., Doyle J. C., *Essentials of Robust Control*, Prentice Hall, 1998

[37] Tøffner-Clausen S., Andersen P., Stoustrup J.,*Robust Control*, Aalborg University, 4^{th} Edition, 2001

[38] Ljung Lennart, *System Identification: Theory for the User*, Prentice-Hall,1987

[39] Stoica P., Moses R. L., *Introduction to Spectral Analysis*,Prentice Hall,1997

[40] Kowalik J., Osborne M.R., *Mothods for Unconstrained Optimization Problems*, American Elsecier, 1968

[41] Thomson P., Nalbantoglu V., Balas G. J., *Benefits of Passive SMA Elements in Active Vibration Control*, Proceedings of the First European Conference on Structural Control Barcelona Spain, 1996

[42] Zhou K., Doyle J. C., Glover K., *Robust and Optimal Control*, Prentice Hall, 1995

[43] Four-Channel Programmable Controller User Manual, Sensor Technology Limited, Ontario, Canada, January, 2002

[44] Labview User Manual, National Instruments Corporation, 1992-2003

Appendix A

FEM MODELS OF THE STRUCTURES AND CODES FOR CONTROL APPLICATIONS

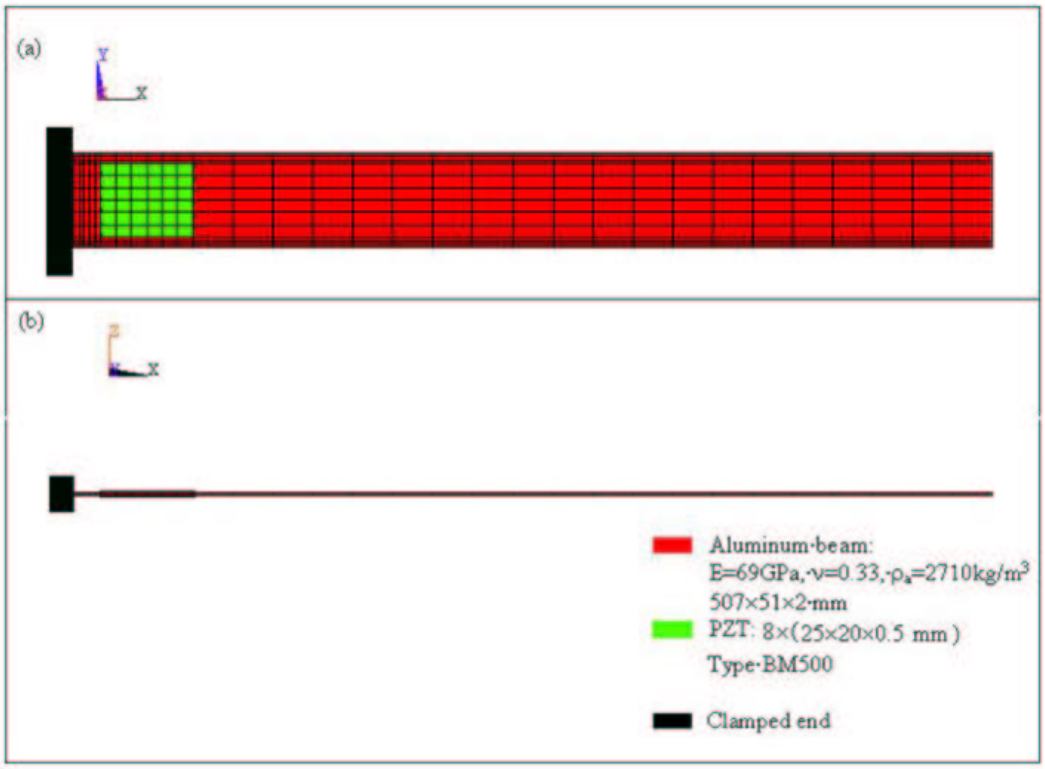

Figure A.1: The Finite Element Modelling of the Smart Beam

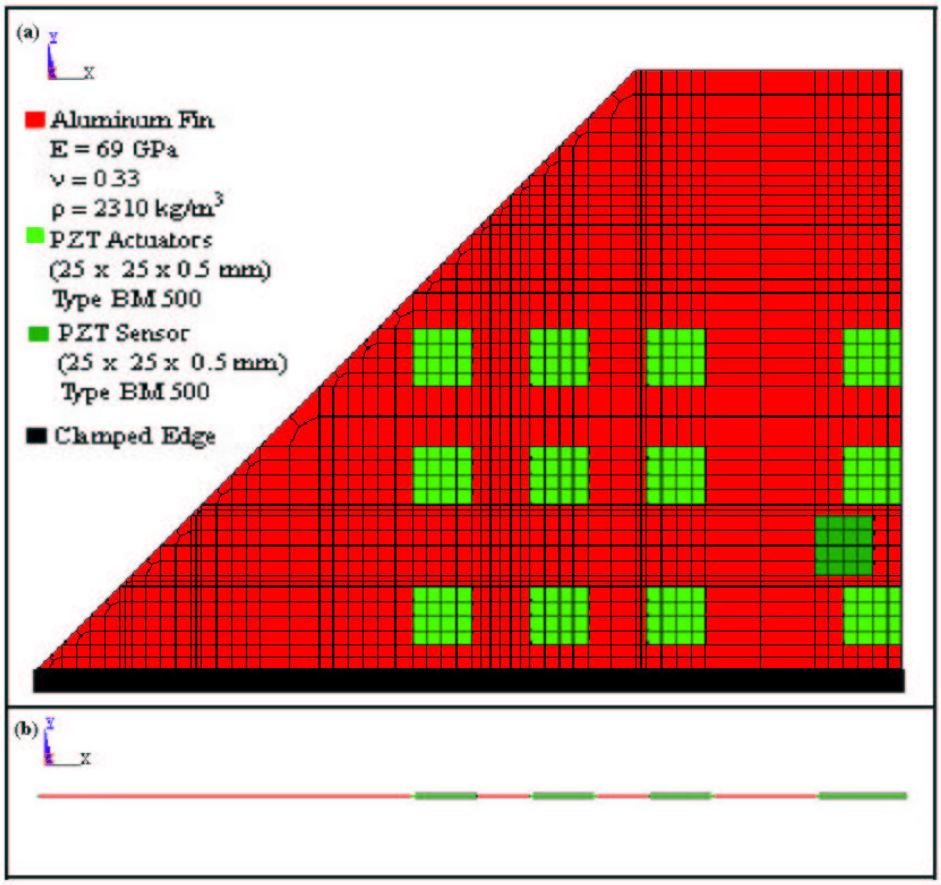

Figure A.2: The Finite Element Modelling of the Smart Fin

A.1 C Code For Strain Measurement Applications

```
/*==========================================*
   This program is used to test 8-ADC and 4-DAC of SBC0486
   C version GNU Development Tools of the Redhat linux 6.2
   *==========================================* */
   # include <stdio.h>
   # include <time.h>
   # include <sys/io.h>
   # include <sys/perm.h>
   # include <stdlib.h>
   # include <termios.h>
   # include <unistd.h>
   # include <signal.h>
   # include <sys/types.h>
   # include <sys/stat.h>
   # include <fcntl.h>
   # include <termios.h>
   # include <string.h>
   # include <time.h>
   # include <math.h>
   /****** Register Address, ADC & DAC of SBC0486 ******/
   # define CFGINDEX 0x350
   # define CFGPORT 0x351
   # define ADCDONE 0x352
   # define DACPORT 0x353
   # define ADC_CONTROL 0x356
   # define ADC_DATA_LOWBYTE 0x356
   # define ADC_DATA_HIBYTE 0x357
```

```
# define HI_CLAMP_PT 4095 /* high limit for output */
# define LO_CLAMP_PT 0 /* low limit for output */
# define TIME_LIMIT 20
# define dt 20/8709
# define NAmax 13
# define NImax 8
# define NOmax 4
void Initialize_IOPort(void);
void Initialize_CFGINDEX_CFGPORT(void);
void Differential(float*, float*, int);
void DAC_Update(int,int);
int ADC_Sample(int);
void Initialize_DAC();
void RungeKutta(float *);
int NA,NO,NI;
float A[NAmax][NAmax];
float B[NAmax][NImax];
float C[NOmax][NAmax];
float D[NOmax][NImax];
float AD_I[NImax];
float AD_Iold[NImax];
int Port_DAC[NOmax];
/**** End of Register Address, ADC & DAC of SBC0486 ****/
unsigned int DAC_Port = 0x3000;
unsigned int ADC_Port = 0x48;
void AD_DA_test(void);
void Choose_input_channel(void);
void Choose_output_channel(void);
```

```
void Show_Channel(void);
long int Cycle_number = 0;

void SigHandler(int SigNum)
    {
       Initialize_DAC();
       printf("\ n Cycle_number=%ld", Cycle_number);
       Cycle_number = 0;
       Choose_input_channel();
       Choose_output_channel();
       Show_Channel();
       alarm(TIME_LIMIT); /* Exit if it exceeds certain time */
       printf("\ n Test will last 30 seconds! \ n");
       return;
    }

void Choose_input_channel(void)
    {
       int ch;
       struct termios old, new;
       tcgetattr(0,&old);
       new = old;
       new.c_lflag &= ~ ICANON;
       new.c_cc[VMIN] = 1;
       new.c_cc[VTIME] = 0;
       tcsetattr(0, TCSANOW, & new);
/**** 0x48– ADC 0;
0x49 – ADC 1;
0x4A – ADC 2;
```

```
0x4B – ADC 3;

0x4C – ADC 4;

0x4D – ADC 5;

0x4E – ADC 6;

0x4F – ADC 7; ****/

/******* Input Channel *******/

printf("\ n Inputing 'n' will end the AD-DA test");

printf("\ n Input the Channel Number of STRAIN GAUGE INPUT or n:");

        do

          {

          ch = getchar();

          printf(" n Your INPUT is : % c  n", ch);

          }while((ch != '1')&& (ch != '2')&& (ch != '3')&& (ch != '4')&& (ch != '5')&& (ch
!= '6')&& (ch != '7')&& (ch != '8')&& (ch != 'n'));

        if(ch == '1') ADC_Port = 0x48;

        else if(ch == '2') ADC_Port = 0x49;

        else if(ch == '3') ADC_Port = 0x4A;

        else if(ch == '4') ADC_Port = 0x4B;

        else if(ch == '5') ADC_Port = 0x4C;

        else if(ch == '6') ADC_Port = 0x4D;

        else if(ch == '7') ADC_Port = 0x4E;

        else if(ch == '8') ADC_Port = 0x4F;

        else if(ch == 'n')

          {

          tcsetattr(0, TCSANOW, & old);

          exit(EXIT_SUCCESS);

          }

        tcsetattr(0, TCSANOW, &old);
```

```
    }

void Choose_output_channel(void)
    {
       int ch;
       struct termios old, new;
       tcgetattr(0, & old);
       new = old;
       new.c_lflag & = ∼ ICANON;
       new.c_cc[VMIN] = 1;
       new.c_cc[VTIME] = 0;
       tcsetattr(0, TCSANOW, &new);
/***0x3000 – DAC 0
0x7000 – DAC 1
0x0b000 – DAC 2
0x0f000 – DAC 3 ***/
/******* Output Channel *******/
       printf("\ n Inputting 'n' will end the AD-DA test.");
       printf("\ n Input the Channel Number of OUTPUT or n:");
       do
         {
         ch = getchar();
         printf("\ n Your INPUT is : % c \ n", ch);
         }while((ch != '1') & & (ch != '2') && (ch != '3') && (ch != '4') && (ch != 'n'));
       if(ch == '1') DAC_Port = 0x3000;
       else if(ch == '2') DAC_Port = 0x7000;
       else if(ch == '3') DAC_Port = 0xb000;
       else if(ch == '4') DAC_Port = 0xf000;
```

```
        else if(ch == 'n')
          {
           tcsetattr(0, TCSANOW, &old);
           exit(EXIT_SUCCESS);
          }
        tcsetattr(0, TCSANOW, &old);
    }

void Show_Channel(void)
     {
    if (ADC_Port == 0x48) printf("\ n Sampling ADC 0 or Strain Gauge Input 1 \ n");
    else if (ADC_Port == 0x49) printf("\ n Sampling ADC 1 or Strain Gauge Input 2 \ n");
    else if (ADC_Port == 0x4A) printf("\ n Sampling ADC 2 or Strain Gauge Input 3 \ n");
    else if (ADC_Port == 0x4B) printf("\ n Sampling ADC 3 or Strain Gauge Input 4 \ n");
    else if (ADC_Port == 0x4C) printf("\ n Sampling ADC 4 or Strain Gauge Input 5 \ n");
    else if (ADC_Port == 0x4D) printf("\ n Sampling ADC 5 or Strain Gauge Input 6 \ n");
    else if (ADC_Port == 0x4E) printf("\ n Sampling ADC 6 or Strain Gauge Input 7 \ n");
    else if (ADC_Port == 0x4F) printf("\ n Sampling ADC 7 or Strain Gauge Input 8 \ n");
    else printf("\ n ADC-Port address is wrong! \ n");
    if(DAC_Port == 0x3000) printf("\ n Updating DAC 0 or OUTPUT 1 \ n");
    else if (DAC_Port == 0x7000) printf("\ n Updating DAC 1 or OUTPUT 2\ n");
    else if (DAC_Port == 0xb000) printf("\ n Updating DAC 2 or OUTPUT 3\ n");
    else if (DAC_Port == 0xf000) printf("\ n Updating DAC 3 or OUTPUT 4\ n");
    else printf("\ n DAC-Port address is wrong! \ n");
return;
    }

void Register_Signal(void)
    {
```

```
        if(signal(SIGALRM, SigHandler) == SIG_ERR)
          {
          printf("\ n Couldn't register signal handler!\ n");
          exit(EXIT_FAILURE);
          }
      }
/********************* Signal of Linux ********************/

int main( void )
      {
        Register_Signal();
        Initialize_IOPort();
        Initialize_CFGINDEX_CFGPORT();
        Initialize_DAC();
        AD_DA_test();
        return 0;
      }

void Initialize_IOPort()
      {
        if((iopl(3)) == -1)
          {
          printf("\ n The iopl(...) is not called rightly! \ n");
          exit(EXIT_FAILURE);
          }
        printf("\ n Initialize_IOPort()...passed!\ n");
      }

void Initialize_CFGINDEX_CFGPORT()
```

```
{
 unsigned int OriginalState;
 outb(0x00, CFGINDEX); /**** CFGINDEX Register of SBC0486 ****/
 OriginalState = inb(CFGPORT); /**** CFGPORT Register of SBC0486 ****/
 /* LED4 OFF, RS232 for COM1 and COM2 of SBC0486 */
 outb((OriginalState & 0x0f), CFGPORT);
 printf("\ n Initialize CFGINDEX & CFGPORT...passed! \ n");
 printf("\ n LED4 OFF, RS232 for COM1 and COM2 of SBC0486 \ n");
}

void Initialize_DAC()
{
   int i;
   /*int Port_DAC[NOmax];
   for(i=0;i¡NO;i++)
    {
     Choose_output_channel();
     Port_DAC[i]=DAC_Port;*/
     DAC_Update(2047,Port_DAC[i]); /* DAC SBC0486 = 2.5v, High Voltage=0v */
    }
}

void AD_DA_test()
{
   FILE * fp;
   FILE *fp1;
   int AD_Input[NImax];
   int DA_OUT [NOmax];
   int i,j,k,s;
```

```
float y[NOmax];
float x[NAmax];
int Port_ADC[NImax];
int Port_DAC[NOmax];
float bias[NImax];
int bcn,bcmax=1000;
printf(" n AD-DA test! n");
fp1=fopen("fcmt.txt","r");
fscanf(fp1,"% d",& NI);
fscanf(fp1,"% d",& NO);
fscanf(fp1,"% d",& NA);
/******READ CONTROLLER MATRIX FROM FILE ******/
for(i=0;i¡NA;i++)
 {
 for (j=0;j¡NA;j++)
  {          fscanf(fp1,"% f",&A[i][j]);          }
 }
for(i=0;i¡NA;i++)
 {
 for (j=0;j¡NI;j++)
  {          fscanf(fp1,"% f",&B[i][j]);          }
 }
for(i=0;i¡NO;i++)
 {
 for (j=0;j¡NA;j++)
  {          fscanf(fp1,"% f",&C[i][j]);          }
 }
for(i=0;i¡NO;i++)
```

```
{
for (j=0;j¡NI;j++)
 {          fscanf(fp1,"% f",& D[i][j]);          }
}
/****** STRAIN GAGE INPUT CHANNEL SELECTION *****/
for(i=0;i¡NI;i++)
 {
 Choose_input_channel();
 Port_ADC[i]=ADC_Port;
 AD_Iold[i]=0;
 }
/****** CONTROL SIGNAL OUTPUT CHANNEL SELECTION *****/
for(i=0;i¡NO;i++)
 {
 Choose_output_channel();
 Port_DAC[i]=DAC_Port;
 }
Show_Channel();
Cycle_number=0;
printf("\ n Test will last 30 seconds! \ n");
/* alarm(TIME_LIMIT);
Exit if it exceeds certain time */
Initialize_DAC();
fp=fopen("mimodata1.txt","wt");
for(k=0;k¡NA;k++)
 {          x[k]=0;          }
/***** BIAS CALCULATION AT EACH CHANNEL ****/
for(i=0;i¡NI;i++) bias[i]=0;
```

```
        for(bcn=0;bcn¡bcmax;bcn++)
          {
          for(i=0;i¡NI;i++)
           {
            AD_Input[i] = ADC_Sample(Port_ADC[i]);
            bias[i]+=AD_Input[i];
           }
          }
        for(i=0;i¡NI;i++) bias[i]=bias[i]/bcmax;
        printf("bias1= % f bias2=%f  n",bias[0],bias[1]);
        printf("\ n ENTER 0 TO EXIT 1 TO CONTINUE \ n");
        scanf("% d",&i);
        if(i==0)return;
        alarm(TIME_LIMIT);
/****** MAIN CONTROL LOOP STARTS****/
        do
          {
          for(k=0;k¡NO;k++)
           {
            y[k]=0;
            DA_OUT[k]=0;
           }
          for(i=0;i¡NI;i++)
          {
            AD_Input[i] = ADC_Sample(Port_ADC[i]);
/*If the Noise is different for each channel modification must be done*/
            AD_I[i] = 20.*(AD_Input[i] - bias[i] ); /*There is bias on the strain gage*/
           }
```

```
            RungeKutta(x);
            for(s=0;s¡NO;s++)
            {
               for(i=0;i¡NA;i++)
                {          y[s]+=C[s][i]*x[i];          }
               for(i=0;i¡NI;i++)
                {          y[s]+=D[s][i]*AD_I[i];          }
/**** Y(s) is CONTROL SIGNAL ****/
               DA_OUT[s] = y[s]+ 2047;
               if(DA_OUT[s] > 4095) DA_OUT[s] = 4095;
               else if(DA_OUT[s] < 0) DA_OUT[s] = 0;
               DAC_Update(DA_OUT[s],Port_DAC[s]);
            }
            for(i=0;i¡NI;i++) AD_Iold[i]=AD_I[i];
            Cycle_number++;
           }while (1);
/****** MAIN CONTROL LOOP ENDS****/
        fclose(fp);
        return;
    }

void RungeKutta(float x[])
    {
        int i,idx;
        float xp1[NAmax];
        float xp2[NAmax];
        float xp3[NAmax];
        float slp1[NAmax] , slp2[NA] , slp3[NA] , slp4[NA];
```

```
float difr[NA];
idx = 1;
Differential(x,difr,idx);
for(i=0;i¡NA;i++)
  {
   slp1[i] = difr[i];
   xp1[i] = x[i] + slp1[i]*dt/2.;
  }
idx = 2;
Differential(xp1 , difr,idx);
for(i=0;i¡NA;i++)
  {
   slp2[i] = difr[i];
   xp2[i] = x[i] + slp2[i]*dt/2.;
  }
Differential(xp2, difr, idx);
for(i=0;i¡NA;i++)
  {
   slp3[i] = difr[i];
   xp3[i] = x[i] + slp3[i]*dt;
  }
idx = 3;
Differential(xp3, difr,idx);
for(i=0;i¡NA;i++)
  {
   slp4[i] = difr[i];
   difr[i] = (slp1[i]+2.*(slp2[i]+slp3[i])+slp4[i])/6.;
   x[i] = x[i] + difr[i]*dt;
```

```
        }
      return ;
    }

void Differential(float x[], float difr[],int inx)
   {
      float sl;
      float u[NI];
      int i,j,s;
      for(i=0;i¡NI;i++)
       {
        if(inx==1) u[i] = AD_Iold[i];
        if(inx==2) u[i] = (AD_I[i]+AD_Iold[i])/2.;
        if(inx==3) u[i] = AD_I[i];
       }
      for(i=0;i¡NA;i++)
       {
        sl = 0;
        for(j=0;j¡NA;j++)
         {        sl+=A[i][j]*x[j];        }
        for(s=0;s¡NI;s++)
         {        sl+=B[i][s]*u[s];        }
        difr[i] = sl;
       }
      return ; }

void DAC_Update(int DA_Output,int DAC_Port)
    {
      int loop;
```

```
        int DACDATA;
        unsigned int Test_bit;
/*************** MAX525 DAC of SBC0486 Start *****************/
/****** Initiate the DACCS and DACCLK of DACPORT *******/
        outb(0x06, DACPORT); /** DACCS = 0; DACCLK = 1 **/
/* 0 to 0V; 2047/2048 to 2.5V; 4095 to +5V for DAC of SBC0486 */
/* Load input register A, all DAC register updated of MAX525 */
/* 0x3000 – DAC 0
0x7000 – DAC 1
0x0b000 – DAC 2
0x0f000 – DAC 3 */
        DA_Output = DA_Output — DAC_Port;
        Test_bit = 0x8000;
/************ Send data to D/A serially ***************/
        for(loop = 15; loop >= 0; loop –)
          {
           if(Test_bit & DA_Output) DACDATA = 0x01;
           else DACDATA = 0x00;
           outb((DACDATA — 0x04), DACPORT); /* DACCS = 0; DACCLK = 0 */
           Test_bit = Test_bit >> 1;
           outb((0x06 — DACDATA), DACPORT); /* DACCS = 0; DACCLK = 1 */
          }
        outb(0x02, DACPORT); /* DACCS = 1; DACCLK = 1 */
/***************** DAC of SBC0486 end ****************/
    }

int ADC_Sample(ADC_Port)
    {
```

```
        int AD;
/****** MAX197 ADC of SBC0486 ******/
/** Channel 1/AD0; -5v - +5v; Aquisition Mode: Internally controlled **/
/*** AD Control register, and start aquisition and conversion of AD ***/
/* 0x48 – ADC 0;
0x49 – ADC 1;
0x4A – ADC 2;
0x4B – ADC 3;
0x4C – ADC 4;
0x4D – ADC 5;
0x4E – ADC 6;
0x4F – ADC 7; */
        outb(ADC_Port, ADC_CONTROL);
/*************** Sample data from A/D 0 ***************/
        while(!(0x01 & inb(ADCDONE)))
          {          /* waiting for A/D conversion completion */          }
        AD = inb(ADC_DATA_HIBYTE);
        AD = AD << 8;
        AD += inb(ADC_DATA_LOWBYTE);
        if(AD & 0x8000) AD -= 65535; /* Adjust minus number */
        return ( AD );
    }
```

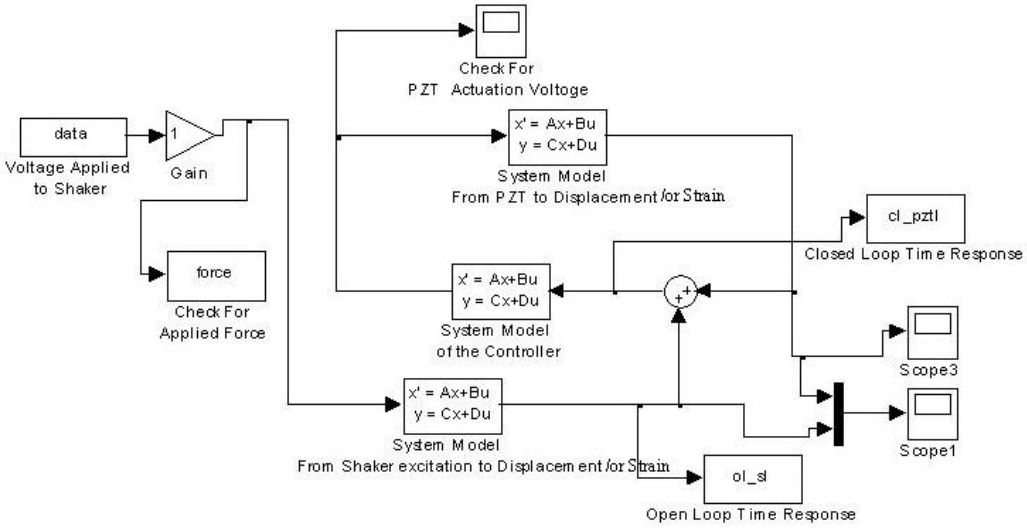

Figure A.3: Block Diagram Representation For Time Response of the System Under Shaker Excitation

A.2 Labview v5.0 vi For Displacement Measurement Applications

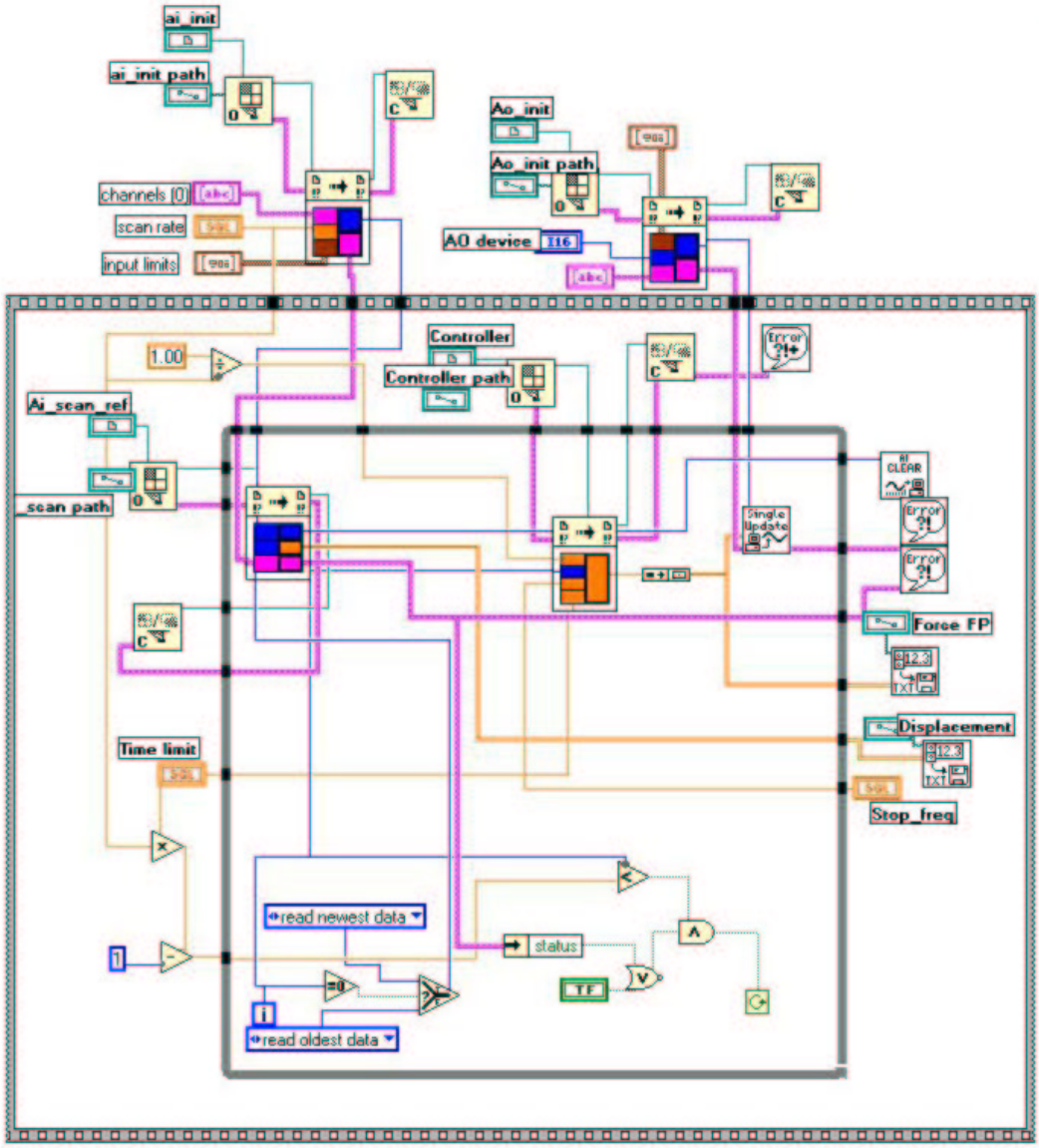

Figure A.4: Data Acquisition Algorithm for Displacement Measurement

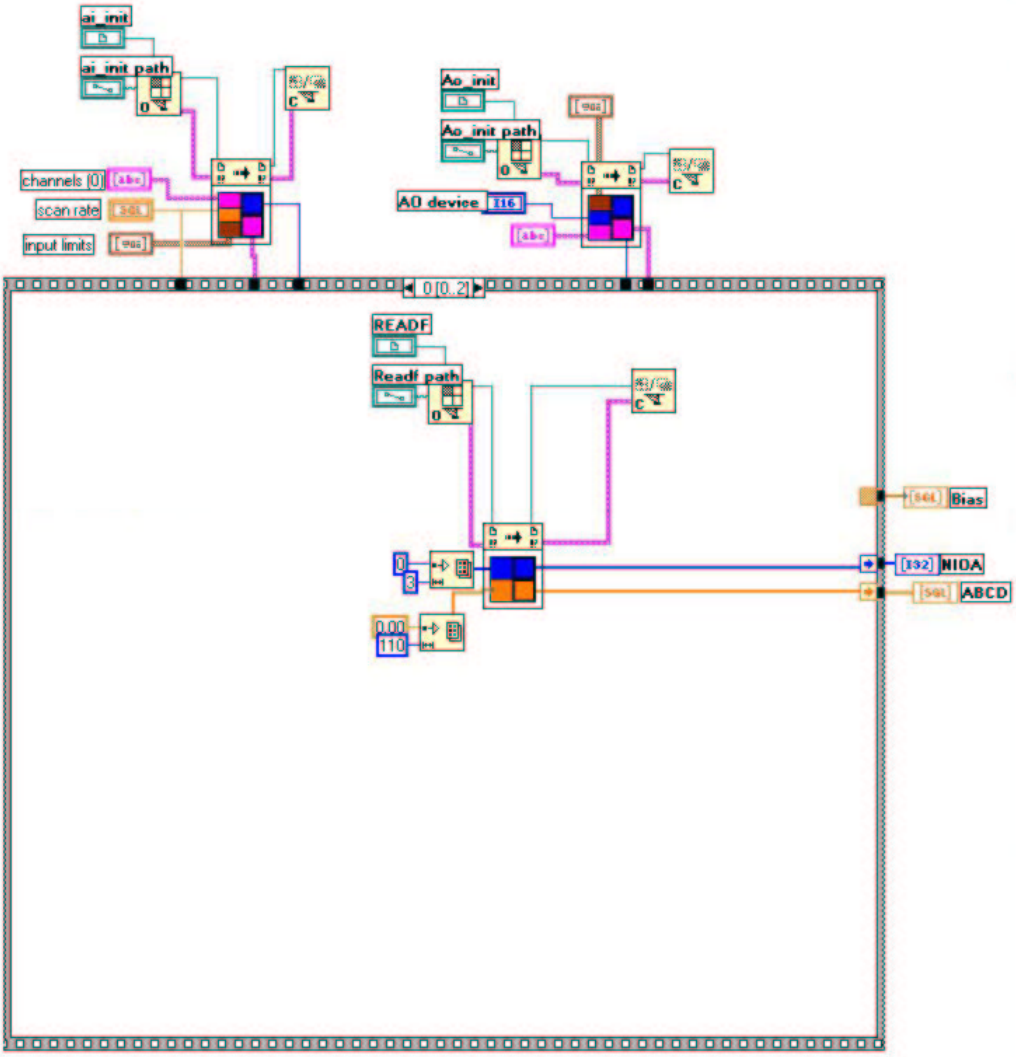

(a) Read Control Matrix From Data

Figure A.5: Controller Algorithm Written in Labview v5.0 for Displacement Measurement

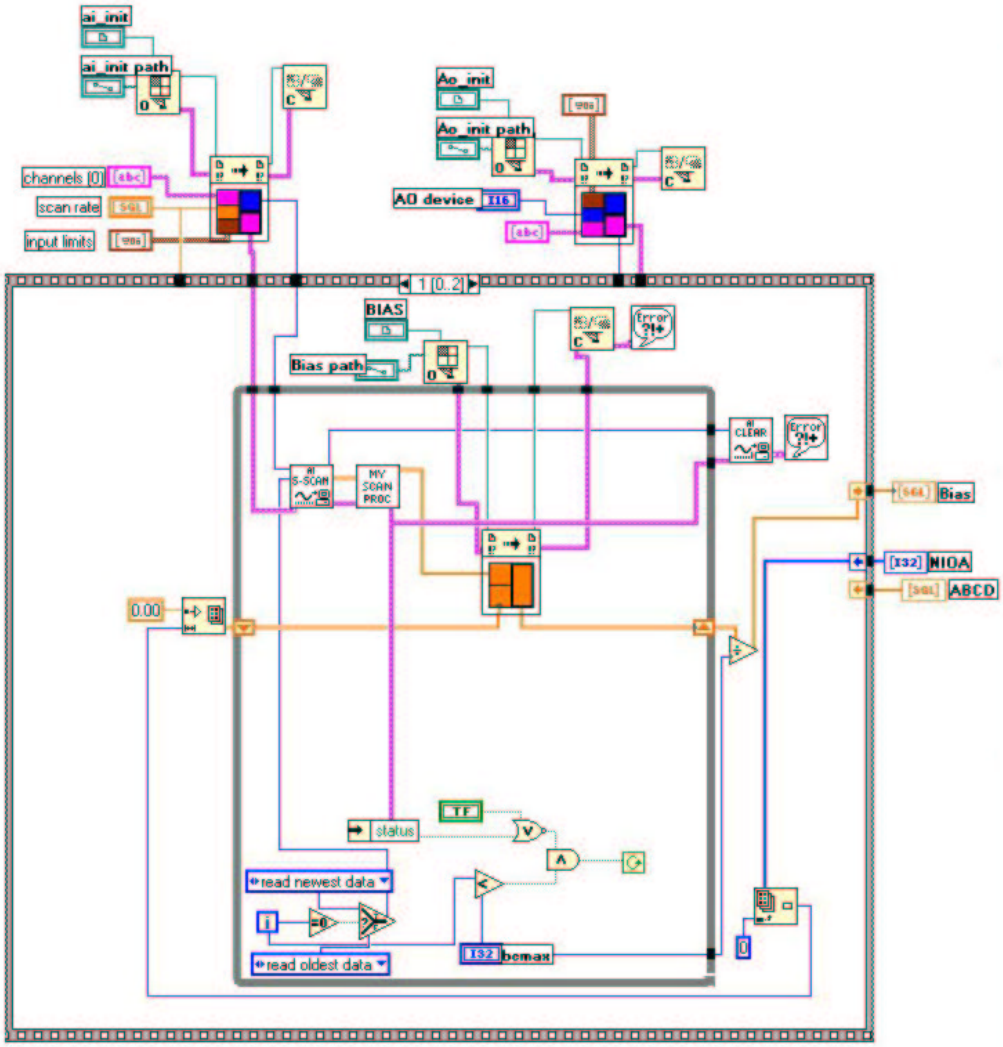

(b) Bias Calculation of Each Input Channel

Figure A.5: Controller Algorithm Written in Labview v5.0 for Displacement Measurement, continued

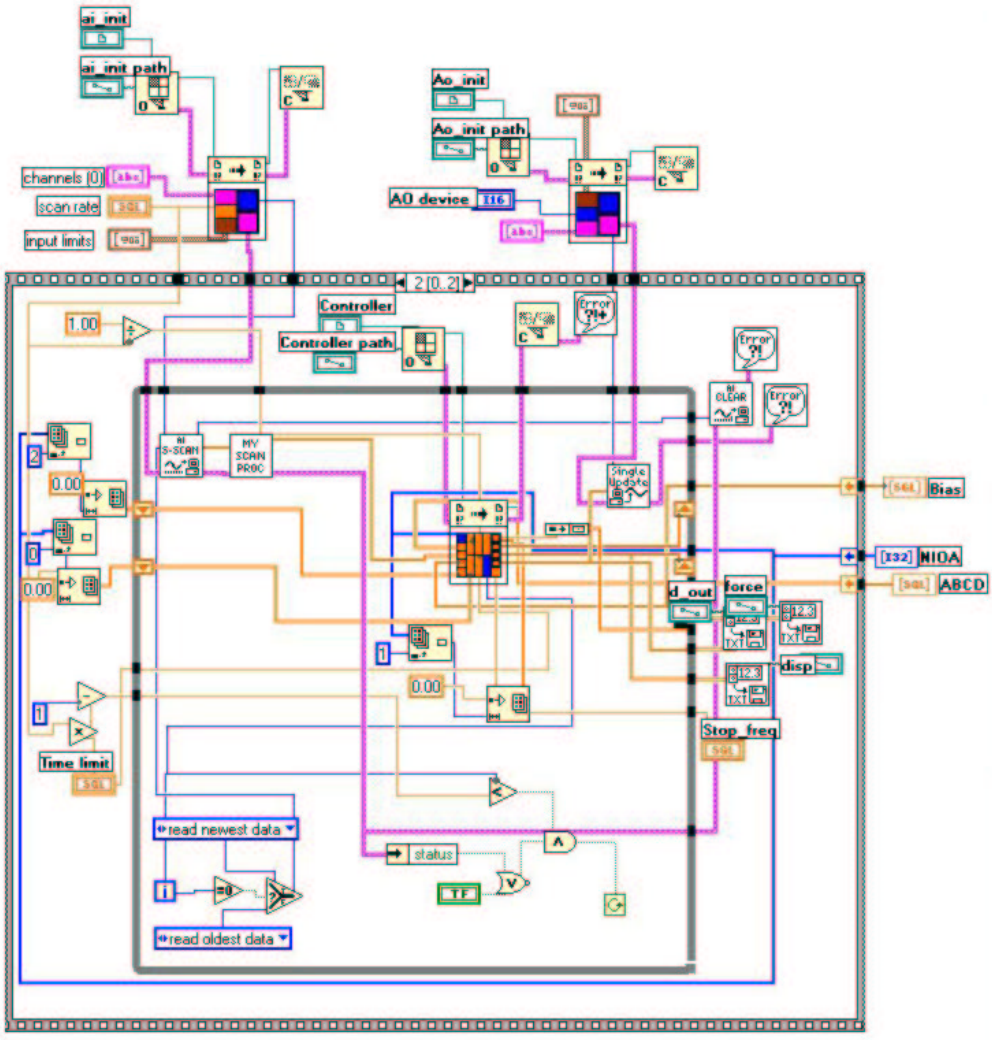

(c) Controller Loop

Figure A.5: Controller Algorithm Written in Labview v5.0 for Displacement Measurement, continued

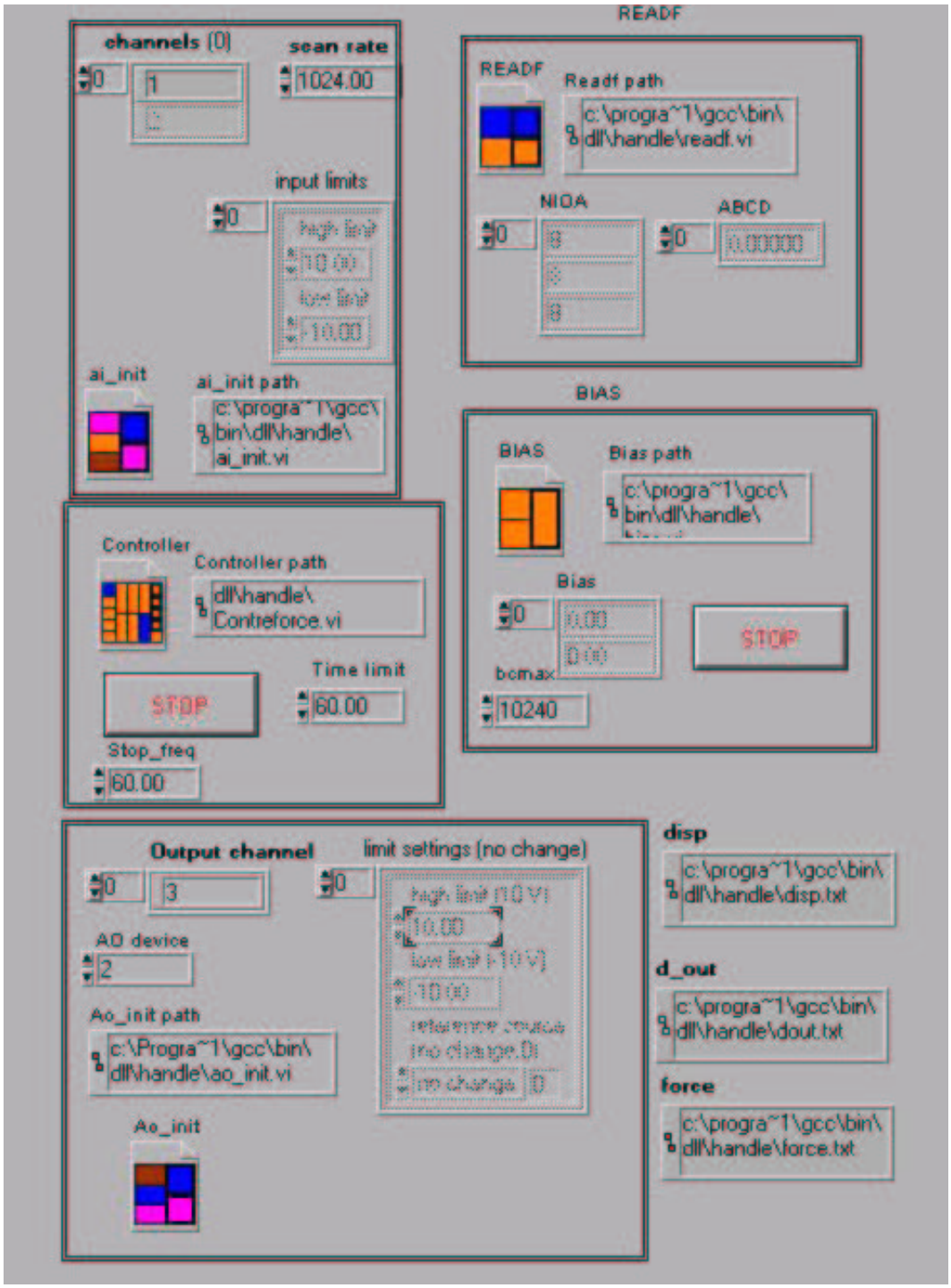

(d) Read-Bias-Control Main Window

Figure A.5: Controller Algorithm Written in Labview v5.0 for Displacement Measurement, continued